DISSERTATIONES
PHYSICAE
UNIVERSITATIS
TARTUENSIS
129

OTT REBANE

In situ non-contact sensing of microbiological contamination by fluorescence spectroscopy

DISSERTATIONES PHYSICAE UNIVERSITATIS TARTUENSIS
129

DISSERTATIONES PHYSICAE UNIVERSITATIS TARTUENSIS
129

OTT REBANE

In situ non-contact sensing of microbiological contamination by fluorescence spectroscopy

UNIVERSITY OF TARTU
Press
1632

This study was carried out at the Institute of Physics, University of Tartu, Estonia and LDI Innovation OÜ, being part of the industrial PhD program in Estonia.

The dissertation was admitted on June 8th, 2022, in partial fulfilment of the requirements for the degree of Doctor of Philosophy in Physics and was allowed for defence by the Scientific Council of the Institute of Physics, University of Tartu.

Supervisors: Prof. Marco Kirm
Institute of Physics, University of Tartu, Estonia

Dr. Sergey Babichenko
LDI Innovation OÜ, Estonia

Opponents: Ilpo Kulmala, PhD
VTT, Finland

Prof. Janis Spigulis, Dr. Habil. Phys.
University of Latvia, Latvia

Defence: August 29th, 2022, at the University of Tartu, Tartu, Estonia

This work has been supported by Estonian Research Council grant PRG629. This work has been partially supported by Graduate School of Functional Materials and Technologies receiving funding from the European Regional Development Fund in University of Tartu, Estonia.

ISSN 1406-0647
ISBN 978-9949-03-963-0 (print)
ISBN 978-9949-03-964-7 (pdf)

University of Tartu Press
www.tyk.ee

CONTENTS

LIST OF PUBLICATIONS INCLUDED IN THE THESIS

I M. Bentahir, S. Babichenko, A.S. Piette, L. Poryvkina, **O. Rebane**, B. Smits, I. Sobolev, N. Soboleva, J.L. Gala, Non-contact, real-time laser-induced fluorescence detection and monitoring of microbial contaminants on solid surfaces before, during and after decontamination. *Journal of Biosensors & Bioelectronics*, **9** (2018). DOI: 10.4172/2155-6210.1000255

II **O. Rebane**, H. Hakkarainen, M. Kirm, L. Poryvkina, I. Sobolev, P. Wilska, S. Babichenko, Real-time monitoring of hydrogen peroxide vapour decontamination of bacterial spores by means of UV fluorimetry, *Proceedings of the Estonian Academy of Sciences*, **70** (2021) 51–61. DOI: 10.3176/proc.2021.1.06

III **O. Rebane**, M. Kirm, L. Poryvkina, H. Hakkarainen, S. Babichenko, Bacterial spore fluorescence dependence on vaporised hydrogen peroxide concentration, *Proceedings of the Estonian Academy of Sciences*, **71** (2021) 117–126. DOI: doi.org/10.3176/proc.2022.2.02

IV J.-L. Gala, **O. Rebane**, J. Ambroise, S. Babichenko, Omar Nyabi, Thierry Hance, Acaricidal efficacy of ultraviolet-C irradiation of *Tetranychus urticae* adults and eggs using a pulsed krypton fuoride excimer laser, *Parasites and Vectors*, 14 (2021). DOI: 10.1186/s13071-021-05085-7

Author's contribution

The author was responsible for the optical and spectral designs of devices in papers **I–IV**, the experiments and data analysis of the results presented in papers **I–III**. The author prepared samples studied in papers **II** and **III**. The author characterised the samples studied in papers **I**, **II** and **III** using fluorescence spectroscopy methods. The author took part of writing paper **I** and **IV** and was responsible for writing papers **II** and **III**.

Other publications of the dissertant

1. J. Saaring, A. Vanetsev, K. Chernenko, E. Feldbach, I. Kudryavtseva, H. Mändar, R. Pärna, V. Nagirnyi, S. Omelkov, I. Romet, **O. Rebane**, M. Kirm. Relaxation of electronic excitations in K_2GeF_6 studied by means of time-resolved luminescence spectroscopy under VUV and pulsed electron beam excitation. *Journal of Alloys and Compounds*, 883 (2021) 160916. DOI: 10.1016/j.jallcom.2021.160916.

2. J. Saaring, A. Vanetsev, K. Chernenko, E. Feldbach, I. Kudryavtseva, H. Mändar, S. Pikker, R. Pärna, V. Nagirnyi, S. Omelkov, I. Romet, **O. Rebane**, M. Kirm. Time-resolved luminescence spectroscopy of ultrafast emissions in $BaGeF_6$. *Journal of Luminescence*, 244 (2022) 116729. DOI: 10.1016/j.jlumin.2022.118729.

3. P. Saari, **O. Rebane**, I. Besieris, Energy-flow velocities of nondiffracting localized waves, *Physical Review A*, 100 (2019), ARTN 013849. DOI: 10.1103/PhysRevA.100.013849.

4. S. Babichenko, L. Poryvkina, I. Sobolev, **O. Rebane**, Compact HLIF LiDAR for marine applications. *International Journal of Remote Sensing*, 37 (2016), 3924−3937. DOI: 10.1080/01431161.2016.1204479.

LIST OF ABBREVIATIONS

BA	*Bacillus atrophaeus* (bacteria)
CCD	charge-coupled device
CFU, PFU	colony forming unit, plaque forming unit
CMOS	complementary metal-oxide semiconductor
DNA	deoxyribonucleic acid
DPA	dipicolinic acid
EEMS	excitation emission matrix spectroscopy
FLIM	fluorescence lifetime imaging
GS	*Geobacillus stearothermophilus* (bacteria)
HLIF	hyperspectral laser induced fluorescence
HPV	hydrogen peroxide vapour
IR	infrared
LED	light emitting diode
LiDAR	light detection and ranging device
LIF	laser induced fluorescence
LOD	limit of detection
LTW	long-time window
NAD	nicotinamide adenine dinucleotide
MALDI	matrix-assisted laser desorption/ionization
OD	optical density
PCR	polymerase chain reaction
ppm	parts per million
RNA	ribonucleic acidSEM scanning electron microscopy
SFS	spectral fluorescence signature
SiPM	silicon photomultiplier
SR	synchrotron radiation
STW	short-time window
TI	time-integrated
TOF	time of flight
Trp, Tyr, Phe	tryptophan, tyrosine, phenylalanine
UV, VUV	ultraviolet, vacuum ultraviolet
VHP	vaporised hydrogen peroxide

1. INTRODUCTION

This thesis summarizes optical and spectral design developments as well as the experiments and their results forming a basis for the detection of various bio-organic compounds using optical fluorescence spectroscopy methods. Most of the methods described here are based on the fluorescence properties of various micro-organisms in the ultraviolet range, but some attention is also given to the influence of ultraviolet radiation itself on the viability of micro-organisms.

1.1. Importance of pathogen detection, identification and monitoring

Among the billions of microorganism species on Earth, there exist a bit more than a thousand known species of bacteria, viruses, protozoa and other micro-organisms that pose a danger to human health [1]. Microorganisms capable of causing disease or harm are called pathogenic microorganisms or just pathogens. Detection and identification of such pathogens is a key problem in infectious disease control efforts [2], including the decontamination procedures of various rooms and surfaces. Decontamination is any activity (including sterilization, disinfection and antisepsis) that reduces microbial load to prevent pathogen contamination of people and other living organisms. Nowadays this prevention is especially important in clinical settings due to the appearance of multidrug-resistant bacterial strains [3] as well as viral diseases that have a significant economic impact or have no applicable cure yet. It is shown that patients admitted into hospital rooms previously occupied by people suffering of multidrug-resistant bacterial infection have twice the probability of getting the same infection [4] compared to being in any other unexposed room. Moreover, decontamination is also relevant in many public rooms [5], public transport [6] and other places where a multitude of infected people have been travelling and/or passing through and have potentially contaminated some surfaces with dangerous pathogens. This thesis is primarily focused on detection of pathogens in the framework of decontamination procedures.

Microorganisms are way too small (in the order of 1 micrometer) to be visible by the naked eye – in fact most are too small to be visible even under a classical optical microscope [7]. Nevertheless, large collections of micro-organisms could potentially be visible as (*e.g.*, white) stains on various surfaces, but these stains are indistinguishable from any other type of stains by their visual appearance alone, if at all visible. Therefore, even with very highly contaminated surfaces, the visual appearance will not give a good understanding about the presence of pathogens. To get a better awareness about the pathogens present in the inspected area, multiple locations in the area typically need to be swab sampled, which in addition to the not-well-defined selection of the swabbing area is in itself not highly efficient from many surfaces [8]. After

careful collection of swab samples, these need to be transported to a properly equipped biological laboratory where the samples have to be cultivated in growth media for at least one day to have enough microorganisms present for *e.g.,* mass spectrometry analysis. Of course, in contrast to the slow classical microbiological growth method and multi-hour gene sequencing, some molecular labelling (*e.g.,* antibody) type tests can give results much quicker on a preselected set of pathogens, but this method also needs sampling, as well as specially synthesized chemical counterparts and pre-treatment. As a result, such method only identifies the same selected set of pathogens and not much else [2]. In this thesis, we consider another solution to this pathogen detection problem, which – compared to aforementioned methods – is extremely quick, giving an answer in seconds, and can cover a much larger spatial area with not many demands on the shape of the area. It also does not require any sampling or additional chemicals and can therefore be used as a quick indicator about the success of any decontamination procedure.

The current method is based on the detection of the pathogen microorganism's autofluorescence signal. Autofluorescence is the process where natural (*i.e.*, non-labelled) cells emit light (radiation) of a certain set of wavelengths when being excited at some other (shorter) wavelength(s) [9]. Admittedly, autofluorescence signal peaks for microorganisms are spectrally wide and this limits the extraction of the information from such spectra, so this method is naturally less specific when compared to *e.g.*, gene sequencing and antibody detection. Nevertheless, the limited sensor specificity and selectivity can in many decontamination situations be an acceptable trade-off to get the measurement speed up high enough. The quick result about the surface being clean versus the surface still showing spectral signs of contamination is mostly enough for the decontamination team to decide on how to proceed. If any contamination-related signal has vanished, it is time to end the decontamination process, otherwise it should continue until its completion without any detectable signals.

1.2. Benefits of using autofluorescence-based pathogen sensors

The term autofluorescence is used to differentiate naturally occurring fluorescence from fluorescence caused by chemical or genetic labelling. In contrast to fluorescence labelling the autofluorescence effect occurs in any wild type (*i.e.,* unmodified) natural cell, because many molecules that are present in living cells exhibit fluorescent properties with reasonably high quantum yields (*i.e.,* reasonable fluorescence efficiencies). The list of natural fluorophores in various cells [9] includes collagen and elastin, reduced pyridine NADH, NADPH, flavins, porphyrins, lipofuscins, pyoverdine, some vitamins (A, B2 – riboflavin, B6 – pyridoxine, E), cellulose, chitin, chlorophylls, some neurotransmitters, etc. Even the nucleic acids of DNA/RNA fluoresce (at ~260 nm excitation and 334 nm emission), although ~100 times weaker compared to tryptophan [10].

Among other factors, the change of autofluorescence signals related to some of these fluorophores can be connected to cell ageing, the presence of tumours and can be used to monitor cell energy transfer mechanisms [9], most of which are unrelated to the current PhD thesis topics. But the aforementioned list of fluorophores also must include proteins containing 2 to 3 common amino acids containing aromatic rings: phenylalanine, tyrosine and tryptophan (although Trp is not present in some proteins), with most of the fluorescent light emitted by tryptophan, if present. The fluorescence signal from tryptophan is often used in this research work as one of the key markers indicating the presence of micro-organisms [11, 12]. The other 2 fluorescent amino acids, tyrosine and phenyl-alanine, also emit fluorescence in close-by spectral regions at shorter wave-lengths (around 300 nm and 280 nm respectively, compared to 350 nm for tryptophan) [13], but tend to transfer their excitation energy to any local tryptophan molecule with excited states at lower energies via resonance energy transfer [14, 15]. Therefore, these other two entities (Tyr, Phe) typically do not contribute as much into the fluorescence spectrum of cells overall – although sometimes the contribution of tyrosine emission can be significant. The Förster resonance energy transfer at close molecular range is quite efficient because the fluorescence emission energies of tyrosine and phenylalanine fall in the same range where excitation of tryptophan occurs. Also, compared to tyrosine and phenylalanine, the quantum yield and absorbance at UV wavelengths are higher for tryptophan, making its fluorescence even more pronounced [13]. As is the case with most fluorescent molecules, the fluorescence spectrum of tryptophan is significantly affected by the local chemical environment [16]. For example, tryptophan packed into a protein with neighbouring hydrophobic amino acids will fluoresce at shorter wavelengths when compared to hydrophilic neighbours [17, 18]. Although the sum of such spectral change effects is not huge, some studies have actually been able to identify and differentiate between closely related microorganisms by using their spectral fluorescence fingerprints alone [19, 20].

Another commonly used autofluorescent biomolecule is NADH (reduced form of nicotinamide adenine dinucleotide, NAD), which is present in most types of cells and is an integral part of energy-conversion redox processes occuring in cells [9], therefore being highly indicative of cell “breathing” and cell viability. Due to its lower fluorescence efficiency and many other fluoro-phores fluorescing in the same spectral area, the detection of NADH in living cells using fluorescence is much more complicated compared to the detection of aforementioned 3 fluorescent amino acids. The NADH signal is often hidden in autofluorescence signals of various B vitamins, collagen, flavins that also emit fluorescence as wide bands in the same overlapping spectral regions. Therefore, quite often, in addition to the separation spectral domain, the time domain is also applied to detect NADH in cells via the fluorescence lifetime imaging (FLIM) detection methods [21]. Since the oxidized form of NADH – labelled as “NAD+” – does not emit significant fluorescence, while NADH has strong fluorescence, this pair (together with NADPH pair, which is more used in

organic synthesis inside cells, but very hard to separate spectrally from NADH [22]) is rather useful tool for monitoring metabolic activity in cells [23]. Fluorescence of NADH is not the main focus of this work, but some of the spectra in this work likely contain NADH spectra and so it is reasonable to introduce NADH principles here.

Not so frequently used fluorophore, but being also relevant to this work, is dipicolinic acid (DPA), which makes up 5 to 15% of the dry weight of bacterial endospores and has a major role in keeping the genetic material safe in the endospore form of bacteria [24]. The high amount of DPA, its relatively close spectral position to tryptophan emission [25] as well as its different spectral behaviour during hydrogen peroxide vapour decontamination procedure mean that the fluorescence of this autofluorescent molecule could be used in monitoring certain decontamination processes as well as for detection and identification of bacterial endospores.

2. FORMULATION OF THE RESEARCH TASK

The current thesis focuses on the following two research objectives:

1. Detection of different pathogens on selected substrate materials by using their autofluorescence signals.

The thesis mostly considers fluorescence-based detection of pathogens on various surfaces. In the context of the thesis multiple different devices are designed and tested by the author. The experimental research includes measuring model pathogens on clinically relevant background materials used in hospitals. The list of devices developed for pathogen monitoring includes a spectral HLIF lidar (BC-Sense), a fibre-optic spectrofluorometer (SFS-Go) and a multichannel hand-held fluorimeter (H2B-Spectral). The lidar and spectrofluorimeter solutions providing comprehensive spectral analysis are shown to be beneficial and extensively capable. At the same time, more affordable techniques are required for many institutions responsible for biosecurity and biosafety monitoring and decontamination activities. Accordingly, the thesis work pays much attention to the simplified technical solution, physically smaller and faster in time response, which is the multi-channel fluorimeter H2B-Spectral. The development and experimental testing, performed in many iterations of this device are included in the thesis.

2. Real-time monitoring of vaporised hydrogen peroxide decontamination procedure by using the autofluorescence signal from commonly used biological indicators.

A novel approach of using autofluorescence to monitor the decontamination process with vaporised hydrogen peroxide (VHP) has been developed and tested by the author. The small and capable H2B-Spectral sensor was modified to monitor the efficiency of VHP decontamination. This approach suggests that commonly used biological indicators – bacterial spores – are installed inside the sensor and their autofluorescence is monitored continuously, in real time during the decontamination process. It has been revealed that the fluorescence signal of the spores decreases during decontamination, even at small gaseous concentrations of vaporised hydrogen peroxide. The degree of such reduction can serve as a measure for the control and optimization of the decontamination process, thus enabling the increase of its efficiency in terms of the quality and duration. The spectral differences between VHP-killed and still viable bacterial spores in the excitation/emission fluorescence spectral scale as well as in time resolved mode were identified. In addition, the damage caused by the ultraviolet excitation beam of the developed monitoring devices was also taken into account by comparing the dose rates for small macrobiological objects. Finally, the VHP-treated dead and viable spores were imaged using the scanning electron microscope (SEM) to visualize presence of any physical damage of spores and whether it can be correlated with VHP-treatment.

3. OVERVIEW OF THE CURRENT SITUATION OF THE FIELD OF RESEARCH

3.1. Overview of modern solutions for pathogen detection

Widely used modern solutions for the detection and identification of pathogens typically fall into one of two categories: either the genome-based polymerase chain reaction (PCR) analysis or mass spectrometry (MALDI TOF MS) analysis with classical incubation steps included [2]. Even though the genome-based PCR detection is nowadays cheap enough for practical use in most settings, the classical growth-on-Petri-dish approach with the MALDI TOF/MS or even with certain chromogenic, fluorogenic or antibiotic markers is still very widely implemented in clinical settings.

PCR analysis works by first chemically accessing and targeting specific RNA part (16S rRNA) of some biological samples for amplification [26]. The polymerase enzymes are used in cyclic temperature settings to multiply the interesting genetic material exponentially. The nucleic acids at the ends of variable piece lengths of genetic material are then tagged and the genetic sequence established with systematic readout mechanisms and help of specialized software. The result really is highly specific to pathogen species – to the point of identifying clusters of disease outbreak according to the genetic fingerprint. PCR result is achieved in a time-frame of a few hours, so it can be expected that even though the clinical healthcare system has a high inertia to change, the PCR systems will be used more and more in the future, even though there are some drawbacks as well. Namely, PCR is often too sensitive and finds pathogens, which really have a way too low concentration to be clinically relevant or are from a non-viable micro-organism [27]. Secondly, the PCR result might not give a real indication about the actual antibiotic resistance response of the found species as certain antibiotic-resistance plasmons can spread horizontally between bacterial species. It must be noted that in contrast to PCR, the full genome analysis [28] will give the antibiotic-resistance result. Thirdly, some samples are so dense in genetic material that it is highly unlikely that the important genetic information is actually found from an untreated sample by PCR. Whole genome analysis [29] of the measured biological sample (a full mix of bio-substances) will bypass many of the issues with PCR and is probably the direction the world is heading to, but the technology is much more expensive, needs much more reference data for data processing and is overall somewhat slower to give the result needed. The slowness is still an issue with at least at the time of completing this thesis, but the technology seems to improve fast.

A connected, but different and quite important modern method is based on so-called hybridisation (including gene chip technology), where synthetic DNA/RNA fragments either bind or do not bind to the sample of interest, revealing the presence or absence of genes that are investigated. A well-chosen

set of such fragments can be used to assess in a matter of hours the presence or many common pathogens that the DNA fragments are chosen for. The specificity is high, it needs less equipment and it is much faster compared to growth-based methods.

Figure 3.1.1. Left – classical growth method of *Bacillus atrophaeus* bacteria on Petri dish grown for experiments of this work. Right – spore-containing biological indicators grown in growth liquid – taken out of 400 ppm VHP every minute (from right to left) show that growth stops only after ~10 minutes of VHP decontamination (clear yellow liquid denotes growth, purple denotes no growth, credit: Cleamix Oy).

The traditional microbiology approach of growing bacterial samples in a petri dish and identification by phenotypical procedures' criteria is often tedious, time consuming, requires many reagents and is still unreliable [30]. For example, some bacteria require highly specific growth conditions and some colonies appear only after 70 days of growth [27]. The conventional approach (illustrated in figure 3.1.1) is nowadays supplemented by analysing the resulting colonies with matrix-assisted laser desorption/ionization time-of-flight mass spectrometry (MALDI TOF MS), which sometimes is more efficient than modern PCR. The fact that it is possible to add certain colouring or fluorescing agents to the growth medium, which react to the presence of bacterial species or genus-specific enzymes and give a specific colour to the colonies of interest certainly helps there to pre-select target sample. But the main reason for the classical approach to continue to be used in clinical settings is the fact that antibiotic testing on the found bacterial species needs to be done anyways to find the best antibiotic and as this test takes many hours to days to be completed, the relative speed and sensitivity of PCR play a much smaller role in this context. Moreover, growing bacterial cultures has the additional benefit of delivering the bacterial isolate, which can be further examined for the virulence determinants (*e.g.,* toxins) that are highly relevant when investigating some new disease outbreak. MALDI TOF MS technique is not perfect either – certain bacterial mass-spectrometric fingerprints of laser-evaporated mix of molecules

are remarkably similar for pathogenic bacteria when compared to benign species and misidentification is certainly a possibility there. This means that modern clinical labs are equipped with both – PCR and MALDI TOF – systems for their relevant benefits as they are not as sensitive to the factors of weight, cost and usability in the field as are the teams that move a lot as they work on decontamination tasks.

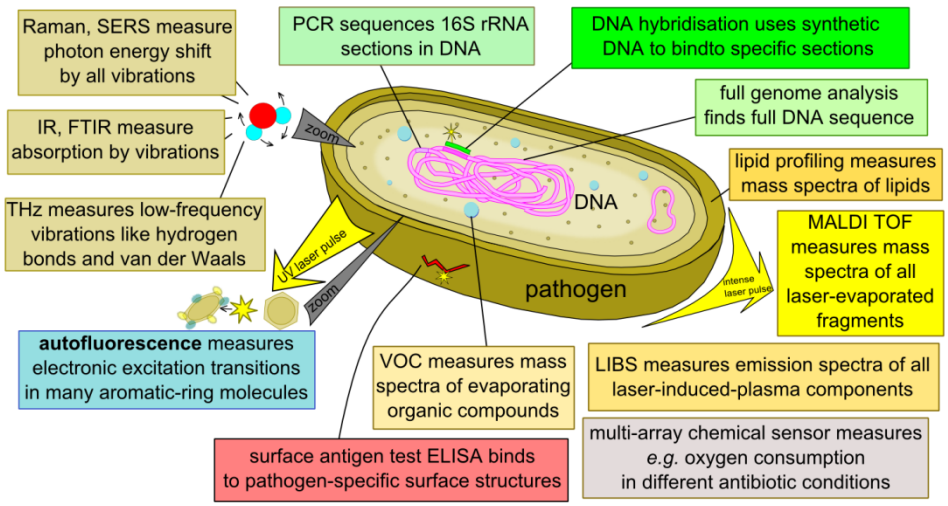

Figure 3.1.2. Comparison chart of bacterial detection and identification techniques that are in use.

Biodetection methods based on proteomic analysis [31], lipid profiling [32] and the emitted volatile organic compounds [33] also exist, but are mostly also based on mass spectrometry. These are not prevailing methods and will not be paid more attention here.

The following IR [34], FTIR [35], Raman [36], SERS [37], LIBS [38], multiarray electrode sensor [39], THz [40], surely ELISA [41] methods all can be used to distinguish bacterial species, but each of these methods have their own limitations and drawbacks when compared to fluorescence methods covered in this thesis. A large set of these bacterial detection methods is briefly described in figure 3.1.2.

3.2. Autofluorescence research, benefits and drawbacks

Fluorescence can be considered as fast photoluminescence process in nanosecond time-scale, in which material absorbs light at a higher energy and emits photons at lower energy (*i.e.,* longer wavelength). Fluorescence is a highly useful physical effect, which among other things can be used for superresolution microscopy [42], optical monitoring of cell functions [43], tagging the nucleic acids in modern genome sequencing applications [44] as well as the detection and identification of various biological objects [45] – as it is relevant to the topic of this thesis. Special chemical fluorescent tags can be developed, which only bind to one particular chemical or even single pathogen species [46, 47], but these always need sampling, sample preparation, fluorescent marker synthesis, which increases the time to get the monitoring result. By using the intrinsic fluorescence – autofluorescence – of the chemicals already present in the biological object, the detection and identification can be done incredibly fast. Of course, the naturally occurring fluorescent molecules can have overlapping spectra and complex interdependencies, which well-chosen fluorescent tags can avoid, but in some certain settings – such as monitoring decontamination process – the speed advantage greatly outweighs the disadvantage of lower specificity in comparison to tagged fluorescence as well as some other competing methods. Also, the fact that the local chemical environment affects autofluorescence of molecules, *i.e.,* their fluorescence intensity, excitation wavelength maximum, emission wavelength maximum and the decay time parameter means that even the non-tagged autofluorescence spectra can contain highly specific information about the biological sample, which is investigated, thus making the phenomenon attractive probes for biological detection and characterization. Autofluorescence spectroscopy offers a rapid, simple, low-cost and label-free solution for the detection and identification of bacteria, of which a few selected examples are pointed out in this section below before proceeding with our own relevant sensor solutions.

In academic research, autofluorescence has been successfully used for the reagentless identification of human bifidobacteria [48], lactic acid bacteria from sausages [49], pathogenic bacteria in the otitis media of the inner ear [50], monitoring of bacterial growth [10], bacterial starvation [51], microorganisms in aerosols [52], spore viability in terrorism context [27], just to name a few examples. Reference 45 even mentions that autofluorescence may be used for investigating bactericidal or bacteriostatic effect of disinfectants (common liquid disinfectants are considered in [53]), something that is aimed in the current research using VHP decontamination process.

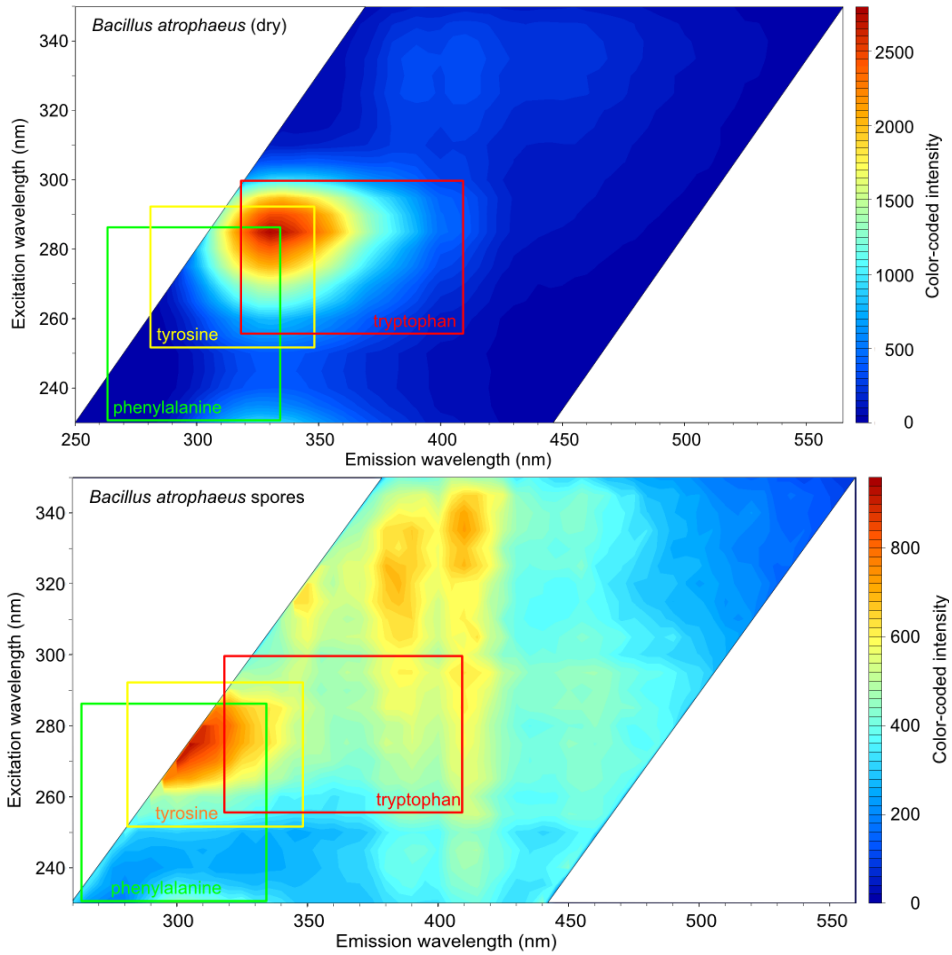

Figure 3.2.1. Spectral fluorescence regions of phenylalanine, tyrosine and tryptophan designated by boxes according to [20] overlaid onto spectral fluorescence signatures of viable *Bacillus atrophaeus* bacteria (upper figure) and *Bacillus atrophaeus* spores (lower figure) which are studied in the current thesis.

In a recent and relevant publication [20] the authors have found non-overlapping spectral regions for phenylalanine, tyrosine and tryptophan (see figure 3.2.1), and recorded synchronous fluorescence (*i.e.,* excitation and emission wavelength are both scanned synchronously while measuring, keeping the wavelength/Stokes shift constant between excitation and emission) of 6 different bacterial species. The principal component analysis on their experimental results showed excellent separation between all 6 identified bacterial species in the studied samples. This result clearly indicates that autofluorescence can indeed be applied in practical detection of biological pathogens only by their autofluorescence signal. Admittedly, these 6 bacteria are from different

taxonomical families, but the identification capability and clear separation between the bacteria is still remarkable. Moreover, the fact that so far there is little to practically no commercial use for this phenomenon obviously points to a business opportunity for those interested. Current research, being part of an industrial PhD program, also takes steps forward in developing similar relevant commercial solutions, the requirements to which are described in the next section.

3.3. Requirements for technical solutions for pathogen monitoring

An important part of this PhD thesis is the conceptual, spectral and optical design of the photonic devices, which are used to detect and/or monitor the biological pathogens. Any design choice is always a compromise for the required properties of the devices – for example, it is immensely difficult to have "low cost" and "high capability" optimised at the same time. This means that the requirements are somewhat subjective and the first-principle approach to reasonable requirements would benefit greatly by input from people who want to use such a device. Here, we have gotten the list of requirements from private communication with Professor Jean-Luc Gala, the head of the CTMA team of UCL in Belgium. The CTMA were one of the teams fighting the 2013 Ebola outbreak in Guinea [54] and therefore they know field hospital needs from their experience really well. Some of the main requirements for the sensor development can be summarised into the following bullet points.

a. The device should have a reasonably small size, mass and power consumption – ideally, it should be handheld for easy and safe handling of highly infectious samples in restricted spaces. Wireless operation on rechargeable battery with compatible charging solutions is part of this condition. Also, ease of packing and unpacking is of relevance.
b. The device should be user-friendly and not need a high level of expertise to deliver reliable measurement results.
c. The cost of the device should be minimal.
d. Device should enable easy, fast and robust sample identification and an efficient data transfer. This means high specificity (true negative rate) and sensitivity (true positive rate) for the measurement results of the device.
e. The device must withstand regular decontamination procedures.
f. On-site quality control, short turn-around time, ease of use of reagents (if any!) are also conditions worth mentioning.

Obviously, one device meeting all of these requirements would need immense development effort with volume manufacturing that is needed to keep the cost down. Investment required for such an effort is out of reach for the academic laboratory and the SME which are part of this research study. Therefore, the device prototypes developed here are a trade-off between their capability, ease of use and cost. The largest developed device – BC-Sense lidar – can operate at long distances and has a good specificity, sensitivity and speed, but is rather

large in size, consumes a lot of power and is difficult to operate. The middle-tier option of SFS-Go spectrofluorometer device has great specificity and sensitivity, but is rather slower, larger and measures just a tiny area at a time. The smallest device – H2B-Spectral – is small, low-cost, low-powered and light-weight, but its specificity is not yet reliably proven to be at a similar level to the more expensive and larger devices. So this device is the main development and research object in the current work, operating not only to detect and identify biological pathogens, but also to monitor decontamination of pathogens in real time.

3.4. Overview of relevant modern decontamination methods

As the devices designed in the framework of the current thesis are meant to operate during pathogen decontamination process, the term "decontamination" must be defined first. Also, a selected set of modern decontamination methods must be introduced, so that the use of vaporised hydrogen peroxide is put into context.

The term "decontamination" refers to any process that reduces microbial contamination on surfaces by some meaningful amount. "Disinfection" refers to just a significant load reduction of almost all pathogenic organisms, whereas "sterilization" refers to the complete destruction of all microbial life [55, 56]. Therefore, disinfection and sterilization are both methods of decontamination. During most of the decontamination experiments in this thesis the pathogenic load after the experiment was not investigated thoroughly enough to claim "sterilisation", so the wider term "decontamination" is mostly used, although sometimes can be used interchangeably with "disinfection".

It is also useful to note here that in this thesis mostly bacteria and bacterial spores are being killed, therefore using the words that refer to lethality to bacteria and spores – *i.e.* "bactericidal" and "sporicidal" are most relevant. Still, as typically the spores are the last form of life to die during decontamination, we can refer to the process as "biocidal" as any biological pathogen will be killed. So under "biocidal" we include terms of bactericidal, sporicidal, virucidal, fungicidal, and even acaricidal (lethal to spider mites).

The most effective widely used biocidal decontamination agent is still low-concentration liquid solution of sodium hypochlorite *i.e.,* bleach. Bleach is more effective, safer and faster compared to other widely used bactericidal agents [53], such as liquid solutions of hydrogen peroxide and formaldehyde, because bleach not only acts on the oxidising power of oxygen, but also that of chlorine. The only downside of bleach is that it will be rapidly neutralized on organic surfaces such as wood – although the same effect is present for most other oxidizing agents. In the case of the 2nd highly effective decontamination agent hydrogen peroxide, it (through mostly free hydroxyl radical mechanisms) oxidises internal parts of the pathogens, such as their genetic material,

membrane lipids and proteins as it easily penetrates cell walls during decontamination [57]. Being a naturally occurring substance, some specific microorganisms have developed catalase-based neutralisation mechanisms against hydrogen peroxide – catalase turns hydrogen peroxide into oxygen and water, making it less effective for decontamination in this situation if higher peroxide concentrations are not used to overpower the catalase-mechanism. Formaldehyde does not operate by oxidising the genetic material or proteins, but rather causes methylization in enzymes and proteins and cross-linking in genetic material, making the cell unviable. Physically the genetic material stays mostly intact when using formaldehyde, while in contrast bleach can physically destroy even the fluorescing molecules inside proteins. Certain bacteria and yeasts are still able to neutralise even formaldehyde by using dehydrogenase enzymes [58]. These 3 decontamination agents are all typically used in liquid form, making the people in charge of cleaning or decontaminating certain surfaces physically wipe down all of the relevant surfaces with a cloth. If this wiping is not done methodically then it is an error-prone process, which often does not reach the cracks, undersides and crevices in the room to be decontaminated, not to mention just missing certain areas in the room during wiping or actually transferring the pathogens from one surface to others with incorrect wiping techniques [59]. Another commonly used disinfectant class based on quaternary ammonium compounds is also based on wiping and will not be discussed here – see [60]. Also, the efficient spore killing disinfectant glutaralaldehyde will not be discussed here.

There are a number of modern technologies that improve the disinfection process [61], like using microfiber wiping cloth instead of cotton [62], using hydrogen peroxide in combination with peracetic acid, hypochlorous acid, or using cold atmospheric pressure plasma, but as long as the process includes manual disinfection, like highly localised wiping or focussing of the disinfectant, they offer little additional benefit. The use of ATP bioluminescence techniques can be used to show the locations where wiping has been performed poorly [63], but this type of quality control is almost never performed in real life. Newer “no-touch” automated systems and antimicrobial surfaces are needed to improve the disinfection efficiency. The “no-touch” systems include UV-C and Xenon light systems, which cover large areas, but also do not decontaminate areas on the undersides or cracks where the UV-light does not reach the object. UV-C decontamination efficiency experiment with an excimer laser is also part of this thesis and will be discussed later in paragraph 6. Last but not least, the “no-touch” systems include aerosol and vaporised hydrogen peroxide, which can reach more areas in the decontaminated room than most competing technologies and are rather easy to use. See figure 3.4.1 for a schematic illustration of the benefits and drawbacks of VHP compared to some other important decontamination methods.

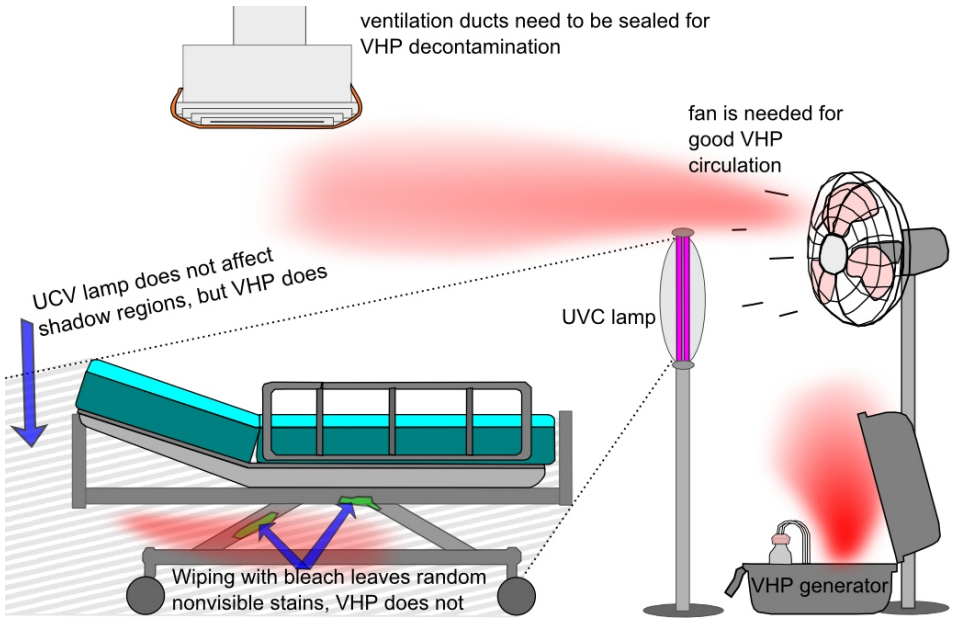

Figure 3.4.1. Technology description, benefits and drawbacks of using vaporised hydrogen peroxide compared to other common decontamination methods.

Consequently, in the case of more difficult and important decontamination processes, the decontamination is done using gaseous disinfectants – called "fumigants" – either in vapour or aerosol form.

3.5. Vaporised hydrogen peroxide usage and its benefits

The options for bactericidal and sporicidal fumigants are formaldehyde, ethylene oxide, methyl bromide, hydrogen peroxide vapour, saturated steam, gaseous ozone [64] and chlorine dioxide [58] as well as a nebulised solution of polymeric guanidine [65]. Due to either their carcinogenic nature, difficulty of use and/or smelly by-products [66], everything other than vaporised hydrogen peroxide is nowadays rarely used. For example, the issues with other fumigants include explosiveness, after smell and discoloration for chlorine dioxide, reactivity with fabrics for ozone, carcinogenicity and high danger when accidentally breathing in for formaldehyde, and methyl bromide being banned due to risk to ozone layer, to name a few. In the case of VHP decontamination, after finishing the VHP decontamination process any left-over hydrogen peroxide itself is either ventilated out of the room or catalysed into harmless water and oxygen, while the remaining small amount slowly decomposes into oxygen and water by itself in a few hours. For vaporised hydrogen peroxide the gaseous form is clearly more effective than the cheaper aerosol form [67]. Although there are

some explosiveness concerns and the doors, ventilation, *etc.* of the VHP decontaminated room have to be sealed off and there can be a significant turn-around time for the room due to safety reasons, this method is still considered one of the best that is currently available. In the second part of the current thesis, it is the vaporised hydrogen peroxide that is chosen as the best disinfection/decontamination agent. The disinfection/killing mechanism of pathogens for hydrogen peroxide vapour is somewhat different from its liquid form when dried samples are used [68] – it seems that the vaporised form of the hydrogen peroxide is much more potent. The decontamination mechanism by VHP on biological objects is not fully known [57] and therefore partly theorised/hypothesised in this work, but it is assumed to work on protein degradation into smaller peptides [57], unfolding and oxidizing key parts of bacterial or spore cell walls, making germination impossible and oxidising the genetic material itself and making copying of genetic material impossible. The fact that vaporised hydrogen peroxide has much more biocidal effectiveness compared to its liquid counterpart can be attributed to the fact that hydrogen molecules in the gaseous form have more kinetic energy and do not have any large solvation shell nor charges around them. This makes it very easy for small neutral H_2O_2 molecules to penetrate deep into proteins, lipids, genetic material, and other internal parts of a cell and oxidise important chemical links inside the deeper structures [68].

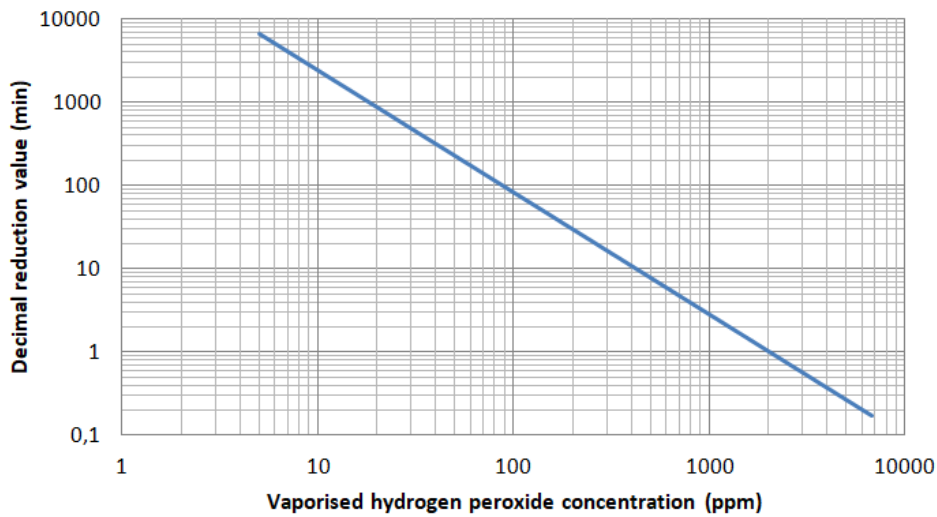

Figure 3.5.1. The time to reduce the concentration of viable *Bacillus subtilis* spores to 10% (decimal reduction value) plotted against VHP concentration, according to [69].

Typically, as illustrated in figure 3.5.1, it takes around 15 minutes to achieve a >6 log10 (i.e. 1 000 000 times less viable pathogens) reduction in pathogen concentration when using high concentrations like 400 ppm of VHP [69], but for dense biofilms of pathogens the decontamination might take somewhat longer [70]. The implemented timescales used for decontamination experiments in the current work are typically in the order of tens of minutes with VHP process.

It is noteworthy that in [53] it is mentioned that the autofluorescence of bio-object can act as a proxy that can indicate viability. A similar experiment with bleach has also been independently carried out in the first paper [**I**] by the author. It clearly indicates that the pathogen fluorescence decreases and even fades completely away during decontamination, inspiring the current PhD study. Clearly, a well-decontaminated surface should not have any pathogen-related fluorescence. To the best of the author's knowledge before the current PhD study this fluorescence fall-off (decrease) effect had never been used to monitor directly with vaporised hydrogen peroxide decontamination process and possibly even any other decontamination process.

4. DETECTION AND IDENTIFICATION OF BIOPATHOGENS

4.1. Description of developed pathogen detection techniques

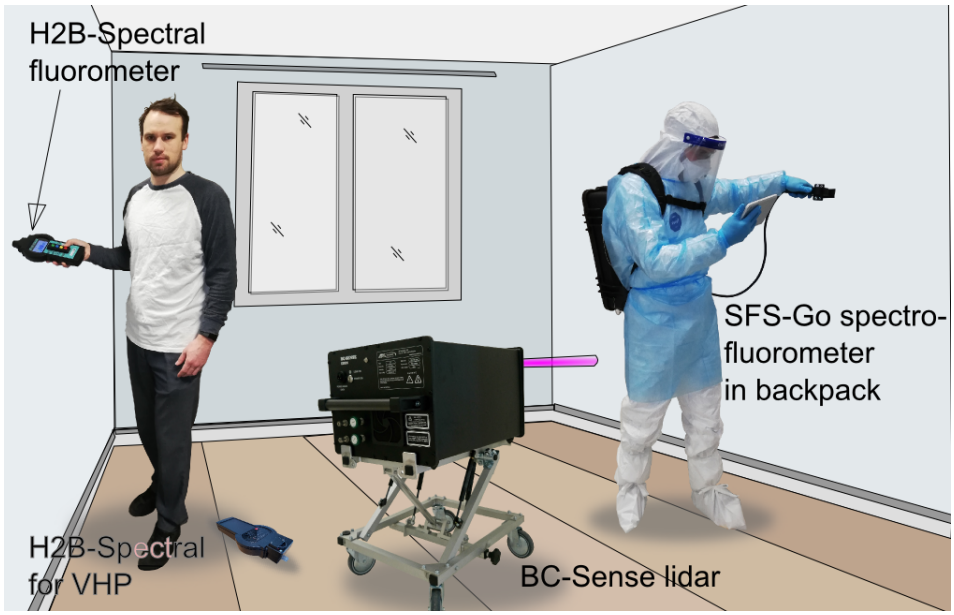

Figure 4.1.1. Size of the developed pathogen detection sensors mounted in a typical room and compared to the size of person operating the devices.

Several sensors developed in the context of the current thesis are illustrated in figure 4.1.1. The small hand-held H2B-Spectral fluorometer is on the left, the BC-Sense lidar is in the centre and the SFS-Go spectrofluorometer in backpack mode is on the right.

4.2. Remote detection of microorganisms with lidar

Many fluorescing objects – including micro-organisms and pathogens – can be detected from quite large distances by applying the hyperspectral laser-induced-fluorescence (LIF or HLIF) lidar technique [71]. Typically, the lidar-type sensors (the “lidar” acronym stands for “light detection and ranging”) are used for optical ranging of objects’ distances and locations, but lidars can also be constructed for the “detection” part of the acronym typically referred to as “stand-off detection”. In such case the lidar device is designed to measure some specific type of emitted radiation or the backscattered lidar light (radiation) – for example it is the fluorescence, the reflectance, even Raman scattering or

plasma spectra of some object that can be measured. So, the backscattered lidar radiation can be used to gather information not only about the distance of the object that was hit by the laser beam, but also about some physical properties of the sample. In this thesis a fluorescence-type lidar called BC-Sense has been designed which is used to determine from more than ten-meter distance whether or not the object's surface has microorganisms on it. The design, construction and experiments with the BC-Sense are integral parts of this thesis and therefore will be explained in more detail in the following sections. The main optical schematic can be seen in figure 4.2.1 and the device itself is in figure 4.2.2.

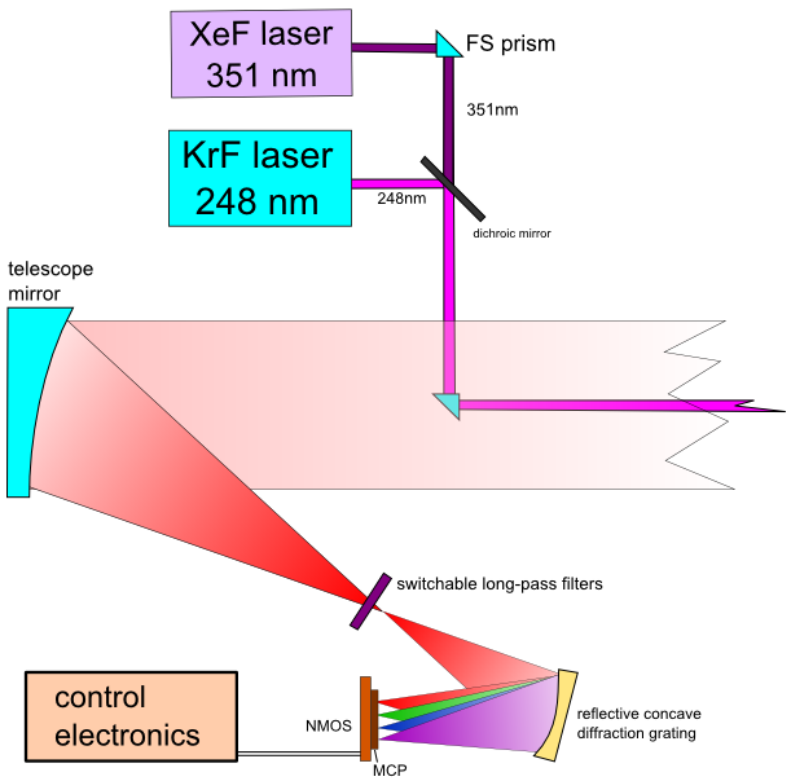

Figure 4.2.1. Functional diagram of the photonic design of BC-Sense lidar. The laser light used for excitation is depicted as a purple line and the fluorescence light coming back from the sample is depicted as a wide red beam. The abbreviation NMOS refers to the linear photodetector type and MCP refers to the micro-channel plate system with fast time response used for signal-amplification before read-out.

The HLIF lidar BC-Sense was developed to detect the induced autofluorescence spectra of pathogens from up to 10-meter distance. During room decontamination procedures, it is envisaged that this device could allow for quick scanning of difficult-to-access areas (*e.g.,* high up surfaces, barred by metal

fence, inaccessible for sampling, *etc.*) and just larger surface areas. The lidar has two different excimer lasers built-in for fluorescence excitation purposes. By using two excitation wavelengths instead of one, the analysis algorithms have qualitatively more information to identify pathogens, separate living micro-organisms from dead ones or separate pathogen fluorescence signal from background material's signal. The first laser was based on krypton fluoride (KrF) gas mixture and produced light pulses at the wavelength 248 nm. The second laser was operating on xenon fluoride (XeF) gas mixture and produced laser pulses at the wavelength 351 nm. Due to the lidar being able to generate short and quite powerful laser pulses – in the order of 2 mJ to 5 mJ with a duration of 10 ns providing up to 200–500 kW of instantaneous optical power – it could measure induced fluorescence signals in daylight conditions that neither xenon-lamp-based spectrofluorometer nor a LED-based fluorimeter is capable of. Moreover, due to excitation with a parallel laser beam the lidar can do such measurements from fairly long distances. By using laser repetition rates up to 20 Hz and quickly averaging the result from one measured sample point, the signal to noise ratio could be improved even further, extending the pathogen detection distance. To increase measurement speed while reducing the size of the lidar, the two excimer gas laser chambers shared a single high-voltage power supply system and a fast electromechanical switch turns them on one by one to excite fluorescence of the sample.

Figure 4.2.2. Photographs of the BS-Sense lidar on its trolley from the front and back side. In the left photograph the tube of the telescope can be seen as a circular hole top-left. Courtesy of LDI Innovation OÜ.

The emitted fluorescence induced by the excimer laser pulses is collected by a 10-cm-diameter off-axis parabolic mirror and directed into a spectrometer where the returning excitation laser beams reflections are already cut off by interchangeable longpass filters *i.e.,* having different filters to cut off 248 nm and 351 nm laser beam reflections. The received light signal is collected within ~200 nanoseconds during and after the laser pulse to enable the fluorescence signal to pass, while disabling the passage of irrelevant background light after this gated time window. The background light signal itself is measured before each laser excitation pulse and automatically subtracted from the main fluorescence signal. This useful many-colour signal is then spectrally dispersed by a concave diffraction grating onto an imaging plane. The time-gated and spectrally separated light is then amplified up to 10^6 times (the amplification parameter can be changed) by a microchannel plate (MCP), which converts arriving photons to electrons and provides their multiplication depending on applied voltage and finally re-converts electrons by a phosphor into photons, which are detected by a linear CCD or CMOS sensor. By exploiting all of this complexity, a series of pulses of fluorescence light from pathogens on various surfaces can be measured in less than one second – that is from pressing the "measure" button to receiving the spectra on the screen of the control computer.

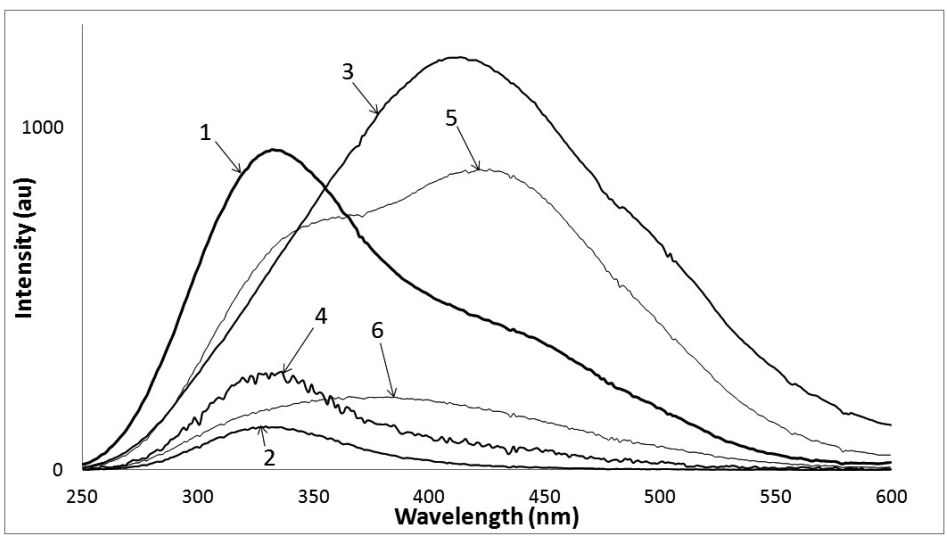

Figure 4.2.3. LIF spectra of biological contaminants at the sample surface, excited by 248 nm photons: 1 – *E. coli* (dead bacteria) 6×10^{10} CFU/ml, 2 – *E. coli* (living bacteria) 1×10^{7} CFU/ml, 3 – *Bacillus* spores 5 g/ml, 4 – *B. thuringiensis* 2×10^{8} CFU/ml (signal multiplied by 10 for visibility), 5 – MS2 Virus 1×10^{9} PFU/ml, 6 – *Cladosporium Herbarum* (unknown concentration).

To demonstrate the possibility of spectral distinguishing of different pathogens with a lidar sensor, a set of different pathogen-simulating micro-organisms was chosen to be measured with the BC-Sense lidar. This included an MS2 bacteriophage virus, a *Cladosporium herbarum* fungus, some bacterial species like *B. thuringiensis* and *E. coli*, the spores of *E. coli* as well as the dead and viable forms of *E. coli*. The details about the preparation of the samples are described in the paper [**I**]. Liquid solutions of these samples were placed onto the non-fluorescing copper background and measured using the lidar from a ~5-meter distance. The resulting emission spectra recorded at 248 nm excitation are shown in figure 4.2.3. Their spectral shapes differ visibly for different micro-organism classes. Although two selected bacterial species do have somewhat similar spectra to each other, slight differences still exist. Even the similar-looking dead and living *E. coli* are actually different enough to be separated by well-chosen analysis algorithms, as will be seen later in the thesis in case of BA and GS bacteria (see figures 5.6.1 and 5.6.3).

During decontamination procedures the identification of pathogens is most of the time not as important as the fast detection of any pathogen contamination on various background materials. The fact that benign micro-organisms can give a similar signal to pathogens is therefore less of a problem as the detected contamination hints at an unsuccessful decontamination procedure anyways. Therefore, as pointed out also in the introduction, the current thesis focuses more on the detection and monitoring than on pathogen identification.

The detection of pathogens on various background materials poses a large problem as the background materials may also fluoresce themselves and in many cases this fluorescence is in a similar spectral region to the pathogens (see figure 4.2.4). To test the capability of the BC-Sense lidar system to distinguish between clean and contaminated surfaces, a set of different real-world background materials were contaminated with bacterial and viral samples [**I**]. These are the same background materials that are used in working field hospitals that are flown around the world to humanitarian missions to combat various disease outbreaks, such as Ebola in 2014 in Western Africa. The tested substrate materials included tent material, PVC, aluminium, steel, PMMA, lab coat (see figure 4.2.4) and the simulated contaminants were *E. coli* bacteria and MS2 bacteriophage virus.

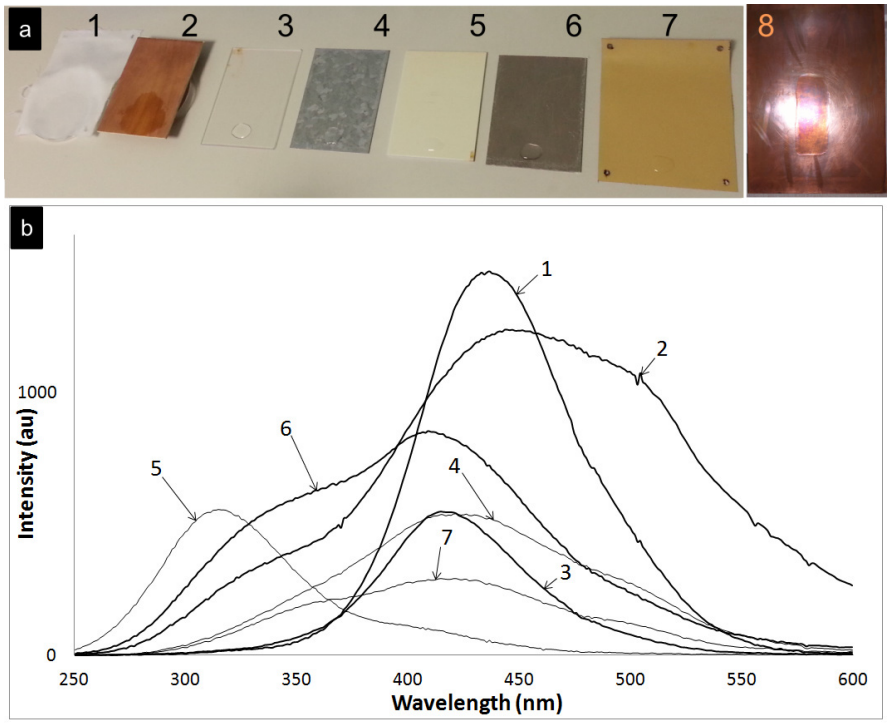

Figure 4.2.4. Tested background materials and their fluorescence spectra excited by 248 nm photons with the BC-Sense lidar.

The background materials were measured with the BC-Sense lidar hundreds of times with and without the simulated pathogen contamination on their surface. Also, all the used bacterial growth media, bleach, and solvents that were used to make the sample suspensions were measured in the same settings. The resulting spectra were then labelled to either contain a pathogen in them or not contain the pathogen. Then the bootstrap aggregation (bagging or "tree-bagging") machine learning method was applied to the spectra. This separates the data randomly into different sets for "training" and "evaluation" and implementation of multiple machine learning methods to choose spectral features that are used to grow "decision trees" – see figure 4.2.5 for illustration. The set of spectral features that makes the best prediction (least amount of spectra in the "evaluation" set fall out of the right prediction class) together with the best-predicting machine learning methods is chosen for the final pathogen-on-background classification (clean vs contaminated) system.

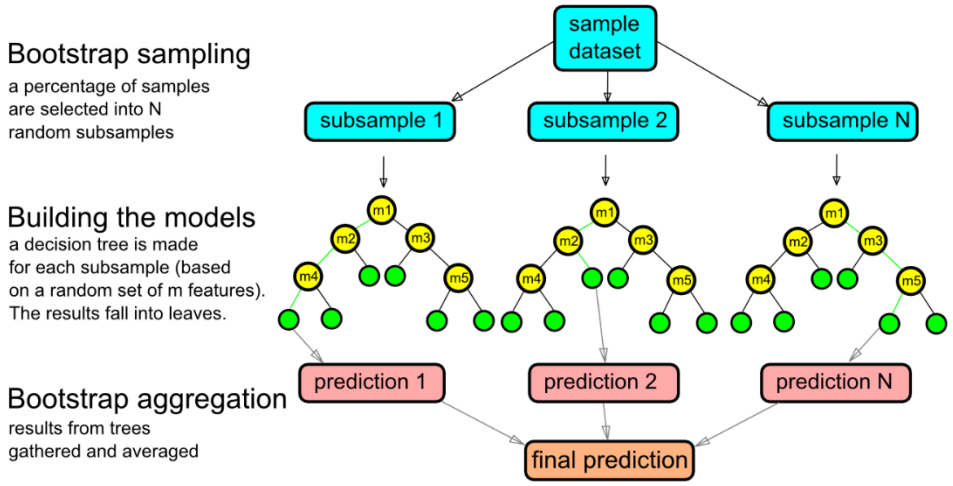

Figure 4.2.5. Simplified explanation of "tree-bagging" machine learning algorithm.

Most contaminant and background combinations showed good and well-defined classification results as shown in figure 4.2.6. The only problems were with the transparent and fluorescent PMMA, where the result was inconclusive and also *E. coli* on stainless steel substrate was constantly misclassified due to unknown reasons.

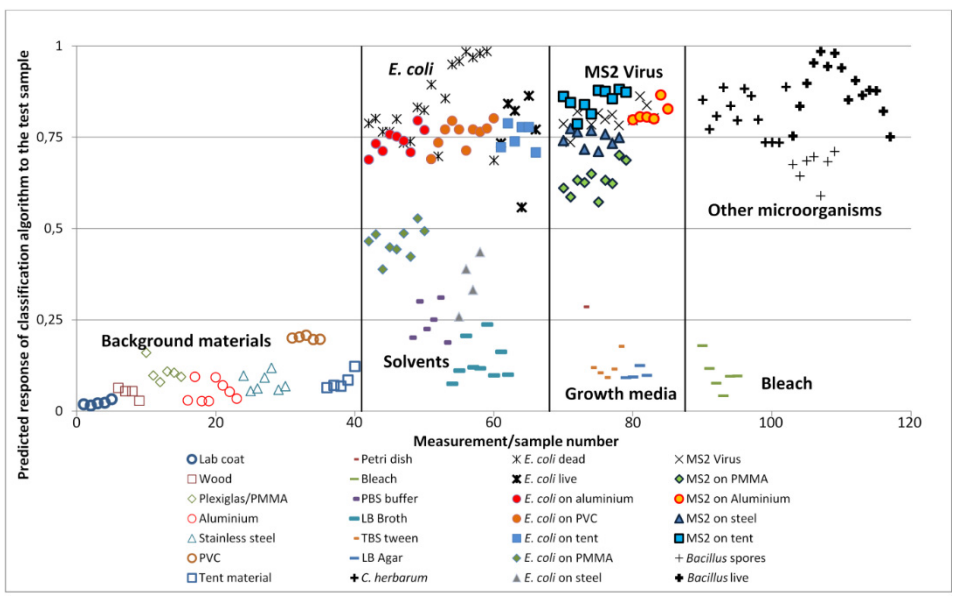

Figure 4.2.6. Classification result of >0.5 classifies the spectra to contain contamination, while the result <0.4 classifies it to be non-contaminated.

The detection of biocontamination with HLIF lidar proved to be highly capable for the specific stand-off applications in a built and open environment. At the same time, its size, complexity of the operation, requirement of a trained operator, and high cost are limiting factors to the wide use of this technique for regular monitoring of pathogenic micro-organisms on various surfaces. For many practical cases of random and selective point inspection, more portable and even hand-held devices are required. Therefore, these results were carried into the development of smaller and easier-to-use devices described in the next sections.

4.3. Spectral Fluorescence Signatures technique and SFS-spectrofluorometer

While it is typical for HLIF lidars to excite fluorescence at one single wavelength and record a comprehensive emission spectrum at every laser pulse, the lidar in the previous section is already more advanced and excites fluorescence at two different wavelengths, but this could theoretically be improved even further. Since the quantum efficiency of the sample fluorescence depends not only on the emission wavelength but also on the excitation wavelength, much more composition-related information could be collected from a sample if the emission spectra at a large number of excitation wavelengths could be measured. Creating such a multi-HLIF lidar using *e.g.,* an optical parametric oscillator laser system [72] was out of budget for the current PhD project, but reducing the measurement distance to a few millimetres and using a wide-spectrum xenon lamp – *i.e.,* designing a front-face fiber-optic spectrofluorometer – allows all of the relevant information still be gathered and consequently used to develop an even more compact multi-LED-based hand-held sensor which will be introduced in the next section.

A spectrofluorometer is a device that uses a tuneable-wavelength light source to excite fluorescence in a sample and records the fluorescence (or phosphorescence) spectrum at each of these excitation wavelengths, which results in measuring a spectral intensity matrix called Spectral Fluorescence Signature, abbreviated as SFS and often referred as a spectral fingerprint [73]. SFS is also sometimes called Excitation Emission Matrix Spectroscopy (EEMS), but compared to SFS the EEMS usually has not a cut off for Rayleigh (elastic reflection) spectral signal, irrelevant for many measurements, and often the excitation and emission axes are switched due to historical reasons and technique naming conventions.

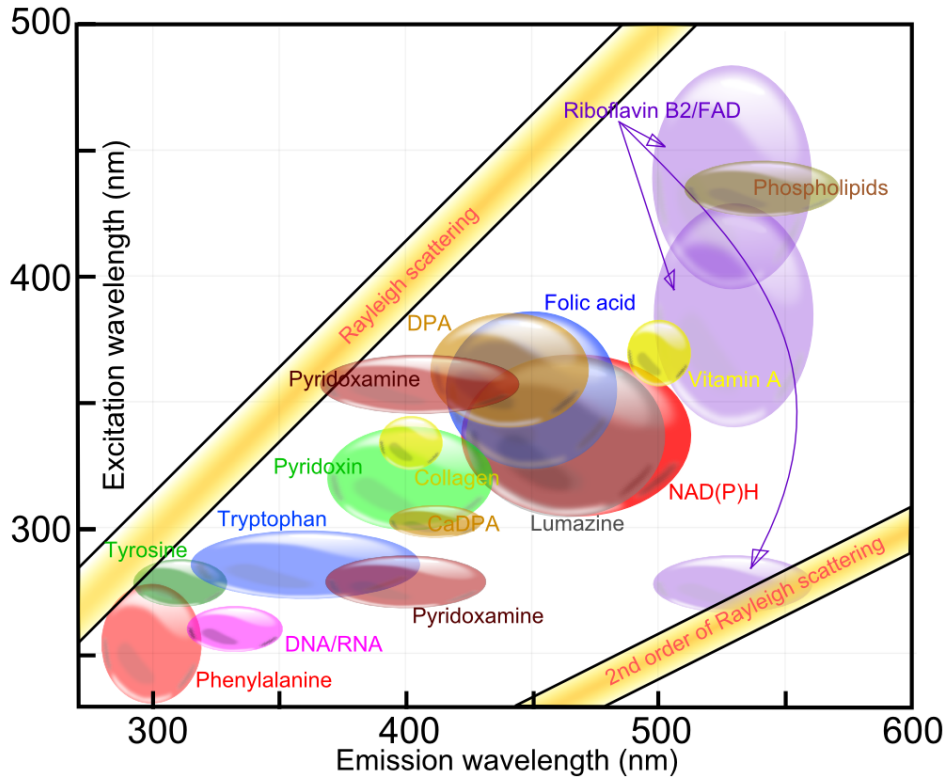

Figure 4.3.1. An approximate SFS spectral map of selected autofluorescent cell constituents according to [74] and [9] shows close-by spectral areas covered by different natural fluorophores. This illustrates how much more relevant information can be collected into a two-dimensional fluorescence matrix compared to the one-dimensional line-spectrum.

Figure 4.3.1 summarizes the spectral positions of typical fluorescence patterns of some of the more common fluorophores inside cells. As the relative fluorescence intensities of the fluorophores can differ by multiple orders of magnitude and the peaks can be slightly shifted, the deconvolution of SFS into constituent spectra can be extremely difficult. Therefore, most of the time, a number of real-world cell samples – technically containing many of these fluorophores in different amounts – are measured and a database (and sometimes machine learning algorithm) is built to detect the empirical differences between various cell types. So in order to find the most indicative characteristic spectral regions for the detection and identification of pathogenic microorganisms, the spectral patterns of the pathogens were investigated using the SFS-Go spectrofluorometer. The author contributed as a principal developer of this device by the R&D and engineering team of LDI Innovation OÜ. The device was developed as a small and light-weight instrument enabling extremely fast measurements of the SFS. The scan time is only 15 seconds for obtaining a full spectral finger-

print – SFS – in which excitation wavelength is scanned from 230 nm to 350 nm and a ~200 nm wide emission spectrum is collected for each of these excitation wavelengths with 5 nm step size and ~10 nm spectral resolution. In addition to scan speed increase compared to all previously designed spectrofluorometers, this SFS-Go spectrofluorometer was designed to be used with fibre-optic input/output cables and connectors. Such fibre-optics probe has the advantage of versatility since the flexible and long fibres can be used to direct the excitation light to almost any surface without collecting a sample – at least when used in the front-face fluorescence configuration, which can be seen in figure 4.3.2. Additionally, the fibre optical solution enables measuring samples with the typical cuvette configuration (the 90-degree fluorescence and 0-degree absorption measurement in liquids) just by using fibre-optic connectors installed in another measurement configuration. This means that the applicable measurement configuration is not fixed, but rather adaptable for measurement requirements.

Figure 4.3.2. SFS-Go spectrofluorometer with a front-face measurement handle. Left - the stand-alone device powered by battery on a table. Right – the device demonstrated in “back-pack mode” for decontamination teams. Courtesy of LDI Innovation OÜ.

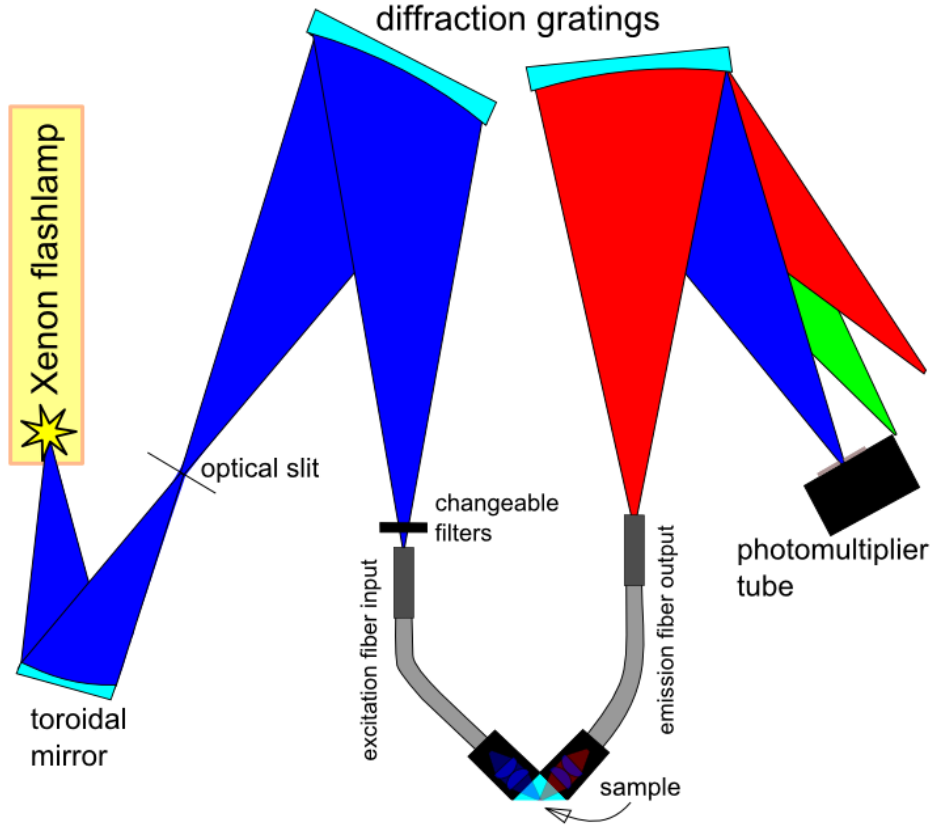

Figure 4.3.3. Illustration of the optical schematic developed for the SFS-Go spectrofluorometer.

The SFS-Go spectrofluorometer device uses a 20-watt continuous spectrum xenon flashlamp directed through a wavelength-selecting monochromator as the excitation source for fluorescence – see figure 4.3.3 for illustration. The monochromator is based on a concave reflective holographic grating, which is used to select the exact wavelength of the excitation light with ~10 nm bandwidth. The excitation light is then directed through an order-cutting filter into the optical fibre bundle that directs the monochromatic light onto the surface or object to be investigated. The surface area and the acceptance angle of the fibre bundle are chosen to match the arc size of the flashlamp and the numerical aperture of the concave grating respectively. The excitation light will then pass through output optical fibre with up to 1.5 meters length and then be focused onto the sample via two small relay lenses. If there is some amount of pathogen on the surface, then its fluorescence will be excited and a pathogen-specific fluorescence spectrum can be recorded. Another set of lenses relays the collected fluorescence light onto the tip of the emission (input) fibre bundle. This fibre directs the light into a second monochromator, which is used to analyse the

emission spectrum. This is performed by measuring the fluorescence emission light for all pre-selected wavelengths one by one in very quick succession by rotating the monochromator gratings with stepper motors. This “excite at one single wavelength and read emission signal at another longer wavelength” procedure is repeated at around 40 times every second, resulting in the acquisition of the full SFS spectrum in less than 15 seconds.

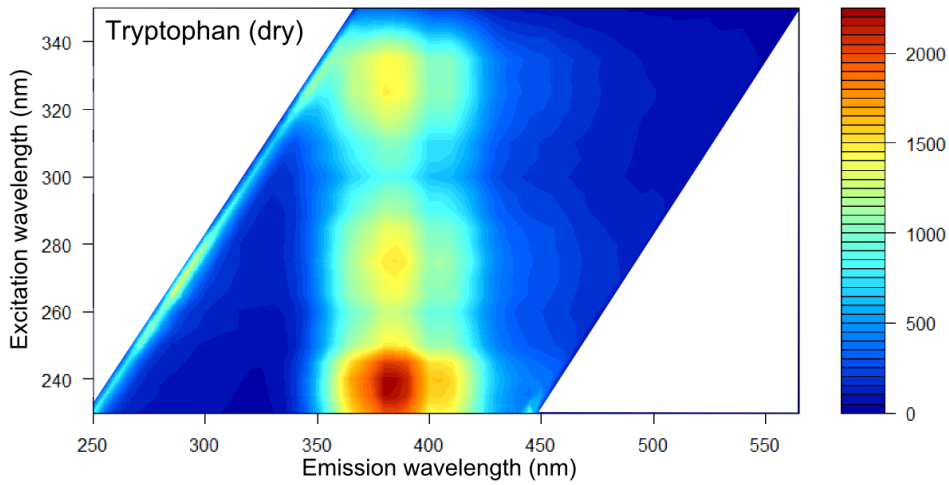

Figure 4.3.4. Example SFS spectrum of dried tryptophan (graphical image from R software).

In such spectra (see figure 4.3.4) the vertical axis stands for the excitation wavelength, the horizontal axis stands for emission wavelengths and the fluorescence intensity is colour-coded (from blue to red) so that blue regions depict low-intensity regions, green regions show the middle-intensity regions and red areas show the highest intensity regions in the spectral matrix (SFS).

In case the object to be detected is in a liquid, in water or water-like solution, the usage of fibre bundles reduces the signal intensity significantly compared to measuring liquid directly in a small transparent cuvette. The main reason for this signal reduction is simply the geometry since the circular fibres in a fibre bundle cannot physically cover all of the area of the multi-fibre bundle – even close-packed fibres will have inactive space between individual fibres, which will not transmit any useful fluorescence light. The second reason why fibres reduce signal significantly is due to the inherent absorption of light in the long fibres – this is especially noticeable at wavelengths below 250 nm even with the best fused silica fibres. Thirdly, when using the cuvette with optical fibres the optical coupling between the fibre and the cuvette is typically realized by using fused silica lenses, which naturally induce axial chromatic aberration in the system and focus different wavelengths at different points in space, thus reducing the average intensity at most wavelengths.

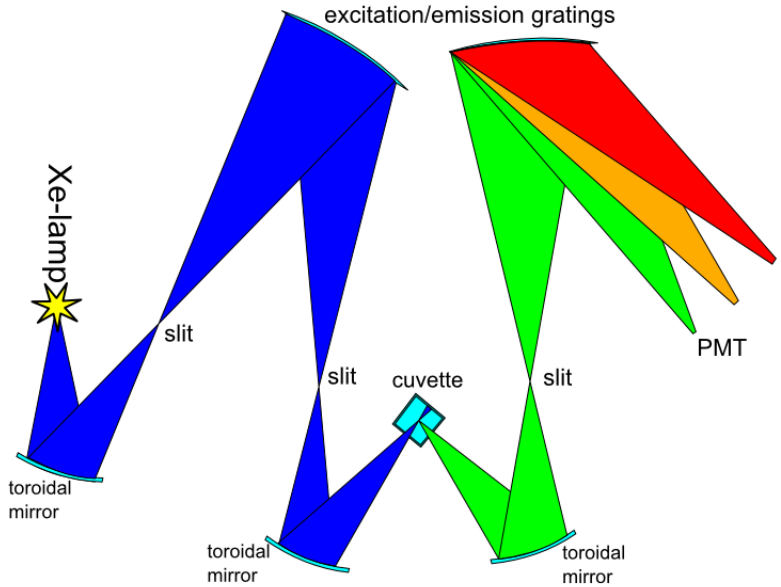

Figure 4.3.5. Illustration of a reflective-only optical schematic (SFS-Cube) developed during the PhD project.

To combat such fluorescence signal loss, a reflective-only spectrofluorometer called SFS-Cube was also developed – the optical schematic can be seen in figure 4.3.5. Such a device uses toroidal mirrors to focus off-axis light to a single spot in the centre of the cuvette and also collects the fluorescence light from the centre of the cuvette to the emission monochromator with a similar toroidal mirror. The emission (detection) monochromator dispersion is in the vertical optical plane to fit such a solution into a compact spectrofluorometer device.

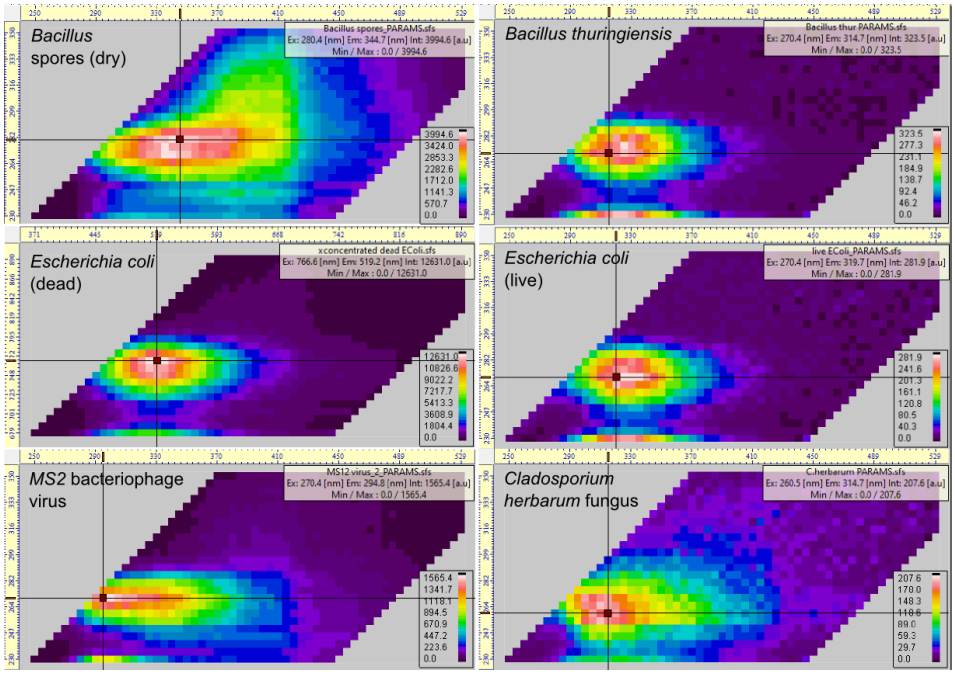

Figure 4.3.6. A selected set of SFS spectra of different biological pathogens demonstrates clear differences in their spectral shapes (graphical images from SFS-Probe software).

Multiplicities of SFS spectra of tens of micro-organisms were recorded to determine the most indicative characteristic spectral fluorescence regions for pathogens. Figure 4.3.6 illustrates the spectral differences of various micro-organisms. The differences enable the identification of pathogens that have been spectrally characterised with their spectral signatures stored in the reference SFS library.

The developed spectrofluorometers use a highly sensitive single-channel detector called a photomultiplier tube (PMT) for the detection of some extremely weak (low quantum yield) pathogen fluorescence signals. The PMT converts light into electrons, which are accelerated between metal dynodes and lead to even more electrons at each stage that will affect the detector output – in effect a PMT can amplify the signal up to tens of millions of times and enable sensitive spectral mapping of any micro-organism.

The experiments that were performed with the SFS-Go spectrofluorometer revealed decently low enough limits of detection (LoD – at the level of 10^5 CFU/ml, see figure 4.3.7,) and rather good identification capabilities. A neural-net-based identification algorithm was implemented in the SFS-Go software, but due to arbitrary selection of pathogens in the library, the small set of background materials, the limited set of growth stages and even the different growth media all influencing the analysis result, the real-world identification

procedure is actually much more complicated than envisioned initially and falls out of the scope of this work.

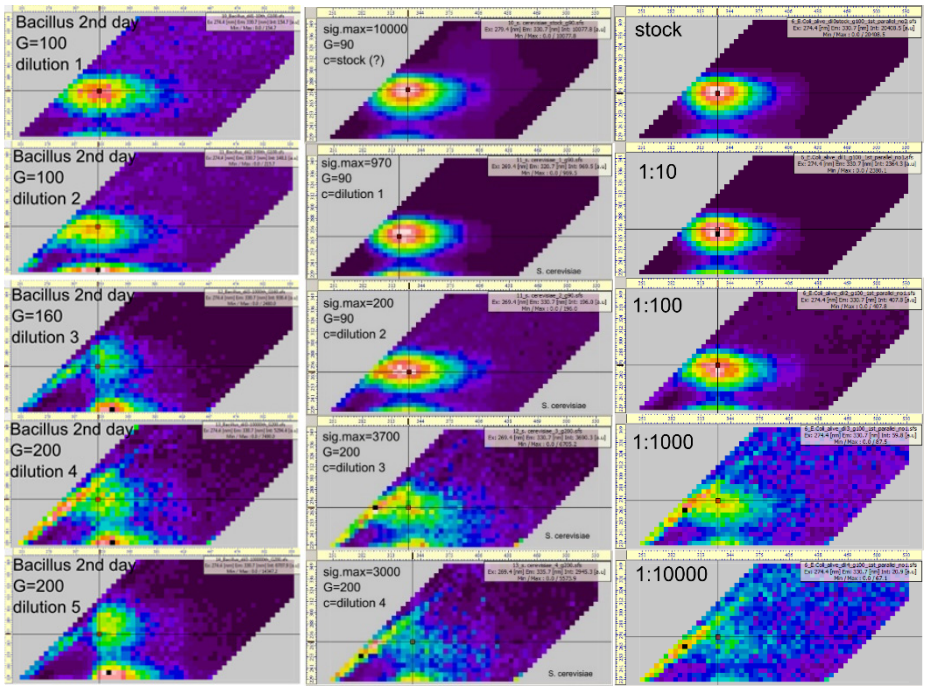

Figure 4.3.7. SFS spectra of the dilution series for liquid solutions of *B. thuringiensis* spores (left column – dilutions of 1/10, 1/100, 1/1000, 1/10000, 1/100000 of 1.7×10^8 CFU/ml stock solution shown from top to bottom), *S. cerevisiae* yeast (central column – dilution steps 1, 1/10, 1/100, 1/1000, 1/10000 of 2.3×10^8 CFU/ml) and *E. coli* (right column – dilution steps 1, 1/10, 1/100, 1/1000, 1/10000 of 3×10^9 CFU/ml), which were used to determine the limits of detection and quantification of the spectrofluorometer device. The lower detection limit was found to be around 10^5 CFU/ml for all of these micro-organisms, while the limit of quantification was found to be two times higher.

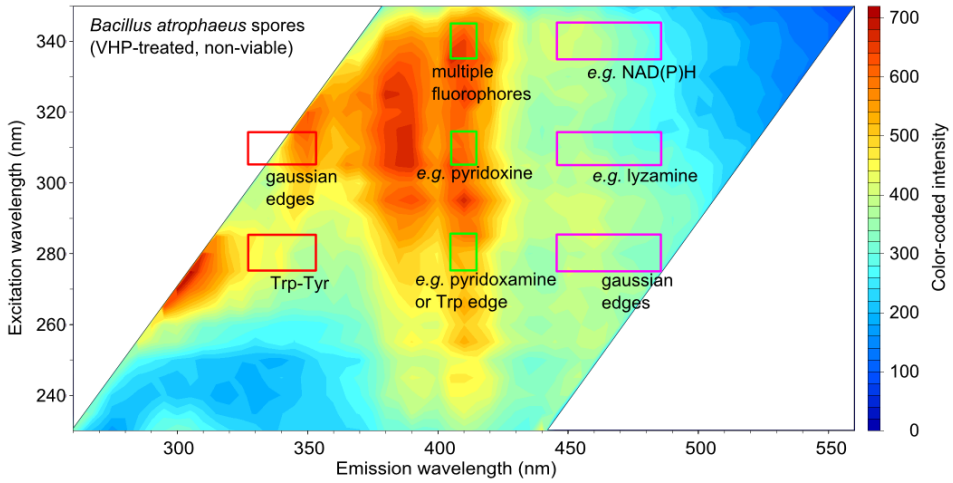

Figure 4.3.8. Wavelength ranges chosen by SFS spectroscopy for developing the H2B-Spectral handheld device. The spectral areas referred to as Gaussian edges are not selected for any particular fluorophore, but are present due to other choices and do contain some useful information about the sample.

Certain applications, like control of the decontamination settings, and especially the cleanliness after decontamination (commonly referred to as "how clean is clean") require more focus on low LOD than on the identification. This requirement was further realised in the development of a simplified version of SFS technique in a form of a small handheld multi-spectral device, which was one of the goals of this PhD work. The three different excitation wavelengths provided by widely available UV LEDs and 3 emission filters, which enable to study 8 spectral regions (9^{th} one contains reflection and is not used) of each standard SFS as shown in figure 4.3.8 were selected for such development. The development was carried out by applying modern UV LED and silicon photomultiplier (SiPM) technology described in the next sections.

4.4. Pathogen detection with LED-based fluorometer H2B

Ultraviolet LEDs with reasonably good radiant efficiency and reasonable price have not been available for too long time in the component market of radiation sources. After the groundbreaking AlGaN research and development phase in the 1990s such LEDs have been in the market only since about 2000s and early 2010s [75]. Compared to other manmade light sources of ultraviolet radiation like Xenon lamps, deuterium lamps, cathode ray tubes and especially UV lasers, these light sources are orders of magnitude smaller and therefore efficiently applicable in the design of conveniently handheld photonic sensors.

The second recent technological advancement that is enabling the development of highly capable handheld photonic devices is the appearance of the so-

called silicon photomultiplier (SiPM) photon detection systems [76]. These detectors are basically matrices of avalanche photodiodes that are coupled with ultrafast counting electronics, in effect acting as photon counters. In a silicon photomultiplier a photon creates a quick avalanche of current in a very controlled (non-damaging) manner in a thin Si layer. The short duration and relatively constant height of avalanche signals are the reasons that allow counting of single photons with fast detection electronics. SiPM-s allow signal amplification of 10^6 times – almost as much as PMT-s. While not matching the exponential signal amplification of PMT-s depending on the gain voltage nor the dynamic range, the SiPM-s operate on much lower voltage and have much smaller dimensions, enabling compact, light-weight and robust mechanical design which is essential for the development of hand-held devices. Furthermore, the smaller dynamic range can be compensated by tuning the intensity of the excitation LED.

Figure 4.4.1. Left – the single-channel H2B device in hand. Right – the H2B usage shown during a technology demonstration show. Courtesy of LDI Innovation OÜ.

Based upon the measurement principles and spectral characteristics of pathogens, which were studied with the UV spectrofluorometer as well the lidar, a number of much smaller and cheaper fluorimetric sensors were developed. The first iteration of this sensor can be seen figure 4.4.1 and is called H2B. This "gun-like" mechanical design has to be placed against the measured surface, then the measurement is triggered by the gun-like trigger and the resulting number can be read on the LCD screen in the back of the sensor. The device can operate on the mounted battery power for half a workday and can transmit recorded data directly to a control computer via WiFi. The excitation light sources for the H2B sensor is a single ultraviolet LED emitting 280 nm wavelength photons with microwatt-level radiant power. The ultraviolet excitation

light is directed through an OD6 high-quality bandpass filter onto the surface to be monitored. The filter is necessary to be used with a LED light source to cut off the long-wavelength spectral shoulder (which is only visible in a logarithmic scale) that can otherwise be reflected from the studied sample surface, spoiling the quality of the spectral fluorescence signal to be detected. In case the sample emits fluorescence, this useful emission is collected by a set of focussing lenses and another OD6 bandpass filter at the tryptophan-related 320 to 360 nm spectral region.

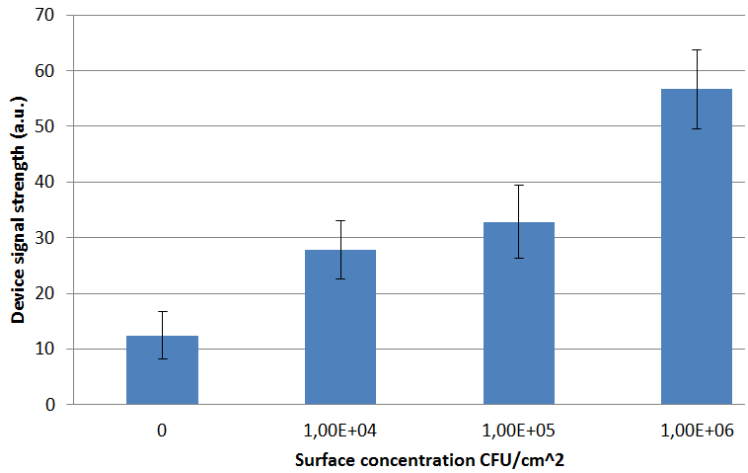

Figure 4.4.2. The H2B detection limit estimation reveals that 3×10^3 CFU/cm^2 of BA bacterial spores could be detectable on low-fluorescing surfaces such as aluminium used in this experiment based on the signal and its standard deviation at 10^4 CFU/cm^2.

The optical detection is realized via a SiPM detector, which is capable of a million-fold amplification of the signal. As this device measures just a few square millimetres from a distance of about 1 centimetre (inside the background-light-exclusion-tube) and has such a high signal amplification, the device was found to be extremely sensitive and work well on certain surface materials. Typically, such a high amplification can cause problems when either operating at high background light levels due to scattering or reflection is present. A set of well-chosen bandpass filters, blackening the internal surfaces of optical path and mechanically light-tight body of the device eliminate these issues and surfaces concentrations as low as 3×10^3 CFU/cm^2 (see figure 4.4.2) have been shown to be detectable on various less-fluorescing surfaces. Obviously, most surfaces do emit some fluorescence and there is always a need to record signal from a clean surface first, otherwise a single-channel approach can contain too little information to determine the need for further decontamination.

4.5. H2B-Spectral design and application

In certain situations, where measurements are being done on monotonous low-fluorescing surface materials the single-channel H2B works fine to detect microbiological contamination on surfaces. But this single-channel approach is found to be too restrictive for the many practical application situations. Most of the time the real world is much more complicated as a variety of surface materials are used even in the simplest settings. Detecting somewhat differently fluorescing pathogens at random surface concentrations makes the task even more difficult. To combat the shortcomings of the single-channel H2B, while still maintaining a user-friendly size, the concept of H2B-Spectral was developed.

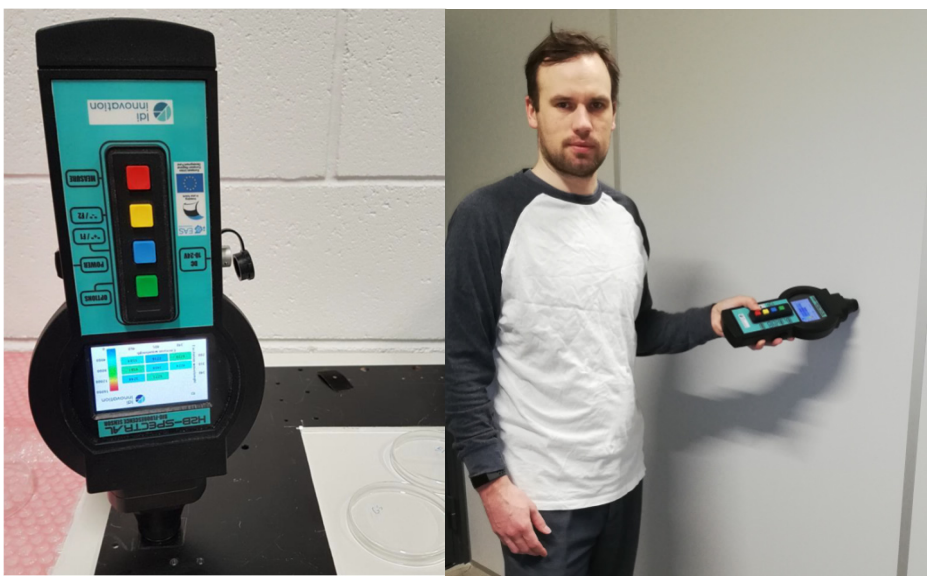

Figure 4.5.1. Left – H2B-Spectral recording GS spores signal on black anodized aluminium surface. Right – the sensor size compared to a person. Courtesy of LDI Innovation OÜ.

The H2B-Spectral illustrated in figure 4.5.1 uses 3 different LED-s to excite the fluorescence and on the emission side the device switches between 3 bandpass filters during any measurement – see figure 4.3.8 for the selection of the spectral areas measured and figure 4.5.2 for the simplified optical schematic. This enables to get more specific spectral information and enable better distinction between the spectra, which are caused on the one side from the background surface material and on the other side from the fluorescence of potential microorganisms on the surface.

The technical design choices for the H2B Spectral were governed in part by end-user needs (described in paragraph 3.3) and convenience factors, while

focussing on the ability to detect low levels of microbiological pathogens on surfaces. The device is designed to be light-weight enough (~1 kg) to be easily hand-held during the check-up of surface contamination associated with decontamination procedures. At the same time the device is large enough (~ 30 cm × 15 cm × 7 cm) to be used with thick gloves through the hazmat suit that is sometimes required for decontamination efforts that are more dangerous. The H2B-Spectral device has the capability to operate fully wirelessly by having data transfer over WiFi and rechargeable Li-ion batteries for 10+ hours of continuous operation. In some cases, wireless option is not good (*e.g.*, military operations) and only wired operation is preferred. Therefore, the device also has the capability to transfer data over RS485 wired protocol and operates (and charges its battery) from 24V DC power input. For measurement in the typical H2B-Spectral configuration the device is simply directed against any surface to be measured and the device will spend one to two seconds per ~10-mm-diameter surface point measuring it at multiple wavelengths and help estimate pathogen amount on the surface – if any.

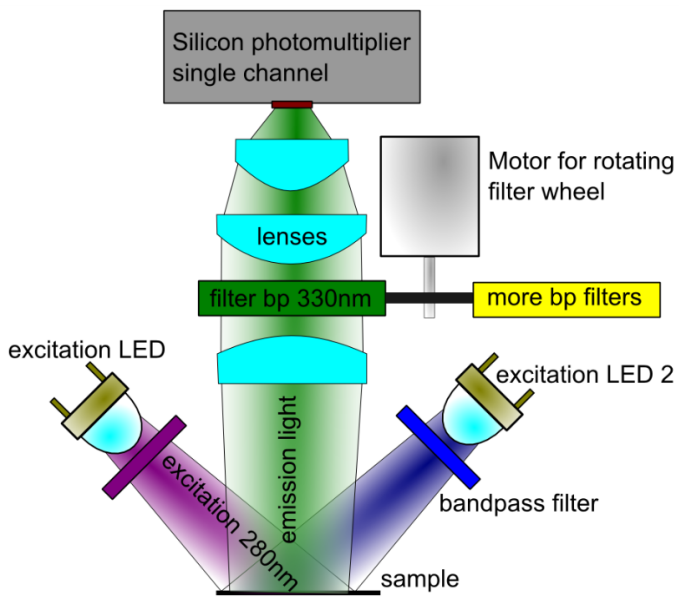

Figure 4.5.2. Simplified optical design schematic of the H2B-Spectral device.

The wavelengths used in the H2B-Spectral were chosen by examining spectral fluorescence fingerprints of multiple pathogenic microorganisms. The main signal typically arises from 280-nm-excited and 340-nm-emitting (later noted as 280/340 nm) tryptophan-related peak, which is complemented by the pyridoxine peak 300/400 nm and NADH peak at 340/460 nm. As already introduced in previous sections, the ultraviolet excitation light is created by

microwatt-level LED-s and spectrally selected with relevant spectral bandpass filters, which have optical densities over 4 in the spectral region where the long-wavelength-shoulder of UV LED-s could otherwise contribute to reflection signal from the sample that could spoil fluorescence signal. For the same reason the emission channels have high quality OD6 fluorescence filters that reject all of the LED excitation light. Such configuration enables high signal to noise ratios for fluorescence signal at the selected wavelength pairs. The sensor also enables software-configurable LED-intensity increase in case extremely low signals are monitored. Furthermore, tuning the power of the excitation LED enables reaching a much larger effective dynamic range and getting more relevant information about the sample.

After the excitation light is exposed onto the sample surface, and its interaction with substances on surfaces generates fluorescence light. The fluorescence light is collected by using a 3-lens configuration (see figure 4.5.2) and transmitted through a servo-motor-selectable emission filter onto highly sensitive silicon photomultiplier (SiPM, Hamamatsu 3×3 mm) that amplifies the signal and enables single-photon-level detection in the sample as described in the introduction to this section. The measured sample area is around 10 mm in diameter and it lies at 50 mm distance from the light collection optics (distance is held by a black bellows). Since the high-intensity background light can easily saturate the SiPM detector, the device has a black tube, which blocks the disturbing background light as well as possible from around the area investigated. As is typical with such devices, the signals are then recorded with and without the LED excitation on at all relevant wavelength pairs. The obtained background light level is subtracted from accumulated signal, improving signal to noise ratio. Single measurement at all relevant wavelength pairs typically takes around one to two seconds and thereafter results are displayed in the screen of the sensor and/or a connected control computer. Using machine learning and calibration of data on these graphs help to interpret the presence of pathogens in front of the sensor.

Whereas the SFS-Go has the advantage of covering hundreds of spectral channels, the H2B Spectral surely has the advantage of sharper spectral cut-offs. It means the better rejection of reflected/scattered light (better signal to noise ratio at selected wavelength pairs) and crucially a low enough UV excitation flux, which is sufficient for fluorescence measurement, but still below the limit needed to kill the microscopic pathogens simultaneously. One should avoid altering the sample under study, which will be important for the monitoring of VHP procedure introduced and discussed in next paragraphs. The H2B-Spectral generates low enough UV radiation flux, saving the battery, to enable measuring the fluorescence of bacterial spores for more than 10 hours period without the fluorescence signal falling any more than around 1 per cent.

As could be expected from a few-channel fluorescence device that measures only the natural autofluorescence emitted from various surfaces, this device cannot distinguish between the extreme multitude of microorganisms present in the world. At best, it can tell the operator either that the surface is clean from

microorganisms or – based on the measured signals – there is suspicion of dangerous amount of pathogenic microorganisms. Therefore, the device acts as an indicator to improve the decontamination efforts at the location being investigated. In some sense this approach is safer and certainly it is cheaper than trying to identify the full known set of pathogenic microorganisms in any sample surface. Studying the full set means sampling, by pre-growing on Petri dish and identifying (*e.g.,* PCR) of a fair amount of different microorganisms, and this effort is too costly in almost any other situation than whenever some new and dangerous pathogen is feared to have been found its way to humans. And as an opposite example, in case the pathogen to be identified is already known – like SARS-CoV2 – then the most efficient approach is to chemically engineer a receptor that only binds to the pathogen of interest (*e.g.*, the spike protein that connects to the ACE2 protein in human cells). If such receptor could be bound to a near-by fluorescent label, the fluorescence energy transfer would be modified in case the virus is connected to the receptor, allowing highly selective detection of the quantity of the selected pathogen present. The main advantage such highly specific detection is also its main draw-back – by detecting just one type of pathogen the device would be actively ignoring all other kinds of pathogens and therefore in a general decontamination setting it would not increase safety as much as indiscriminately pointing out every kind of pathogen. The H2B-Spectral does neither immediately point to a single pathogen like the immuno-sensors do nor needs hours of operation including intense computing to determine the DNA-sequences present. It is just a perfect cheap and small tool, which extremely quickly points out that the surface seems to be containing pathogen-like fluorescence and should be cleaned or re-cleaned from this dangerous substance. Figure 4.5.3 illustrates the ability of such a quick tool to still separate different pathogens on different background materials.

The limit of detection for pathogens (GS spores) of the H2B Spectral is found to be in similar range where the viral/bacterial load starts to become dangerous to humans touching the surface, *i.e.,* ~10^3 CFU/cm^2. Typically, it is considered that pathogen concentrations below such values do not have much probability to infect people or [77, 78]. The detection limit for the H2B-Spectral device can further be improved by increasing the excitation LED intensity, applying the whole dynamic excitation range of the LED and increasing the signal collection time.

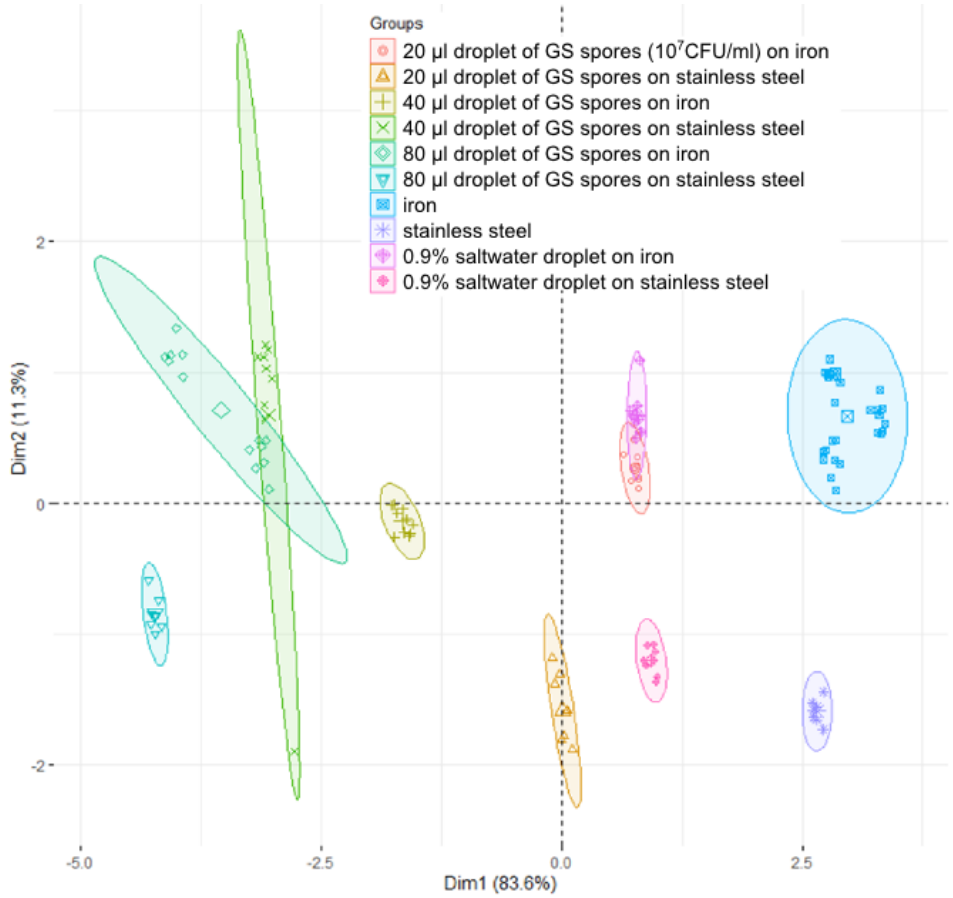

Figure 4.5.3. Principal component analysis (1st and 2nd component) of H2B-Spectral measurement results of GS spores on iron/steel background shows some separation between similar objects.

5. MONITORING OF VAPORISED HYDROGEN PEROXIDE DECONTAMINATION PROCESS USING A MODIFIED H2B-SPECTRAL SENSOR

5.1. Fluorescence as a marker for pathogen viability

When concluding the pathogen measurements described in paper [**I**] the lidar was left measuring during the decontamination with bleach – *i.e.*, sodium hypochlorite – when the bleach was poured onto the samples, the fluorescence was continuously measured. An immediate fall-off of the fluorescence signal was observed, which was slower for the more decontamination-resistant pathogens like spores and faster for living viruses – see figure 5.1.1.

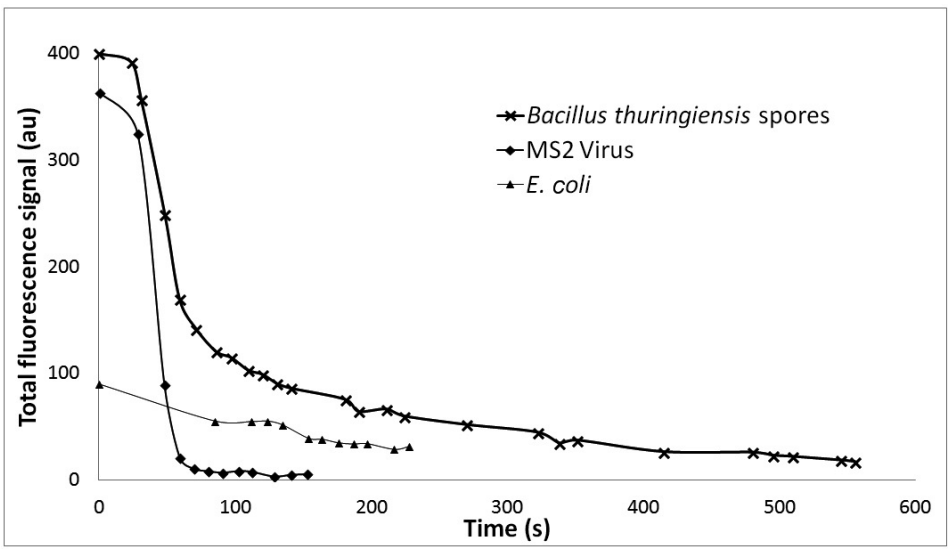

Figure 5.1.1. Lidar 248 nm excited fluorescence signal intensity fall-off when pouring bleach onto the samples. For E. coli the long tail of the fall-off is only visible.

A similar effect was observed with the spectrofluorometer device when measuring the full SFS spectra of a small concentration of bleach acting on liquid solution of *Bacillus atrophaeus* bacteria – as can be seen in figure 5.1.2. The main tryptophan-like peak intensity falls very clearly even with no mixing and just a small concentration of bleach added. Common knowledge tells that the bacteria are killed with bleach, so there surely is a correlation between the fluorescence intensity fall-off and death of the micro-organisms. As the bleach oxidizes many of the building blocks of life like amino acids, cell wall lipids and genomic material, this result is to be expected.

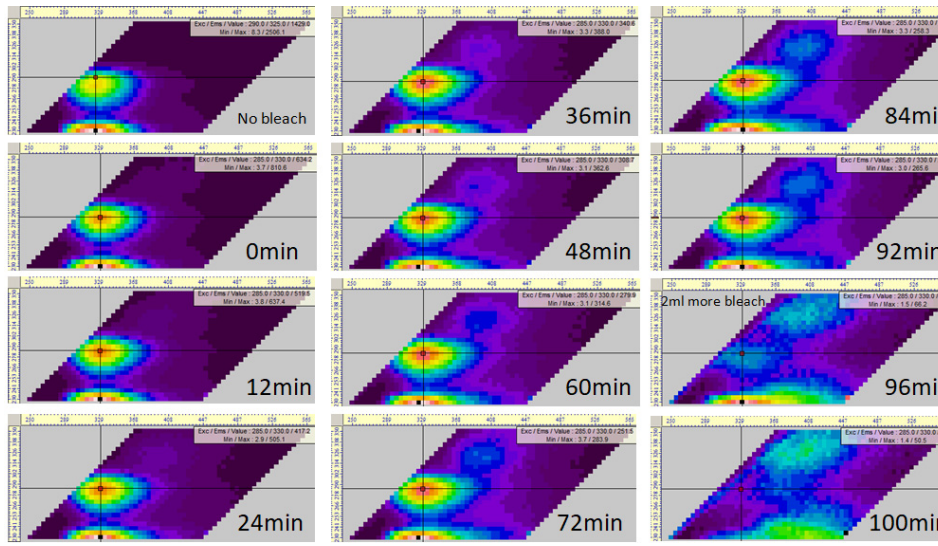

Figure 5.1.2. A series of SFS spectra of 1 ml 10^8 CFU/ml *Bacillus atrophaeus* liquid sample with added 1 ml of 1% bleach solution.

In [53], the authors even found a connection between the probabilities of germination for bacterial spores and their fluorescence. More intensively fluorescent spores were found to be more likely viable compared to the less fluorescing spores.

As the effect was so obvious, there also appeared a need to monitor vaporised hydrogen peroxide decontamination in real time and there was very little research performed in this field, a similar effect was chosen to be experimentally studied throughout the course of the PhD work [**II**, **III**]. The following sections briefly describe some key findings from papers [**II**] and [**III**].

5.2. Modified H2B-Spectral for VHP process monitoring

As already described in the introductory paragraphs, hydrogen peroxide vapour decontamination is a highly effective method for killing any biological microorganisms that come in contact with the air atmosphere in the room and are influenced by the small amount of gaseous H_2O_2 present. This decontamination method is chosen due to its efficiency, but also because it can be automated for room disinfection [4]. It is more effective than using hydrogen peroxide aerosol [67] and it leaves no bad smell into the room after its proper use. Consequently, among the vapour-based decontamination methods, VHP is unsurprisingly number one among of the more popular ones to be used in various studies [79]. After the decontamination procedure the hydrogen peroxide is simply catalysed into regular water and oxygen, with the residual

small concentration either being ventilated out of the room or quickly reacting to the organic matter (dust) always present in the room.

Figure 5.2.1. Modified H2B-Spectral device for the VHP monitoring configuration viewed from the front side. A fresh bioindicator sample on stainless steel is installed into the sample slit (on the right side in the photo) for each VHP decontamination effort. Courtesy of LDI Innovation OÜ.

The H2B-Spectral was modified to operate specifically in the VHP decontamination monitoring configuration – see figure 5.2.1. In this configuration, the modified H2B-Spectral device contains the "biological indicator" (industry standard uses spores of *Bacillus atrophaeus* and *Geobacillus stearothermophilus*) strip on stainless steel substrate. The plate is fixed in place in front of the sensor's light beam and room air is directed over the sample using a small fan. In this way the VHP concentration in front of the biological indicator is assumed to be exactly the same as in the air of the room that is being decontaminated with VHP. Most of other technical specifications of the modified H2B-Spectral remained the same as the H2B-Spectral in its original configuration. In addition to the stainless steel strip implemented, the device operates at lower exciting LED-powers to reduce UV-killing effect and uses just 3 wavelength pairs instead of 8 (exc/em pair of 310/405 nm is skipped).

5.3. Choice of biological indicators

The bacterial spores are biological objects that are typically installed to the room where VHP decontamination is carried out. Their representatives are *Geobacillus stearothermophilus* (GS), particularly resistant to hydrogen peroxide gas, and the spores of *Bacillus atrophaeus* (BA), which are biologically similar enough to simulate behaviour of the highly dangerous anthrax spore contamination. Anthrax attacks have been a real danger in recent decades [80, 81], so even though anthrax itself might be even more resilient and surely a lot more tenacious than these simulants [58], but the selected spores are similar enough and typically the last type of biological objects to survive a disinfection procedure. It is therefore assumed that if these biological indicators are dead then every other type of pathogen is deceased as well.

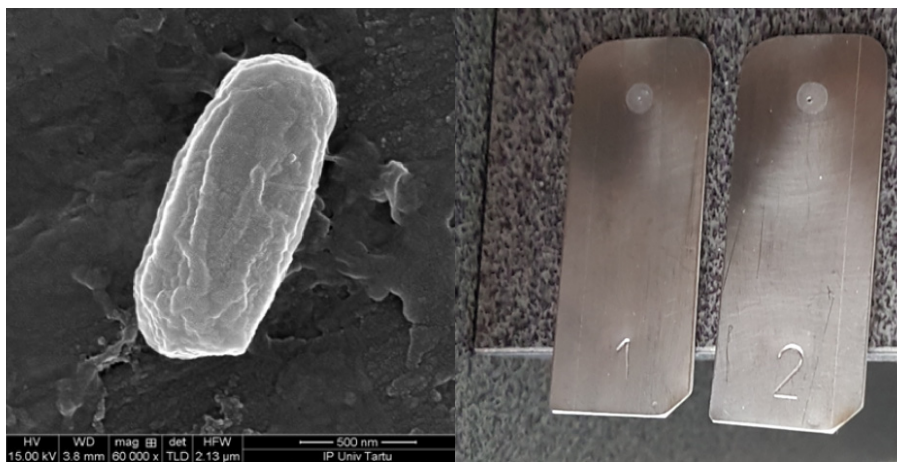

Figure 5.3.1. Left – SEM image of single BA spore. Right – stainless steel plates with BA spores sample at the top.

Spores have a typical size of ~0.5 µm in diameter and ~1 µm in length (see figure 5.3.1 left side). Such bacterial spores have evolved to withstand high and low temperatures, many corrosive chemicals, very dry and even vacuum conditions, *etc.* The spores have multiple cell wall layers to prevent their germination mechanisms to be injured by chemicals exposed outside and they cushion their genetic material in loads of dipicolinic acid (DPA) [82]. Spores that are decades or even centuries old can often still germinate if the proper environmental conditions occur. The chosen spores germinate easily in liquid or agar-based nutrient broth at the typical 37-degree settings and therefore, allow classical viability test to be carried out after the decontamination procedure has been finished.

The BA and GS spores were obtained from VTT through Cleamix Oy as liquid solutions of 10^7 or 10^8 CFU/ml concentrations. Approximately 10 micro-

litre droplets of these solutions were pipetted onto stainless steel substrates and then placed into the modified H2B-Spectral sensor, resulting in a surface concentration around 10^6 CFU/cm^2.

5.4. Experimental design of VHP monitoring setup

Surprisingly, the influence that vaporised hydrogen peroxide (VHP) has on the autofluorescence of bacterial spores is found to be unexpectedly strong and immediate. As soon as introduced hydrogen peroxide vapour gets into contact with the microorganism, the main fluorescence peak near 320 nm is found to decrease in intensity and its spectral position shifts slightly towards shorter wavelengths. Figure 5.4.1 shows the intensity fall-off as a function of the time, being reproduced in 10 independent experiments. The VHP concentration applied was 600 ppm at room temperature and non-condensing conditions.

To establish the reproducibility of the fluorescence fall-off effect, experiments were conducted to determine the spectral changes during the VHP decontamination effort of *Bacillus atrophaeus* and *Geobacillus stearothermophilus* spores [**II**]. A one cubic metre stainless steel box shown in figure 5.4.2 was sealed off. The modified H2B-Spectral device with a freshly made spore sample was installed inside the cube together with a VHP-generation device VCS-100 manufactured by Cleamix Oy. The latter device was used to generate hydrogen peroxide vapour with the foreseen concentration and duration.

As can be seen in figure 5.4.1, the relative fluorescence (compared to the initial fluorescence level) signal fall-off was found to be highly reproducible when using similarly prepared pathogen simulant samples as well as the same VHP concentration in every experiment. Interestingly, after the VHP exposure ended and the residual VHP was removed from the enclosure and its concentration was reaching zero value, the fluorescence signal did not stay as low as during the VHP exposure. Its intensity increased again and it reached somewhat similar (although mostly lower) values than its initial level at the start of VHP exposure. The recorded fluorescence signals demonstrated a slight spectral shifted before and after VHP exposure. The permanent change in autofluorescence signal intensity was too small and slow response in its accumulation to be really useful in determination of the viability of the microbiological sample. At the same time the fast-changing/dynamic fall-off of the fluorescence signal as a function of decontamination duration gives enough and reliable information to determine the approximate logarithmic death ratio of the pathogens.

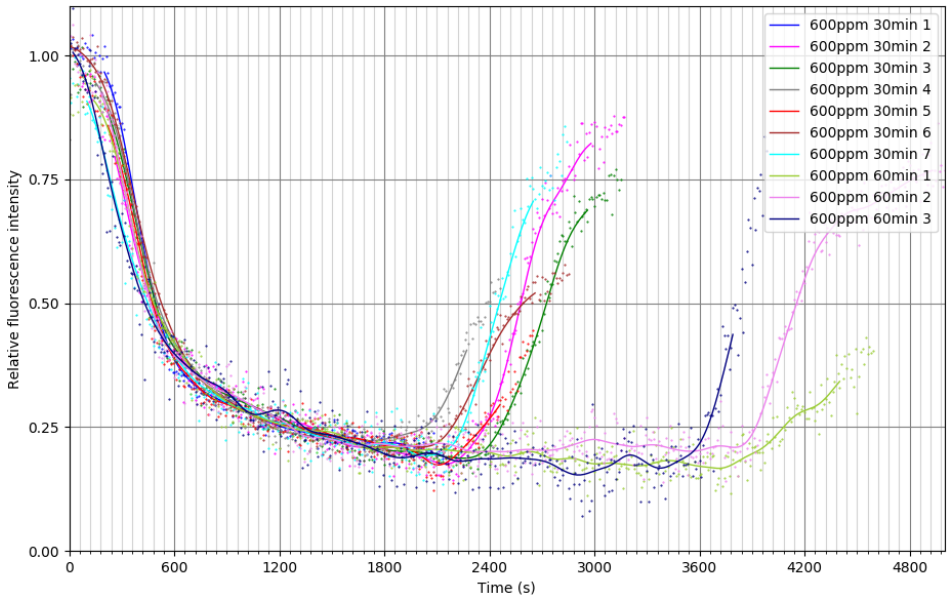

Figure 5.4.1. The fluorescence signal (at 280 nm excitation and 320–360 nm emission) intensity fall-off was found to be very reproducible under similar experimental conditions. Here are results of 10 independent measurements plotted against time from the start of VHP exposure. The end times of the experiments are dissimilar.

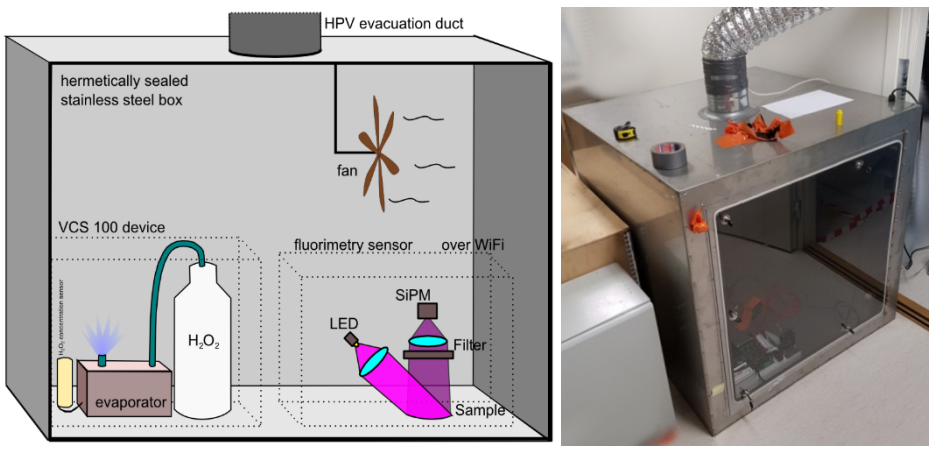

Figure 5.4.2. Left – schematic of the small 1 m^3 experimental volume including devices used. Right – photograph of the 1 m^3 experimental volume.

The slow fall-off of the permanent change in fluorescence can is observed to be in the timeframe of hours (figure 4 in [**II**]), possibly indicating that the oxidation of the fluorescing subcomponents is occurring at a much slower rate than the log6 (1 in a million spores may survive) death process takes place, which

happens in the time-frame of minutes. In the time-frame of minutes the really small and uncharged single hydrogen peroxide molecules penetrate or diffuse easily through any cell walls and inside of key proteins, they will come in close proximity to the fluorescing molecules and quench the fluorescence (*i.e.*, create a nonradiative pathway for the excited molecules to get back to ground state). Most of the quick signal fall-off is probably just based on quenching emission of the 3 fluorescent amino acids. At the same time, this indicates that H_2O_2 molecules get deep into the proteins and break hydrogen (and maybe sulphide) bonds, causing unfolding of the structure and therefore breaking the protein's structure and function. The longer-term oxidative effect on genetic information and important molecules is also present, but is no immediate cause of death for the bacterial spores during VHP decontamination. Figure 5.4.3 illustrates how the short-term and long term effects are tentatively explained here in this work.

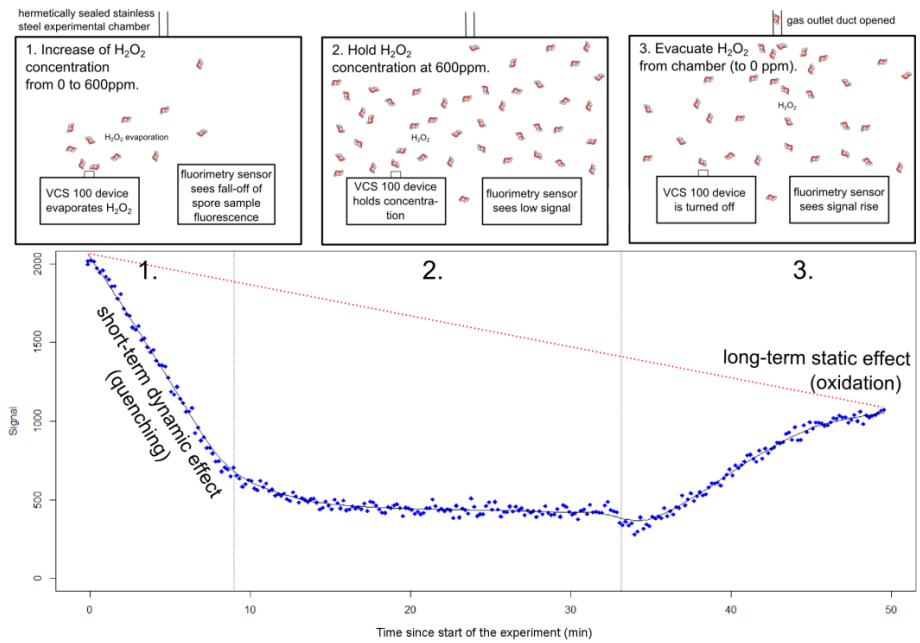

Figure 5.4.3. Short-term and long-term effects of VHP exposure on the fluorescence intensity of bacterial spores.

As a side note, it is worth mentioning that at first it was thought that maybe the effect of hydrogen peroxide molecules on fluorescing molecules inside living cells is entirely physical and connected to quenching effect only. As seen in the graph in figure 5.4.4 pure L-tryptophan with a surface concentration that has a similar fluorescence-intensity was measured in exactly the same conditions as the spores and was found to decrease in fluorescence at a much smaller rate

compared to the spores. Therefore, it was concluded that inside the spores the fluorescence quenching – even if it is just a proxy signal for the presence of hydrogen peroxide – is much more effective and really connected to the viability of the spore, not just to the decrease of the strength of the fluorescence signal by any other effects.

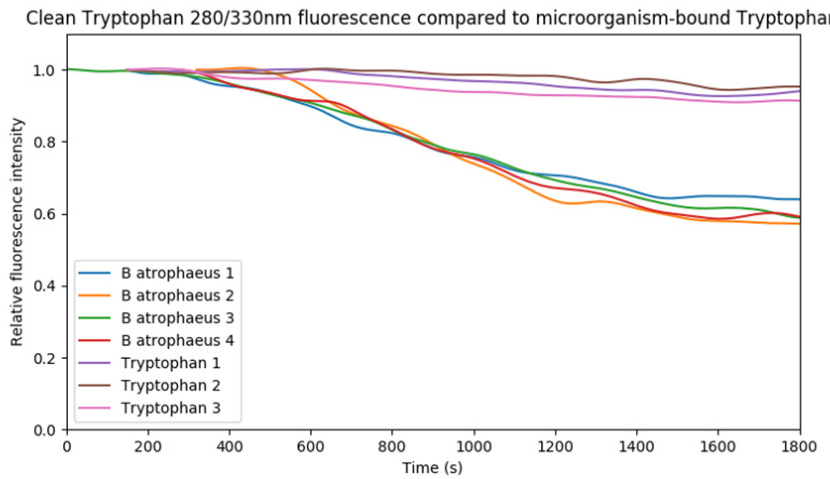

Figure 5.4.4. Pure L-tryptophan fluorescence shows much smaller signal intensity decrease as a function of VHP exposure when compared to signal from spores.

When performing the VHP decontamination experiment using same sample multiple times in a row (*i.e.,* not removing it from the chamber), it is possible to see that the signal path from viable spores to dead spore state takes a different spectral "route". It is particularly well seen when comparing the dead spore state without VHP surrounding to the dead spore state with VHP surrounding (see figure 5.4.5). The signal intensity decrease of the viable spores during the first VHP exposure has a longer duration than the next ones for already dead spores. The signal recovery occurs nearly to the initial value in all cases. Note that the different axes are 280 / 460 nm and 280 / 340 nm spectral features that are used in monitoring of the VHP influence.

As a side note, it is useful to mention that throughout this thesis (including figure 5.4.5), if the decontamination parameters are not stated explicitly, these are set to be ~500 ppm and ~20 minutes of VHP.

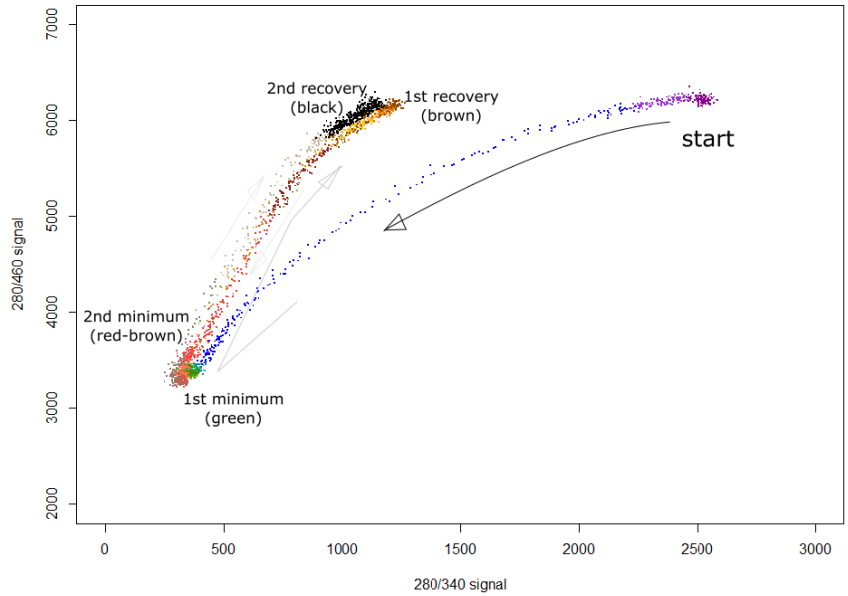

Figure 5.4.5. The viable spore has a different 280 nm / 460 nm versus 280 nm / 340 nm signal intensity "path" when compared to the signal path of dead spores. The plot shows one intensity plotted against the other and time scale (sequence) is shown with different colours, starting with magenta, blue, green, red, orange, brown, grey, black.

5.5. Monitoring decontamination at various VHP concentrations

The fluorescence decrease effect together with the decontamination (a duration of VHP exposure) time can be used to make a very good estimation of the quality of the decontamination process at the selected location, where the sensor is installed during the VHP decontamination procedure. The main aim of such sensor is to monitor decontamination efficiency in hard-to-reach corners inside the room-to-be-decontaminated – *i.e.,* behind some piece of furniture or at several corners at once, where the air (and therefore VHP) flow is not as good as in the open room area (*e.g.,* in a centre). Typically, the VHP device (*e.g.,* VCS-100) as well as one or more large ventilators/fans are mounted inside the room to distribute the vapour evenly. Since VHP is highly reactive with organic matter, even common household dust will get affected by the vapour, and without thorough mixing the room will have some unknown VHP concentration gradient throughout the room. Thus, without proper monitoring this might mean that some distant corners of the room still have viable pathogenic micro-organisms present and the VHP decontamination effort cannot be considered successful. Installing a sensor with replaceable real pathogenic microorganisms in the most-hard-to-reach places eliminates this problem.

Of course, another important problem remains – how can decontamination team be sure that every microorganism within the room-to-be-decontaminated is dead or incapacitated? To solve this, experiments have been carried out with multiple microorganisms and it is found that the endospores (mostly called "spores" in this thesis) or some *Bacillus* bacterial species are the most resilient to VHP decontamination [83]. As stated in previous sections, this means that every other pathogenic microorganism in the room is already dead when these spores finally lose their viability. Such bacterial spores are commercially available by *e.g.,* Mesalabs. The modified H2B-Spectral sensor that was developed uses either one of the aforementioned bacterial spores and measures the spectral fall-off during VHP decontamination procedure, enabling to calculate also the log-kill ratio for the spore sample and answer the question risen above.

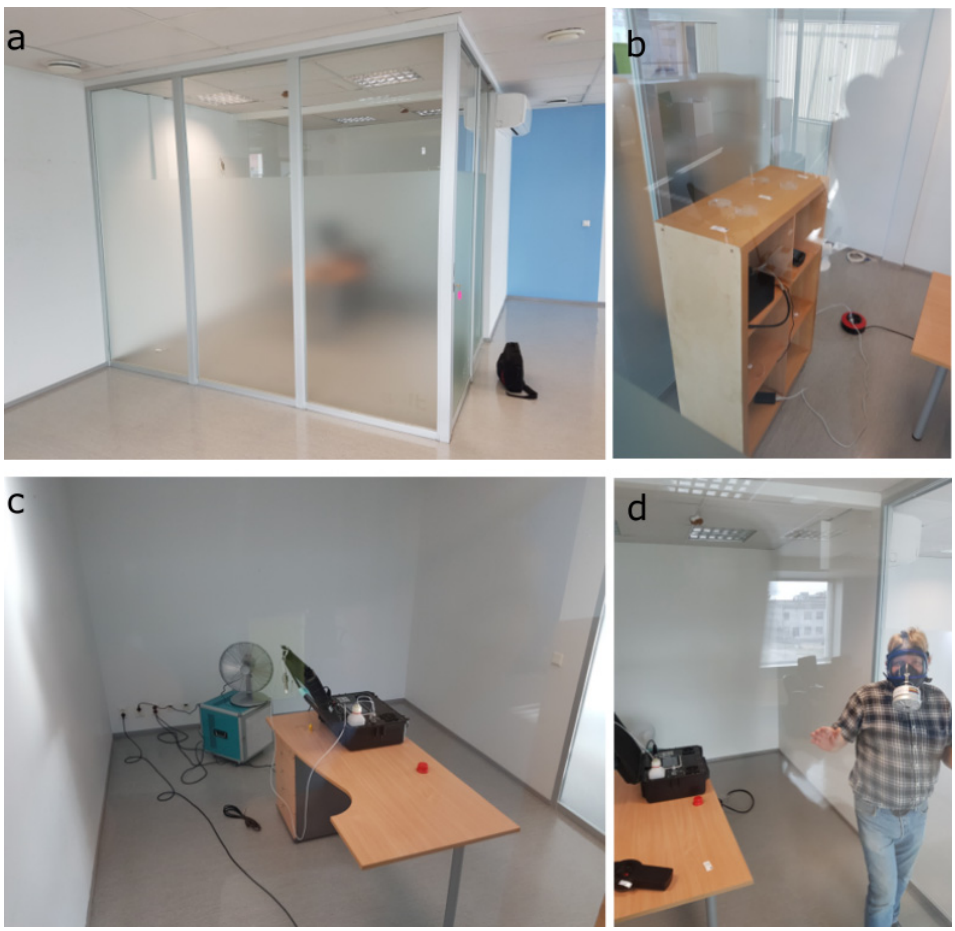

Figure 5.5.1. a) 30 m^3 enclosure (empty corner office); b) the experimental fluorometry measurement devices in the enclosure; c) the VHP generation machine VCS-100 and a fan; d) the experimenter entering into the enclosure. Courtesy of LDI Innovation OÜ.

A much larger enclosure (empty corner office room of ~30 m^3 volume) was used during experiments with different hydrogen peroxide vapour concentrations [**III**]. Since vaporizing the hydrogen peroxide to achieve the required VHP concentration in such a large enclosure takes many minutes (if not tens of minutes) and even longer time to catalyse the VHP back into water vapour and oxygen, the experiment was carried out by installing the sensors into the room under decontamination when the VHP concentration selected earlier was achieved. This required using gas masks and other safety measures due to VHP leaking out of the experiment room each time when the device is taken out or moved in. Such enclosure size also means using a large ventilator to homogenize the hydrogen peroxide gas concentration throughout the room to be decontaminated (see figure 5.5.1). All communication with monitoring devices, controlling of VHP concentration, was handled wirelessly, providing that the decontamination process can be done safely without need to enter the dangerous VHP environment for operator. Even the catalysis of H_2O_2 back into H_2O and O_2 can be controlled outside with the small tablet PC that generally runs decontamination procedure.

With the modified H2B-Spectral sensor, it was found that the tryptophan spectral region (280 nm / 340 nm) gave the highest quality signal and it was affected most by the presence of VHP. Other fluorescence channels (340 nm / 460 nm and 280 nm / 460 nm) had a much smaller intensity fall-off during the decontamination procedure and were much more erratic in their signal's behaviour. The shape of the fluorescence-intensity as a function of time can be described a bi-exponential fall-off function with an almost constant background signal (*i.e.,* exponential fall-off to constant plateau slightly above zero value). The fall-off speed (decay time) as well as the remaining background signal level both depend on the VHP concentration as can be identified in figure 5.5.2.

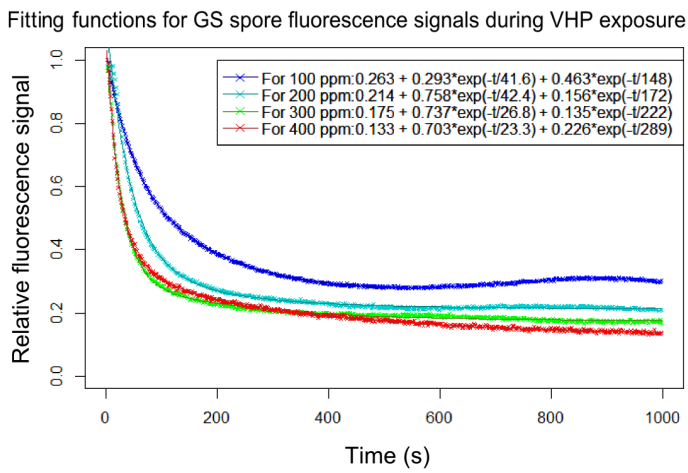

Figure 5.5.2. Bi-exponential fits (solid curves) together with raw data (symbols) for 280 nm / 340 nm fluorescence channel fall-offs for 4 different VHP concentrations (100 ppm, 200 ppm, 300 ppm, 400 ppm, see [III]) in the 30 m^3 experimental room.

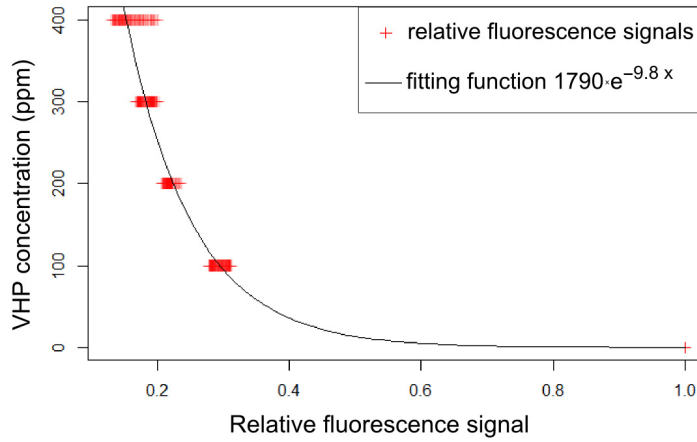

Figure 5.5.3. Relative fluorescence signal level of the 280 nm / 340 nm monitoring channel (at the "plateau" level, the averaged signal intensity from 300 s to 1000 s) plotted as a function of the VHP concentration shows that the effect is highly sensitive in the lower concentration ranges.

Plotting the almost constant "plateau levels" (the averaged signal intensity value from 300 s to 1000 s, see figure 5.5.2) of the fitted data as a single exponential function of the VHP concentration values, one identifies the following. There is a converging and well defined exponential mathematical model between these two quantities, which means that the H2B-Spectral output signal enables estimating local VHP concentrations and its real influence to the behaviour of the biological samples (in particular, for the GS spores). This derived exponential approach is more precise at the lower VHP concentrations (0–100 ppm) and has a larger error at large concentrations (over 500 ppm), which is typically used in real-life applications. Real life applications also need to account for the inhomogeneity of the VHP distribution as well as VHP losses (*e.g.,* due reactions in the far-away at the corners of the room-to-be-contaminated). Thus, a more precise global estimate of the influence VHP is beneficial for monitoring the efficiency of the VHP decontamination procedure. According to the experimental data (figures 5.5.2 and 5.5.3) there is no big exposition difference between using 300 ppm or 400 ppm of VHP, whereas there is a huge decontamination time increase when using the lower 50 ppm or 150 ppm VHP concentrations. Also, it demonstrates that the sensor is sensitive in a way that prohibits over-estimation of the influence of small VHP concentrations.

As a next step, the so-called Weibull formula can be used on this relative-fluorescence-intensity derived concentration relationship and the integral logarithmic death rate estimation (under-estimation by design) is calculated as a sum of each time-constrained concentration estimate – see figure 5.5.4. Constants for the Weibull formula were established from the published literature [69] when matching it with the experimental data of this work. The formula

used is $\frac{C}{C_0} = 10^{-(\frac{t}{D})^p}$, where C/C_0 is the proportion of viable spores, t is the time since start of procedure, the time decay factor $D = k \times c^m$ depends on the VHP concentration, according to fit obtained k value is 69451, m value is −1.462 and p is taken to be neutrally 1. The value of p indicates whether the spores get more resistant to decontamination over time ($p<1$) or less resistant ($p>1$), the latter option being the more probable case for BA and GS spores used in this research. This formula is used to estimate logarithmic death ratios – that means the log 6 death rate corresponds to 1 viable spore for every 10^6 killed spores – log 6 level is typically considered sufficient to determine that the decontamination procedure has been successful. At lower VHP concentrations the achievement of log 6 death rate takes much longer time compared to higher VHP concentration values. The Weibull formula can give indication of the decontamination time for the achievement of log 6 kill as well when drawing a horizontal line through the real-time calculated integral effect graphs at log 6 level. The calculated result for 5 different VHP concentrations is shown in the following figure 5.5.4.

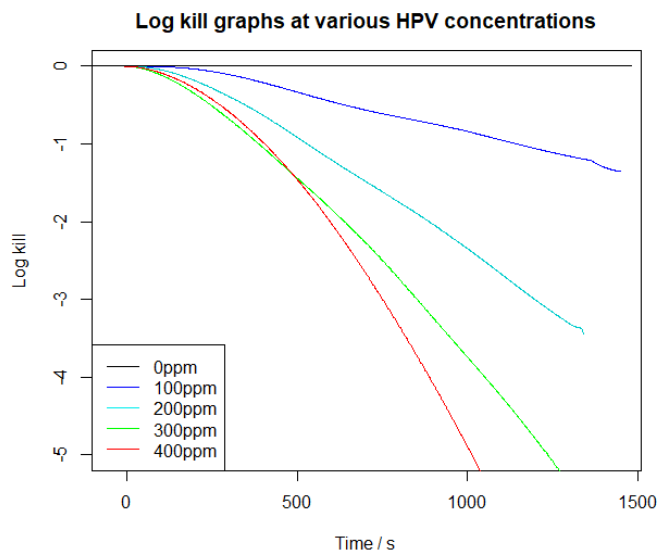

Figure 5.5.4. Calculated log-death rate ratios based on the experiments in the 30 m^3 office at several VHP concentrations (shows the preferred underestimation).

To sum up the potential of H2B-Spectral device, one has to compare its properties with the classical methods. The classical method would be to place the spore (or the so-called "biological indicator disks") samples for the decontamination period into the hard-to-reach places in the room and then let them grow in nutrient solutions to see if there remain any viable bacterial spores after the procedure. This method is the typical reference for all such deconta-

mination procedures, but it has a crucial flaw in speed because the results are only revealed after 24 hours to 7 days after the decontamination has been carried out. This, in turn, means that the decontaminated room cannot be safely released for use until the results from classical biological indicator growth tests are delivered. The modified H2B-Spectral sensor gives direct fluorescence signal from the same biological indicator disks, but in real-time during the decontamination process, allowing the operators of the VHP device to leave a safe margin to the decontamination process. Thus, the room can be taken into use directly after the VHP decontamination procedure is completed successfully and the remaining VHP removed by catalysis reaction forming water and oxygen or ventilated out of the room. The classical method can be used as an additional safety test, but continuous autofluorescence feedback from test microorganisms will give direct and immediate information about the influence of VHP.

5.6. Spectral differences between viable and dead bacterial spores

H2B fluorometer experiments showed that the tryptophan-tyrosine-like signal intensity can recover to a higher value when the VHP concentration is reduced after completing the decontamination process. Also, because the real reasons of spore cell death are not entirely clarified in the published scientific literature, the multi-concentration experiments were made in parallel (to the H2B-Spectral measurement) by using the SFS-Go device placed also inside the 30 m^3 experimental enclosure. SFS spectra contain not only the intensity of selected spectral peaks, but also reveal small shifts in their spectral positions, possibly giving more clues to researchers about the cause of cell death of the spores.

Experiments carried out with the spectrofluorometer SFS-Go on living (vegetative state) *Bacillus atrophaeus* (BA) bacteria before the VHP decontamination procedure showed a large spectral difference when compared to measuring the endospores of the same bacteria. The bacteria were grown from commercially available Kwikstik-type of source for 3 days at room temperature on LB broth agar Petri dishes and were gently scraped off onto the detection areas of SFS-Go sensors with small amounts of nutrient agar possibly still attached. Therefore, the living bacteria were in the growth phase and the spectra could be contrasted to the dormant spores' spectra. Although the emission spectrum of tryptophan-related (280 nm / 330 nm) peak shifted towards shorter emission wavelengths for both of them, the spectrum of dried endospores showed much more monotonous behaviour (*i.e.,* constantly becoming less intense during decontamination process), while the living bacteria even showed some intensity rise at tryptophan-like wavelengths during and after VHP exposure ended – see figures 5.6.1 and 5.6.2. At NADH-related (or oxidation-product-related) wavelengths (340 nm / 450 nm) the spores showed almost no signal change, while the living bacteria showed a remarkable rise, seemed to

contain more spectral features (peaks) and thus providing more information on ongoing processes.

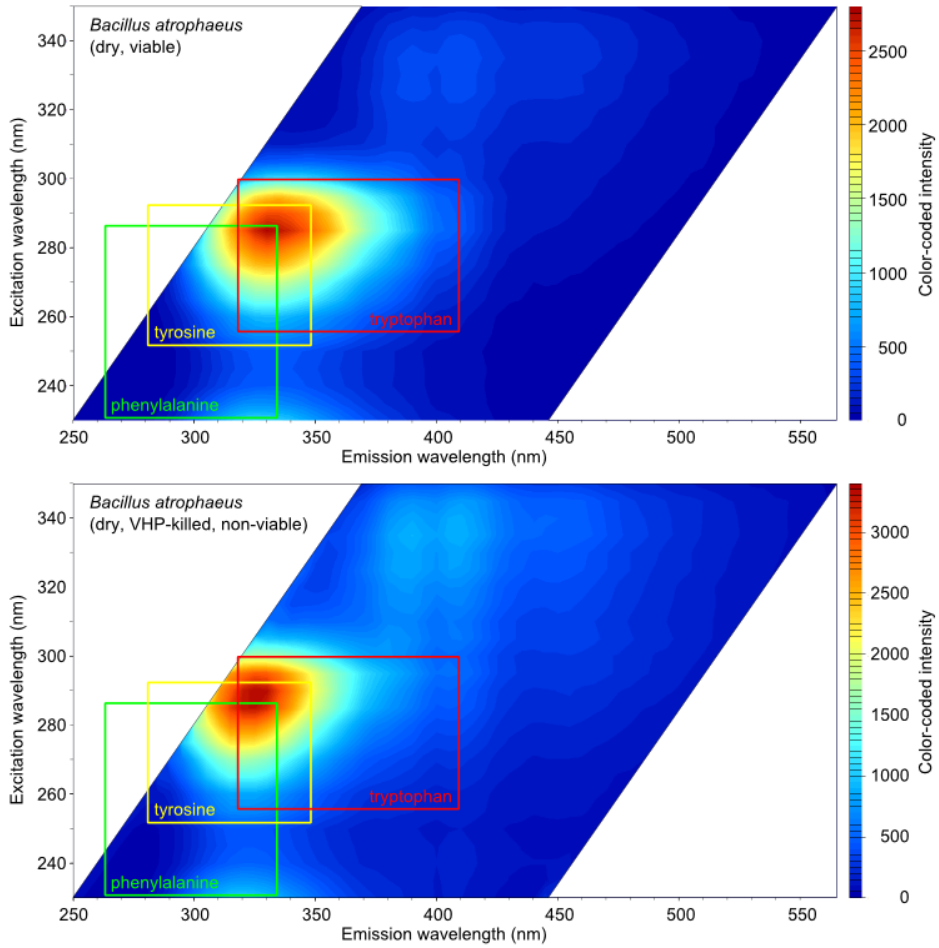

Figure 5.6.1. In the SFS spectrum of BA bacteria before (upper SFS graph) the VHP decontamination show higher autofluorescence intensity in the tryptophan region. After the VHP decontamination (lower SFS graph) the peak shifts towards tyrosine region and even rises in its intensity. During VHP decontamination, the intensity of Trp-peak becomes 2 times lower. The boxes designate spectral regions typical for the 3 fluorescent amino acids.

The spore autofluorescence spectra were very different from their parent bacteria as can be seen in figure 5.6.2. There is clearly less fluorescence at tryptophan spectral region, more in the tyrosine region and relatively more information available in the long-wavelengths (*e.g.*, DPA region) regions.

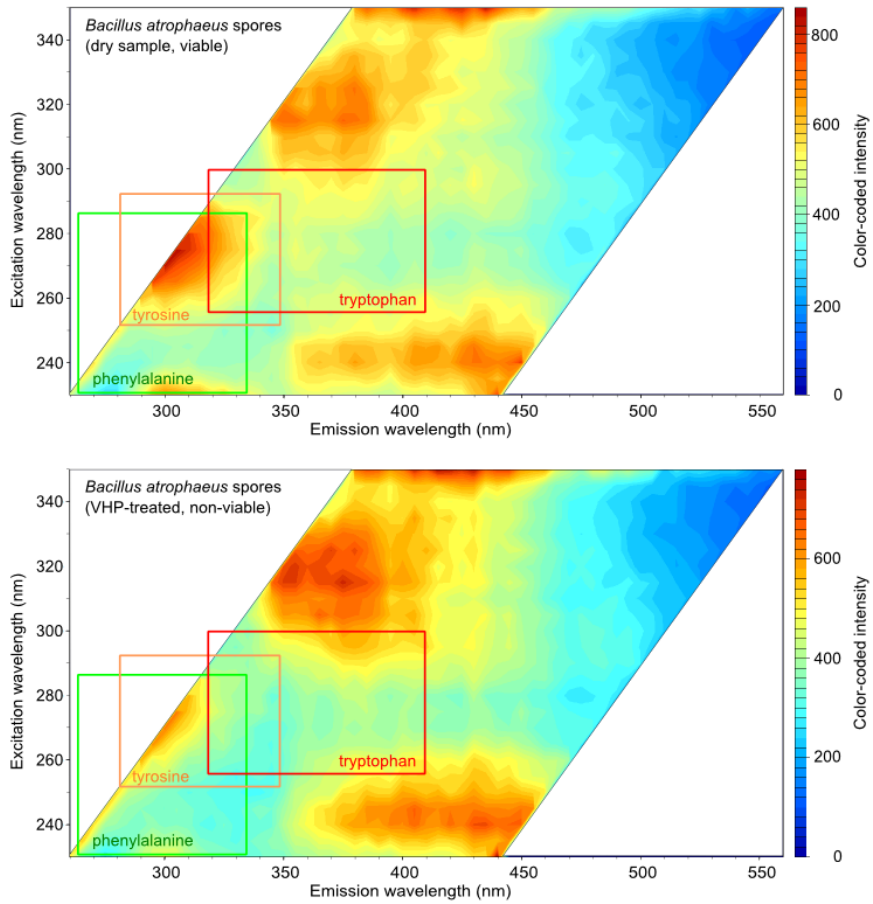

Figure 5.6.2. SFS spectra of BA spores (upper SFS graph) shows that the "tryptophan-like" peak is actually located in the tyrosine region, but in addition to reduction of its intensity, it does shift to the left towards shorter wavelengths during VHP decontamination (lower SFS graph). The lower graph is recorded at the end of ~20 minute 600 ppm VHP cycle. The boxes designate spectral regions typical for the 3 fluorescent amino acids.

It must be noted that the SFS spectra for the vegetative state bacteria have been studied before and after completing the VHP decontamination procedure, but the spores have been measured only in real time and the "dead" spectrum is

recorded at the end of a VHP cycle when VHP concentration is not yet turned off.

The 2nd commonly used biological indicator based on *Geobacillus stearothermophilus* was also studied before and after completing VHP decontamination in bacterial and spore form (see figures 5.6.3 and 5.6.4) so that more general conclusions could be drawn from the spectral change of recorded data.

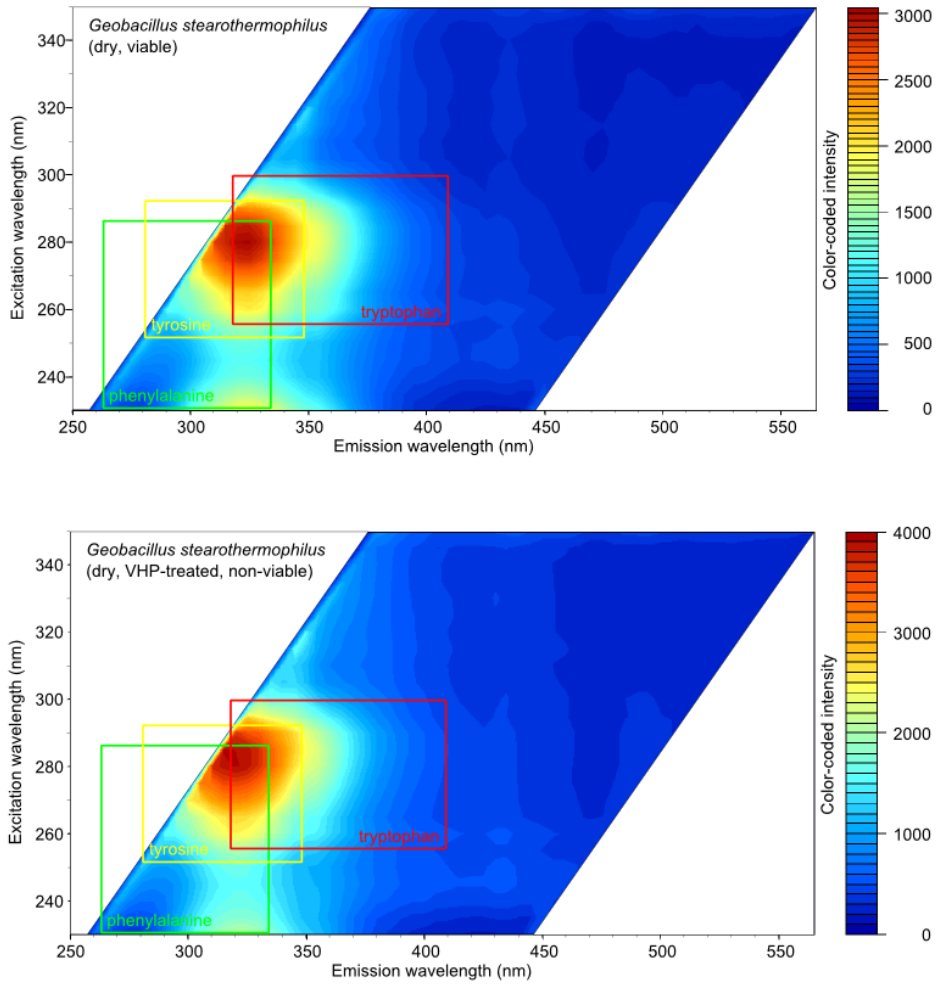

Figure 5.6.3. GS bacteria also show the same tendency as BA bacteria – the main spectral peak shifts towards shorter emission wavelengths and its intensity actually rises. SFS spectrum before decontamination treatment is in the upper SFS graph and after VHP decontamination treatment (~400 ppm for ~15 min) in the lower SFS graph. The boxes designate spectral regions typical for the selected amino acids.

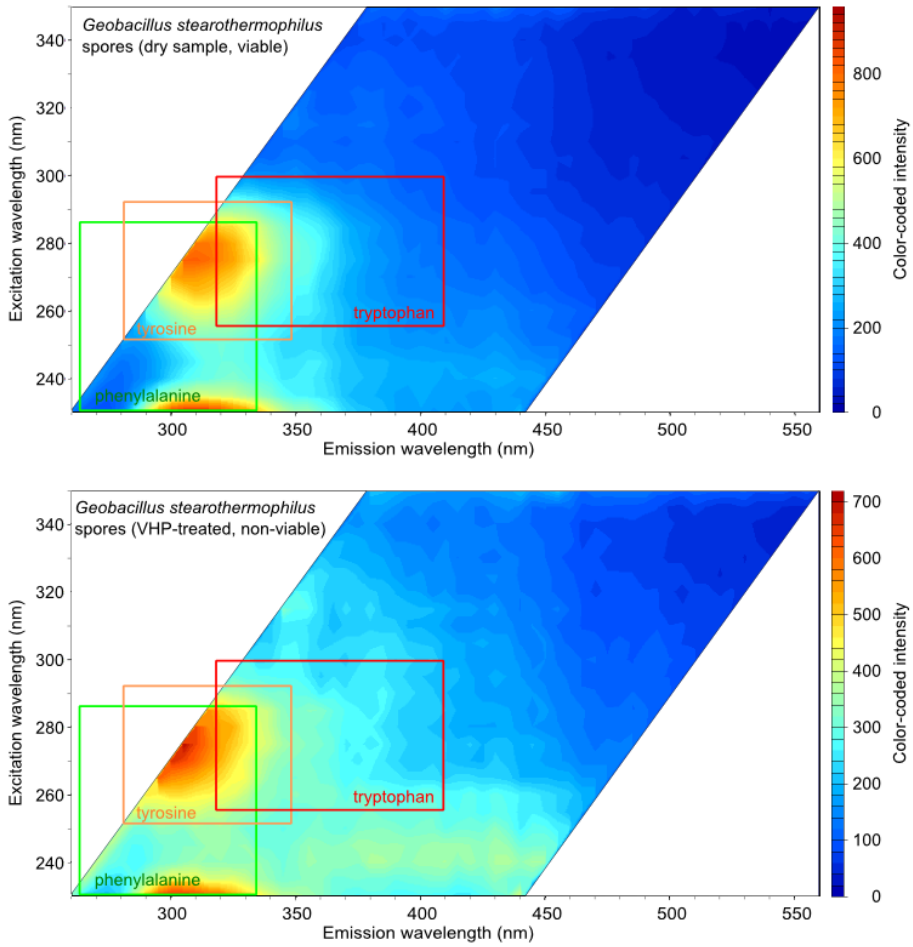

Figure 5.6.4. SFS spectrum before decontamination treatment shown in the upper SFS graph and after VHP decontamination treatment in the lower SFS graph. During VHP decontamination the GS spores' main spectral peak also moves to shorter wavelengths and reduces in intensity – similarly to the behaviour of BA spores. The applied VHP concentration on GS spores in this graph was ~300 ppm, compared to ~600 ppm for BA spores. The boxes designate spectral regions typical for fluorescent amino acids.

When comparing the spectra of the spores to spectra of the bacteria (in the typical tryptophan and tyrosine regions) it seems there is a trend that while the bacteria have their main fluorescence peak mostly near tryptophan region, the dry spores exhibit the main peak shifted to tyrosine region. The possible explanation is that the spores could either contain more tyrosine (this is more likely) or their tryptophan could be in an even more hydrophobic local environment compared to their "parent" bacteria.

After finalizing the VHP decontamination procedure a remarkable spectral shift of maxima towards shorter emission wavelengths was observed for the

main ~320 nm emission band under ~280 nm excitation. The observation was similar for the bacteria as well as the bacterial spores. The cause of this spectral shift is speculated [**II**, **III**] to be that the H_2O_2 molecules go deep inside of protein structures and break structural bonds, unfolding the proteins and disconnecting amino acids so that energy transfer from phenylalanine to tyrosine and from tyrosine to tryptophan is reduced. The distances between amino acid units increase, some oxidative damage might occur also and integrity of the fluorescing molecules becomes reduced.

The fluorescence intensity fall-off effect of the spores after VHP decontamination seems more easily explainable by the same mechanism. As the fluorescence yield decreases in the row Phe – Tyr – Trp and the energy transfer is disconnected in the same manner, a shift towards shorter wavelengths should be associated with a decrease in intensity. Also, any oxidation occurring should decrease the amount of fluorescing molecules and therefore the fluorescence intensity.

Contrary to the previous point, it was found that for the bacteria, the intensity of the shifted peak is actually increased after VHP exposure. From literature [84] it appears that enclosed inside a protein structure the tyrosine's fluorescence is actually weaker than it is for more free-floating tyrosine. As less energy is transferred to tryptophan at the same time, this could explain why the fluorescence intensity could also increase after VHP decontamination. Different effects mean that the protein structure of the spores is significantly different for the dormant spore form and living bacterial form, which is obvious.

At the same time, the broad emission peak at longer wavelengths centred around 460 nm when excited by 340 nm radiation barely changed its position and intensity or was rather increased than decreased during VHP killing procedure of spores. As for the rise of 340 nm / 460 nm peak, this can partly be attributed to the oxidation products of tryptophan-like molecules, which are centred around 340 nm / 460 nm according to [85] and [86]. In the case of bacteria the appearance of oxidation-induced molecules in this spectral region is more strongly connected to NAD(P)H fluorescence and longer wavelength excitation would have been needed to disentangle the real cause of this fluorescence [87].

The SFS-Go was also used to measure autofluorescence fall-off shown in figure 5.6.5 in real time during the VHP decontamination, but the measurement without any VHP influence (black line in figure 5.6.5) showed also a fall-off. It is likely that the high UV intensity of the SFS-Go damaged the samples together with very small air movement above the sample in the chamber may result erroneous and incomparable measurement of fall-off signals.

To the best of our knowledge, this is among pioneering studies where the spectral changes of the full autofluorescence spectra of micro-organisms were recorded for the first time during the vaporised hydrogen peroxide decontamination in real time.

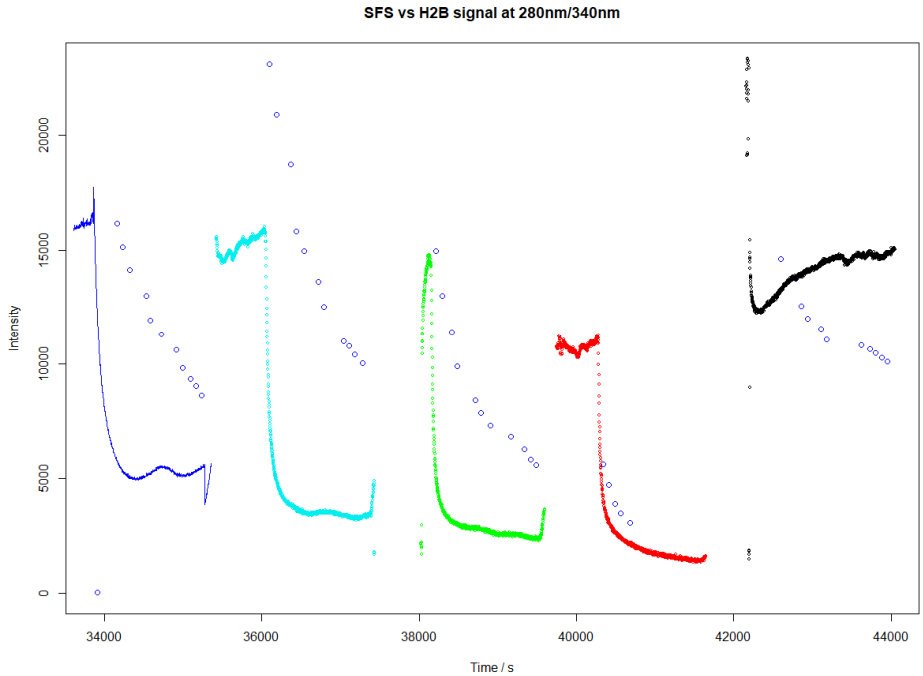

Figure 5.6.5. Illustration of the simultaneous measurements by SFS-Go (open blue symbols) versus H2B 340 nm autofluorescence signals (colored line of blue, small open circles of cyan, green, red, black) excited by 280 nm photons during 4 consequent 100 ppm, 200 ppm, 300 ppm and 400 ppm VHP decontamination runs (not normalised). Last curve on the right (black symbols) shows autofluorescence fall-off with smaller VHP influence. The fall-off speed of SFS-Go is slightly slower due to very small air gap letting the VHP in the measurement area.

During the death of the studied microorganisms only a few major spectral changes were observed. In special conditions, where the microorganism was in its active stage of life at first and then killed afterwards, it was mathematically possible to extract the NADH-spectral-area's change from the spectra, but this was far from being an obvious change. As noted, the fluorescence of bacterial spores was found to be extremely stable at the dipicolinic acid's spectral peak (region) (~340 nm / 450 nm, similar to NADH). DPA is a compound that is present in high concentrations around the DNA or RNA of the spore, protecting it from many types of attacks (chemical, thermal, electromagnetic). The stability of DPA's peak could be used as a reference, when comparing with the tryptophan-like signal that is highly dependent on hydrogen peroxide vapour concentration in the air surrounding the sample. Figure 5.6.6 reveals that even the "stable" DPA/NADH-related peak increases slightly during VHP run.

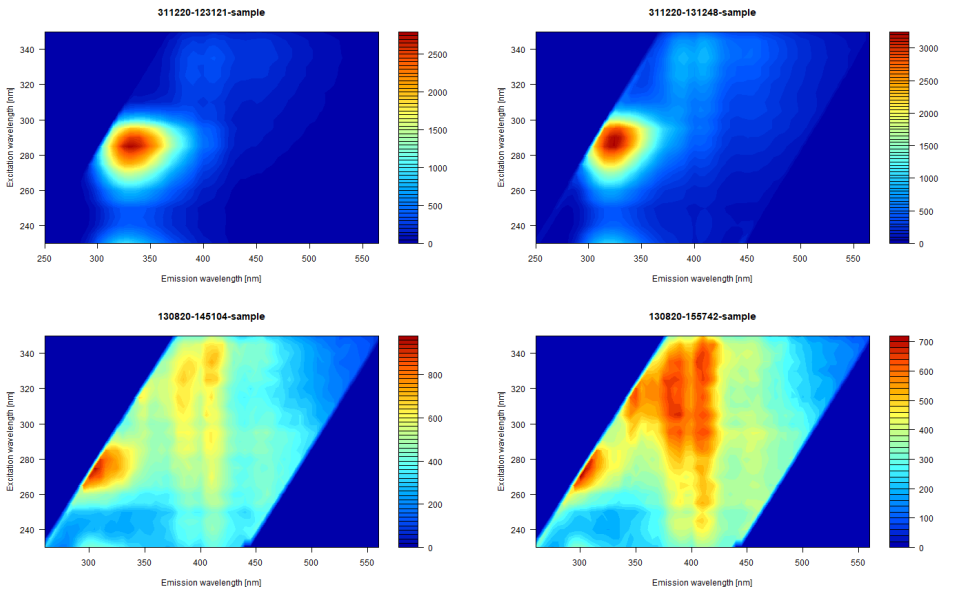

Figure 5.6.6. VHP-non-treated and VHP-treated vegetative bacteria compared to BA spores non-treated and treated spectra during VHP decontamination in one image. Top left – SFS spectrum of living BA bacteria before VHP procedure; top right – SFS of BA bacteria after the VHP procedure. Bottom left – BA spores before VHP treatment; bottom right – BA spores after VHP treatment. Note that for the spore samples the bottom-row SFS window the shorter wavelength edge has been moved 10 nm towards longer wavelengths due to very high reflection signal.

5.7. Differences of dead and viable spores in time-resolved mode

Although there certainly are differences in spectral distribution as well as total fluorescence intensities between viable spores and VHP-treated non-viable spores, there exists at least one more dimension in fluorescence spectroscopy that should be explored for a better understanding. Namely, it is possible to study the fluorescence in time-resolved mode and see if in the nanosecond time scale there are differences in the decay kinetics of viable and non-viable spore samples. If large differences appear, it would be possible to use modern electronics to design a small handheld sensor to exploit this result in a device with time-resolved operation mode. Obviously, the detection of already dead pathogens is not as important to the decontamination team as revealing still viable and dangerous pathogens. Here, a study was carried out by using time-resolved luminescence spectroscopy to find differences in time-resolved decays of emissions in the relevant spectral regions for the same bacterial spores already introduced in this thesis – mainly for GS spores. The study was carried out at the P66 beamline at Petra III storage ring DESY (Hamburg, Germany) and

FinEstBeAMS beamline [88] at MAX IV Lab synchrotron facility (Lund, Sweden). Both of these beamlines provide ultrashort excitation pulses in the UV range, including the important 230 nm to 280 nm wavelength range and also enable to measure the time-resolved emission spectra and luminescence decay kinetics with good enough resulting time-resolution (~160 ps for FinEstBeAMS and ~700 ps for P66).

GS spores of 10^6 CFU/cm^2 surface concentration on stainless steel substrate were studied at the P66 beamline at DESY and some measurements were performed also at the FinEstBeAMS beamline at MAX IV Lab. As can be seen in figure 5.7.1, firstly the time-resolved emission spectra recorded at under "far-enough" 230 nm photon excitation were compared for viable and VHP treated dead spores at room temperature. By "far enough" it is meant that the Gaussian shoulder of the scattered excitation photons will not interfere with autofluorescence signal and the disturbing scattered light photons, always present in normal incidence monochromators like P66 has, were suppressed by a cut-off filter WG280 with 50 % transmission at 280 nm. This filter is mounted in the luminescence detection channel of P66 setup. The data was recorded in time-resolved mode (an interval between subsequent pulses 192 ns) and during the analysis, data was separated into the short time-window (STW): summing up all photons that arrived during the first 10 nanoseconds from the excitation pulse (t = 0 ns) (red line in figure 5.7.1 and blue line in figure 5.7.2). In the long time-window (LTW) the photons coming in the time range 10 – 192 ns (black line in figures 5.7.1 and 5.7.2) were summed up. The samples were also studied at spectroscopically similar conditions, but at 10 K using liquid helium cooling and the respective spectra are shown in figure 5.7.2.

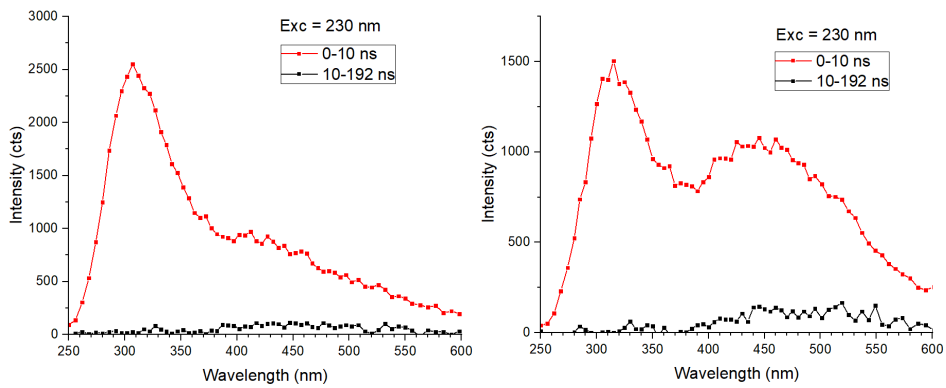

Figure 5.7.1. Time-resolved emission spectra of GS spores' under 230 nm excitation at room temperature. In the short time window (STW) (<10 ns, red line), the viable spores (left graph) show a significantly larger intensity in the tryptophan/tyrosine-related spectral region at ~315 nm, whereas the oxidation-result-related or NADH-related spectral region at 450 nm is more expressed in the VHP treated 'dead spores' samples, depicted on the right graph.

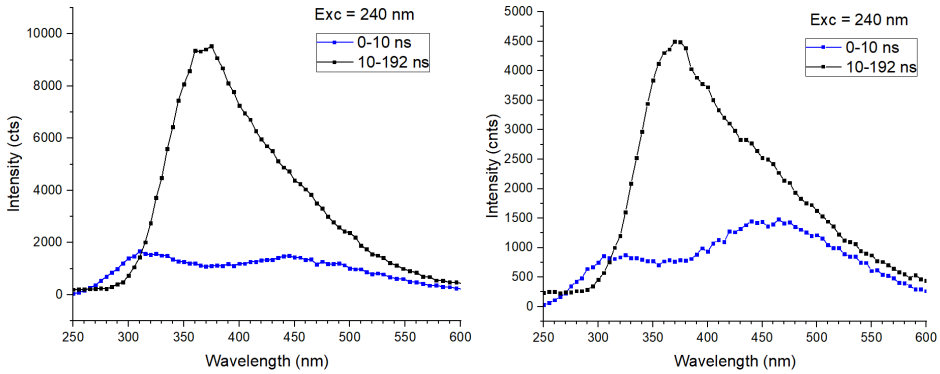

Figure 5.7.2. Time-resolved emission spectra of GS spores' under 230 nm excitation at 10 K. The dominating feature is the emission peak at 370 nm detected in the LTW, which indicates the changes in the radiative relaxation processes in comparison with RT. The viable spores (left graph) still show larger autofluorescence intensities as well as a well visible tryptophan/tyrosine-related peak (~315 nm) in the STW, when compared to the dead spores (right graph). The latter sample exhibits long wavelength peak at 450 nm in the STW due to the oxidation or NADH-related spectral region.

The first observation is that autofluorescence of viable or VHP treated GS spores is very fast process as most of luminescence is emitted during the first 10 ns, and practically nothing is left in the LTW (see Fig. 5.7.1). Also, the emission spectra show an enhanced Tyr-Trp-related ~320 nm peak for the viable spores, whereas the dead spores exhibit more pronounced feature at 460 nm at both temperatures. At 10 K, the wide peak at ~460 nm in the STW became dominant feature for the dead spores. At the same temperature, there is a large difference in the autofluorescence intensities between dead and viable spores, the latter ones having several times higher intensity. This can be tentatively assigned to the influence of VHP treatment as this was for confirmed for several unique samples in different measurements. At 10 K the dominating spectral feature is the emission peak at 370 nm detected in LTW. It indicates the changes in the radiative relaxation processes occuring in GS spores at low temperatures in comparison with room temperature. However, the origin of the 370 nm autofluorescence peak itself is not entirely clear. Wavelength-wise, its spectral position somewhat matches with the pyridoxine spectral features, but physically DPA would be a much better candidate [74] as the spores contain ~10% of this substance around DNA/RNA. Understanding the low temperature relaxation processes is of high importance for biophysical behaviour of spores, but for sensor development, it is not very fruitful as the devices operate at ambient conditions. Therefore, these low temperature investigations were discontinued.

As for the differences in the time-resolved fluorescence signal, the Trp-Tyr-related region (~315 nm) is typically relatively less intense for the dead spores, whereas the oxidation-result-related >450 nm region is more intense for the dead spores. This result makes sense as the oxidation process decreases the

amount of fluorescing amino acids and increases the amount of oxidation products, which supposedly fluoresce at the >450 nm range [87]. At the same time, gaseous H_2O_2 is not as strong an oxidizer as liquid H_2O_2 [68] so at least some of the fluorescence fall-off effect at ~315 nm should be due to denaturation/ unfolding of key proteins, which inhibit energy transfer between Phe-Tyr-Trp and effectively reduces the average quantum yield of the process as Phe has a lower quantum yield than Tyr and Tyr has a lower yield than Trp. The energy transfer disruption hypothesis falls slightly apart for GS spores here because under 230 nm excitation the ~315 nm peak does not move towards shorter wavelengths for the dead spores in figure 5.7.1. This is somewhat baffling since the same 230 nm excitation and 320 nm emission peak seems to shift towards shorter wavelengths in the dead GS spores' SFS spectra seen in figure 5.6.4. The main difference between these two studies carried out is that the P66 beamline measurements are performed in ultrahigh vacuum, whereas the SFS measurements occured at normal atmospheric pressure and in few-hundred ppm VHP concentration in air. After the VHP treatment ends, the Trp-Tyr-peak probably shifts back towards its original position. These differences are subject for further investigations beyond the scope of the current PhD thesis.

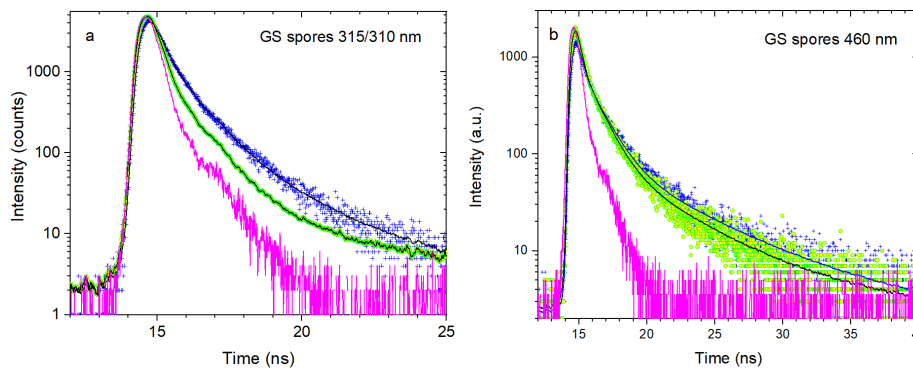

Figure 5.7.3. Decay curves of 315 (a) and 460 nm (b) emissions of GS spores at RT excited at 230 nm. Blue and green symbols designate the viable and VHP treated spores, respectively. Instrumental response function is shown as a line in magenta color. Solid lines show three exponential fits of the experimental data.

Figure 5.7.3 depicts the decay curves of viable and VHP treated GS spores recorded for specific wavelength regions under excitation by 230 nm photons at the P66 beamline. The plotted decay curves show that for the dead spores' Trp-Tyr-peak ~315 nm fluorescence has a slightly accelerated decay in comparison with the viable GS spores (figure 5.7.3.a), while the ~460 nm oxidation-result-related peak has practically similar decay time (figure 5.7.3.b). This means that our assumption was correct about a difference existing in time-resolved fluorescence decay times, but the difference is small enough not to initiate time-

resolved hand-held sensor development based on this effect. It is obvious that the decay curves are non-elementary and consist of several exponentials. The best approximation was with the 3 exponential functions and corresponding results are shown in Table 5.1.

Table 5.1. Three exponential fitting results of decay curves shown in Fig. 5.7.3.

Viable GS spores 315 nm emission				VHP treated GS spores 310 nm		
	τ (ns)	Light sum	%	τ (ns)	Light sum	%
τ_1	0.08	2576	53	0.06	3497	81
τ_2	0.72	1787	37	0.70	789	18
τ_3	2.49	508	10	3.37	508	1
Viable GS spores 460 nm emission				VHP treated GS spores 460 nm		
τ_1	0.10	785	39	0.08	1158	48
τ_2	1.22	1139	56	1.12	1124	47
τ_3	5.78	109	5	5.01	107	5

The first decay component τ_1 for 310 and 460 nm emissions is too short for the time resolution of detector used in the experiments at P66 and reflects contribution of scattered excitation photons. The second and third decay component for 310 nm emission are the characteristics of spores with decay times of ~0.7 and ~2.5 ns, and ~0.7 and ~3.4 ns for viable and VHP treated spores, respectively. The cause of the change in decay time for dead spores in Trp-Tyr-region needs also further investigations. There is a possibility that oxidative damage and resulting (smaller) aromatic-ring-containing products change decay time and lower quantum yield. At the long-wavelength 460 nm fluorescence region for VHP treated GS spores there is a slight increase of emission intensity in average (right panel in figure 5.7.1). In comparison with the Trp-Tyr-region decay times a bit longer decay times ~1.2 and ~5 ns were obtained and no well pronounced influence of VHP treatment was observed. To summarize, the numerical analysis of the recorded decay curves confirms that changes in the decay times for all emissions are so small and cannot be reasonably exploited in any monitoring device for VHP based decontamination process.

In more pioneering experiments the excitation spectra of the viable and VHP-treated (~20 min, ~500 ppm) dead GS spores at 295 K were comparatively studied at FinEstBeAMS beamline (MAX IV Lab, Lund) as well as P66 beamline (DESY PS, Hamburg) (see figure 5.7.4 for the excitation spectra and 5.7.5 for a photograph of the FinEstBeAMS beamline). The resulting excitation spectra are not completely identical but the main features are repeated and recognisable from studies at both beamlines. This is a natural result because P66 operates on the bending magnet source in normal incidence geometry, whereas an undulator source provides photon flux a few orders of higher intensity for FinEstBeAMS, operating in grazing incident geometry and covering energy

range 4.5 – 1300 eV with a superior energy resolution [88]. It is important to note that the excitation spectrum for ~315 nm Trp-Tyr-related emission is more structured, which can be related to the specific absorption bands of amino-acids. The main excitation peaks are at 230 and 200 nm, which can be tentatively assigned to Tyr absorption and Phe absorption respectively [18]. The excitation spectrum for oxidation-result-related emission at 460 nm is much smoother, repeating the main features of the former excitation spectrum. For the VHP-treated spores, the 200 nm excitation peak is the dominating feature, but viable ones show that along the same peak, the strongest one is at 230 nm. The differences in the excitation spectra are more expressed for 315 nm Trp-Tyr-related emission in both samples. For the 460 nm emission the spectra are more similar when comparing viable and dead spores. If assuming that this long-wavelength emission is mostly excited through various energy transfer processes from amino-acid absorption, the resulting spectra are arising from contributions of different processes forming more smooth excitation curves. To our best knowledge the excitation spectra below 230 nm are not studied before for this type of bacterial spores, therefore more investigations are needed and in this work we do not speculate on the reasons for the observed spectral differences.

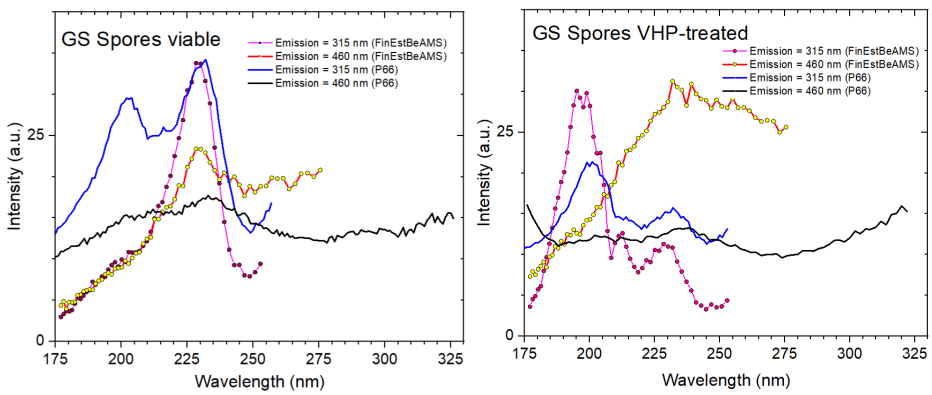

Figure 5.7.4. Excitation spectra of the viable (upper graph) and VHP-treated (lower graph) GS spores at 295 K measured at the P66 beamline (blue line for 315 nm emission, black line for 460 nm emission) and at the FinEstBeAMS beamline (symbols in magenta for 315 nm emission, yellow for 460 nm emission).

Figure 5.7.5. Thesis supervisor professor Marco Kirm is working at the set-up for luminescence investigation at the FinEstBeAMS beamline where the spores were studied by time-resolved fluorescence spectroscopy under UV-VUV excitation.

6. EFFECT OF ULTRAVIOLET RADIATION

In the very first experiments, the H2B device had a microwatt-level 280 nm LED illumination to excite the Trp-Tyr-related fluorescence. As can be seen in figure 6.1, this exciting UV radiation caused almost as much of the fluorescence intensity fall-off (at 280 nm / 340 nm) as the VHP process itself.

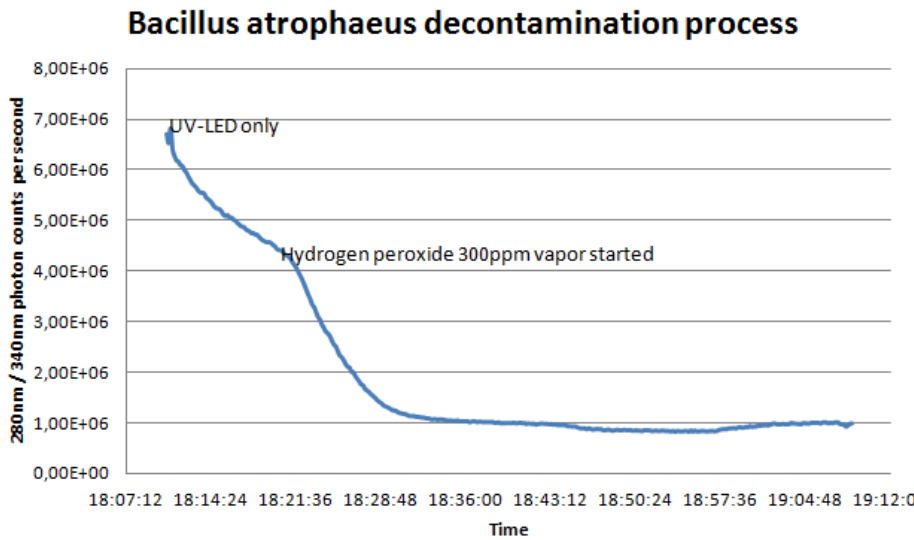

Figure 6.1. The autofluorescence intensity fall-off as a function of exposition time to high intensity 280 nm UV LED radiation and VHP treatment. The incorrectly configured 280 nm UV LED itself caused initially a significant intensity decrease that is associated with the cell death even before the start of VHP delivery in the initial tests.

Therefore, the LED power and duty cycle (*i.e.,* LED-ON-time versus LED-OFF-time) of the H2B device was reduced ~1000 times and the UV-caused fluorescence fall-off effect could no longer be revealed. Even after 16 hour irradiation test, the autofluorescence signal was at the same initial level (plot not shown as it is a straight horizontal line graph over time).

Unfortunately, the same excitation power reduction could not be achieved on the SFS-Go spectrofluorometer as the xenon lamp's pulse energy could not easily be reduced enough as the optimal signal to noise ratio for this sensor has a higher excitation threshold. In figure 6.2 it can be seen that when measuring live vegetative state BA bacteria under VHP treatment, the ultraviolet radiation dose received by the sample under the SFS-Go beam shows a significant loss in autofluorescence signal intensity, while under the low-power LED of the H2B sensor it rises to even higher levels than before starting the experiment.

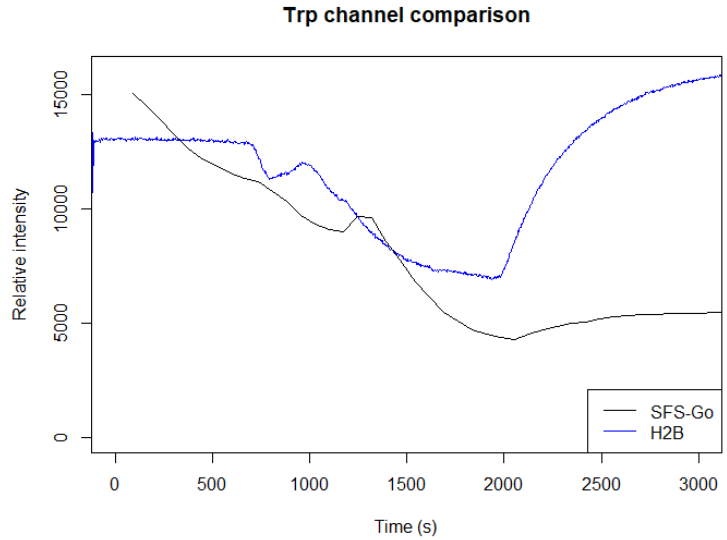

Figure 6.2. Autofluorescence of Trp channel from live BA bacteria recorded simultaneously with the modified H2B-Spectral and SFS-Go device at exposure at few-hundred ppm of VHP. After the VHP was turned off at ~2000 seconds, the SFS-Go signal intensity was not recovered because of the UV damage caused by the sensor itself, which was not the case for the H2B-Spectral operating at lower UV radiation level.

It is well-known that ultraviolet radiation causes damage in the genetic material breaking the structures and nucleic acids, causing them to merge/dimerize [89]. When the cell's repair mechanisms are overpowered by the UV dose per surface area, the cell will become non-viable. The lethal radiation dose rates for bacterial spores are in the range of 1 kJ/m^2, while for example the SARS-COVID-19 dose rate is around 0.2 kJ/m^2 and for reference, the dose around 0.03 kJ/m^2 of 270 nm light is already not safe for humans. In paper [**IV**] it was examined examined what is the lethal radiation dose for some commercially important pests – the two-spotted mites (*Tetranychus urticae*) – so that a decontamination system could be developed to get rid of the pest and at the same time let the affected plants living.

Therefore, in addition to the decontamination of micrometer-scale microorganisms, this thesis includes a summary of the decontamination experiment with an almost macroscopic organism species – millimeter-sized spider mites *Tetranychus urticae*. The applied 248 nm UV beam (see figure 6.5 for the setup) delivered such a large energy density that a water droplet on plastic Petri dish took the shape of the laser beam – as seen in figure 6.3 – rather than its initial circular shape, probably due to the UV light changing the properties of the surface of the plastic, changing the surface tension coefficient.

Figure 6.3. Liquid sample under the 248 nm UV laser beam takes the shape of the laser output beam image on the bottom of a plastic Petri dish.

Industrial food production has benefitted greatly from new growing methods and crop varieties, but at the same time it has suffered from new pests being efficiently spread by our globalised economic model. One of such pests is the two-spotted spider mite *Tetranychus urticae* – see figure 6.4. Originally a European pest, the mites have now been found in many greenhouses all around the world. The mites feed directly on plant matter by sucking the cell contents cell by cell, reproducing fast and – as an aggregate result – leaving the plant partly dead or in a much worse state. Consequently, the spider mites can cause large amounts of financial damage and need to be eradicated or reduced significantly in numbers. One solution is to use various chemicals to combat the mites, but these can leave some amount of potentially toxic chemicals also onto the fruit or plant produce and can long-term damage the soil. Ultraviolet radiation has been proposed as a safe option to combat such type of mites.

Figure 6.4. Two-spotted spider mites on a bean plant leaf photographed at 2 magnification levels.

In the work [**IV**], one step further is taken, using a directed excimer laser beam in the UV-C range (248 nm) as a source of ultraviolet radiation to estimate the killing efficiency at various UV doses on mites.

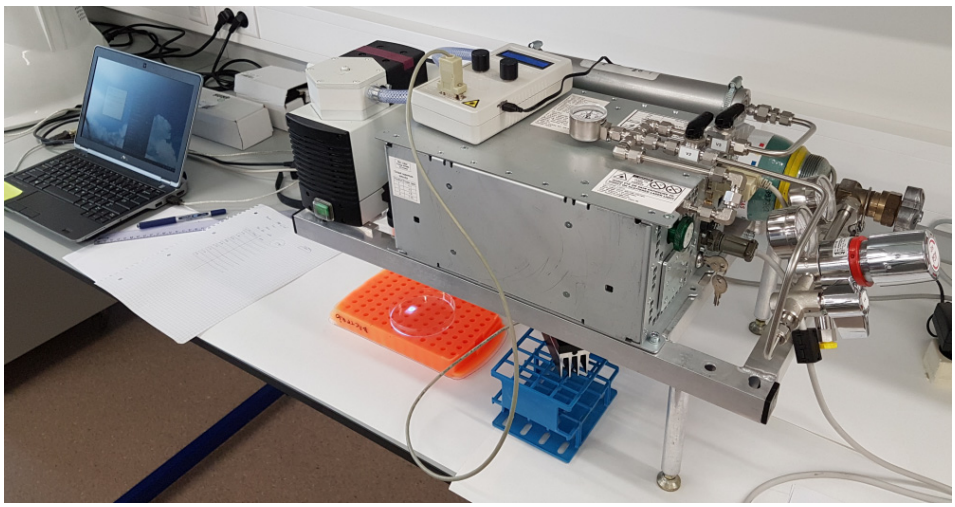

Figure 6.5. Set-up developed to deposit pre-set UV-C radiation doses onto two-spotted spider mites. Courtesy of LDI Innovation OÜ.

It was found that the 24-hour survival rate for living adult female mites is relatively high for small doses of UV-C radiation. A high dose of around 80 kJ/m^2 was needed to achieve a near-100% kill ratio, with ~20 kJ/m^2 50% value was achieved as shown in figure 6.6. At the same time, it was found that much less than 5 kJ/m^2 was needed for the mite eggs to stop hatching, which means that even a single laser pulse scanning along the plant would cause the eggs to become sterile and making a laser-based mite reduction system feasible in some settings. The adult mite eradication would need a too high dose for the plants to survive, so only a reduction of the next mite generation would be a plausible solution for industrial use without any chemicals involved.

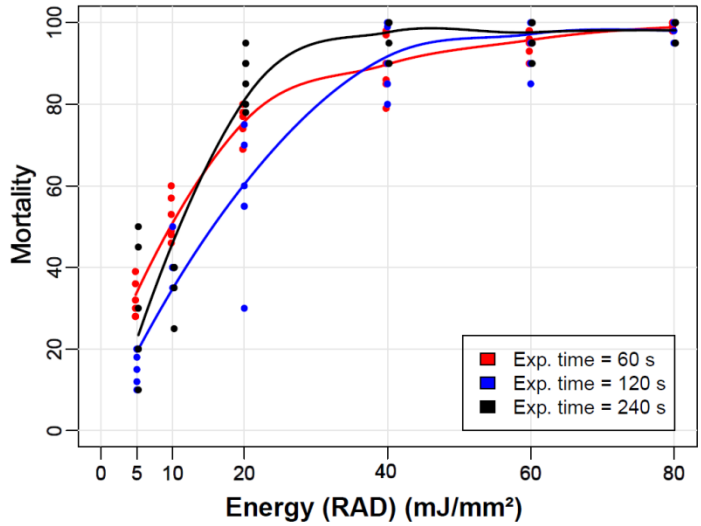

Figure 6.6. Two-spotted spider mite 24 h mortality plotted as a function of the 248 nm radiation dose. Three different intensity levels and UV exposure durations are used to achieve the same radiation doses. The mortality seems to be dependent on dose only at the chosen intensity levels.

7. SEM IMAGE COMPARISON OF DEAD AND VIABLE SPORES

Viable and dead (resulting from VHP treatment) BA bacterial spores deposited on aluminium sample holder were investigated using a scanning electron microscope. The spores were killed by approximately 600 ppm VHP exposure during 20 minutes. The same VHP treatment was applied in experiments with the modified H2B-Spectral device. Visibly intact and broken spores seen in figure 7.1 were counted only in the small areas that were investigated (see figure 7.2) and statistical analysis of the data are summarised in table 1. No statistically significant difference was found between both kind of samples, viable and dead. Therefore, as is confirmed by literature, the main effect of VHP mortality of the microscopic pathogens is not expressed by mechanical damage. The probable main effect of VHP is rather the fact that it penetrates easily into the cell wall and can then denature key proteins, oxidize the DNA or RNA of the pathogen, causing it to be no longer a viable organism.

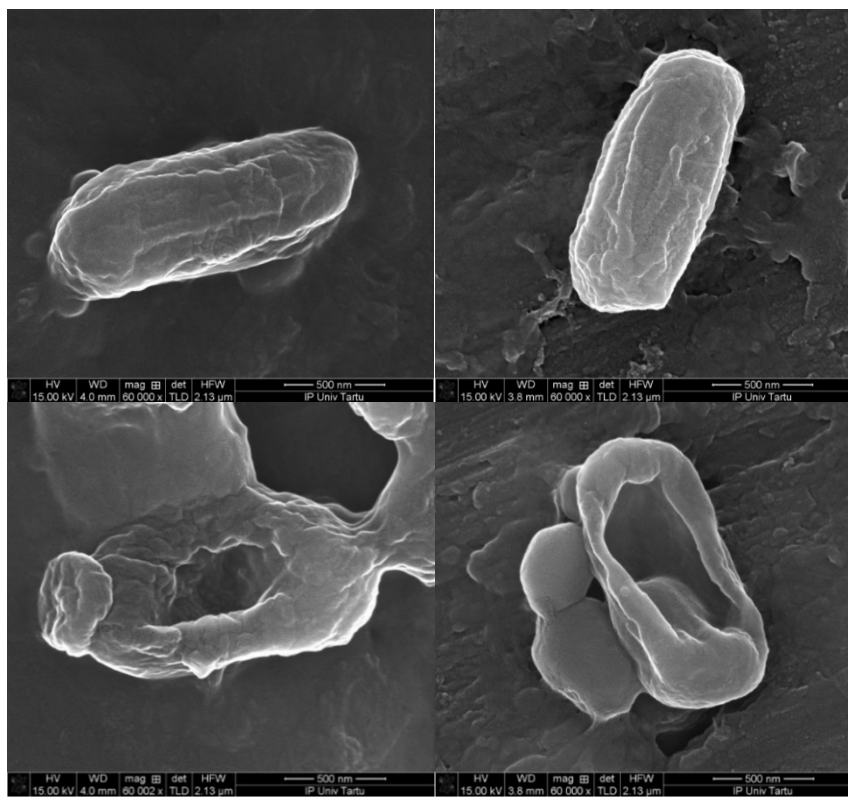

Figure 7.1. The SEM image of viable spores (left column) contained a similar amount of intact spores (upper row) as the VHP-killed sample (right column), while the number of visibly-broken spores (lower row) was also not obviously different. Images by NanoSem 450 (FEI) instrument.

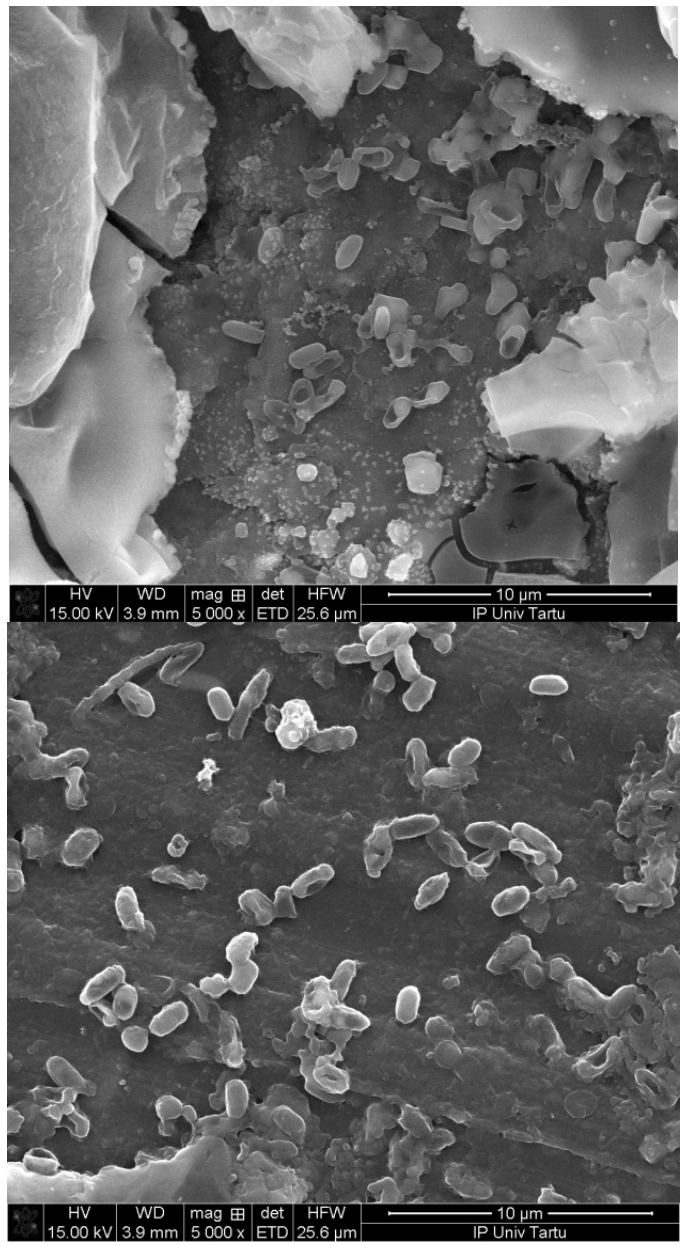

Figure 7.2. The ratio of broken-up spores is similar in dead (upper image) and viable (lower image) spore samples. For the SEM – made using a NanoSem 450 (FEI) instrument – both types of spore samples were covered with 3 nm of gold with Polaron Emitech SC7640 Sputter Coater (1000 V, 15 mA, 3 min).

When taking various images of ~25 micron field of view and counting the visually intact and visually broken spores, the analysis provides statistical result presented in the following table.

Table 7.1. Intact spores and broken spores in SEM images counted.

Name of sample	# of intact spores	# of broken spores
Viable_n1_30	4	20
Viable_n1_05	8	33
Viable_n1_04	1	7
Viable_n2_05	12	17
Viable_n2_15	14	29
Viable_n2_17	3	9
Viable_n2_18	2	13
Dead_n2_03	6	18
Dead_n1_26	2	5
Dead_n1_24	1	5
Dead_n1_25	2	7

Imaging of larger areas covered by dead spores was complicated due to the amount of aluminium corrosion causing the surface to be very uneven. Nevertheless, when applying the statistical t-test for broken spore percentage in the alive spore samples versus the broken spore percentage in the dead spore SEM images, one finds that the p-value is 0.84 and that the intact/broken proportions are very likely similar enough for dead and viable spores: 25%±14% of all distinguishable spores seem intact in these images – see table 7.1 for the data. There is not enough statistics here for a more general conclusion, but this is an indication that a lot of intact-looking spores are still present in the VHP-treated samples. When actually collecting sufficient statistics, it can be found that VHP can actually cause some mechanical damage [90] and the result is even statistically significant [91], but this does not change the fact that intact-looking spores are present in a large part of totally dead spore samples.

This could mean that there is in fact no way to differentiate visibly between viable and totally decontaminated spore samples. The main cause of spore death according to [92] could be that the VHP-treated spores cannot swell properly during spore germination. The VHP-treated spore cores somehow (through denaturation and oxidation of key proteins) become inaccessible to needed chemicals like ATP, reduced flavin, nucleic acids, etc. Also, the fact that the spore coat offers so little resistance to hydrogen peroxide vapor [93], which can pass thought and cause damage inside proteins, seems to support the hypothesis that spore death by VHP is not of mechanical nature, but more chemical nature inside the core.

8. CONCLUSIONS

During the current industrial PhD program, several fluorescence-based photonic device prototypes and their applications were developed and tested – a lidar, spectrofluorometers and fluorometers. Pathogen samples were remotely detected and classified on various field-hospital background materials using the lidar. Various pathogen classes were characterised using the spectrofluorometers and surface contamination was investigated with the fluorometer prototypes. The UV fluorometers were used to estimate the efficiency of vaporised hydrogen peroxide decontamination procedure in real time for the first time. The real fluorescence intensity fall-off effect during vaporised hydrogen peroxide decontamination was investigated not only using the spectrofluorometers developed, but also by using time-resolved measurements in synchrotron facilities and by scanning electron microscopy. The damaging effect of ultraviolet radiation was studied on spider mites and the gained knowledge considered on smaller pathogens studied in this work.

A number of take-aways regarding the main studied samples – the bacterial spores – is summarised in figure 8.1. We definitely see that the small H_2O_2 molecules in vapour form penetrate very easily through all layers of a spore or any other biological sample and cause the signal of the fluorescent amino acids to fall immediately and significantly. The debate about the main killing mechanism being oxidation of the inner connections of key proteins or the denaturation of the proteins is still inconclusive since there seem to be both effects present and oxidation causing more long-term effects. The spectral shifts and time-domain effects after VHP-treatment are mostly explainable with the denaturation and oxidation also. The exact mechanisms remain somewhat unknown for now, but for the development of photonic devices that are usable in real life and could provide future profit, deep empirical understanding could be enough – as is the result of the current PhD thesis.

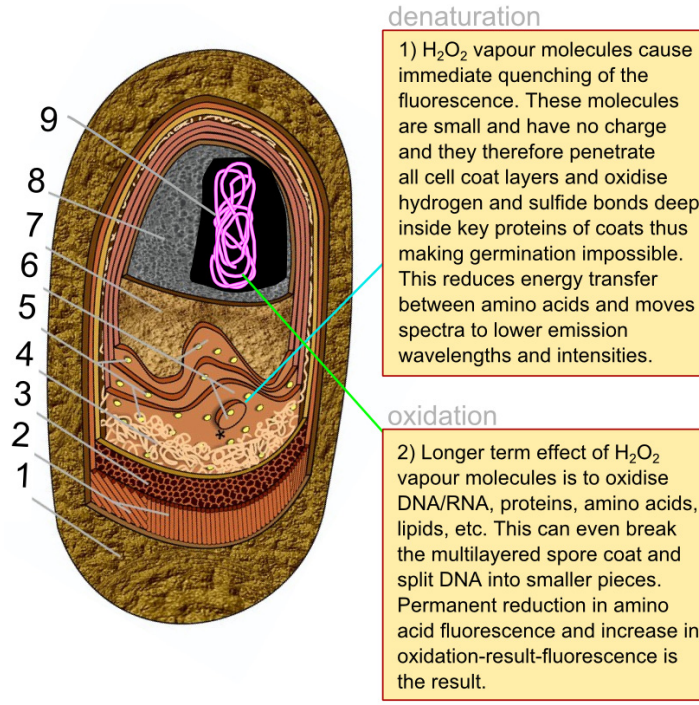

Figure 8.1. Illustration to help visualise and summarize the effects that could explain the spectral shifts seen with BA and GS spores during VHP decontamination experiments.
The figure 8.1 depicts a model of the spore coat architecture of a single B. subtilis spore (similar to BA spores in this work – see chapter 7): (1) the crust; (2) the rodlet layer; (3) the honeycomb layer; (4) the fibrous layer, (5) the nanodot layer on top of a multilayer structure (6) ((with a 2D nucleus (indicated with *) seen on the upper layer)); and the basement layer (7), the cortex's outer pitted surface (8). DNA/RNA in DPA-protection is inside these 8 coat layers. This figure is adapted from [94] according to CC BY 4.0 licence attached and used here just to have a visual illustration along some of the conclusions made in this work.

9. SUMMARY

In this thesis, the optical properties of various biological pathogens are studied using mostly fluorescence spectroscopy methods. Firstly, a chosen set of bacteria, virus and yeast were characterised with laser-induced fluorescence as well as spectral fluorescence signatures to establish the fact that biological pathogens can be separated from each other by their autofluorescence spectra alone. Secondly, two specific biological indicators – the spores of *Geobacillus stearothermophilus* (GS) and *Bacillus atrophaeus* (BA) – were studied before, after and during the highly effective decontamination process with vaporised hydrogen peroxide (VHP).

Main results of this work can be summarised in the following statments:

- Remote detection and identification of biological pathogens is possible when using a specialized laser-induced-fluorescence lidar. The existence of biological contamination can be detected on a set of typical background materials of field hospitals with less than 5% error rate. The developed spectrofluorometer and fluorometers also enable differentiation of pathogens on relevant background materials and the real-time monitoring of the VHP process.
- For the first time, it is observed that GS and BA biological indicators show an immediate response to hydrogen peroxide vapour in their fluorescence signal. By monitoring this signal in real time, it is possible to get an immediate indication about the success of the decontamination process. By using this effect, it could be possible to vastly reduce the time that is needed to verify the success of the decontamination procedure and open up the decontaminated rooms for use.
- The spectra of still viable and dead bacterial (GS, BA) spores show distinct differences in the tryptophan-related spectral region under 280 nm excitation and ~330 nm emission. The viable spores have much greater autofluorescence intensity in this spectral region, whereas the longer-wavelength (related to oxidization products or NADH) spectral regions show an opposite effect where fluorescence peaks become actually more intense after the VHP treatment.
- Scanning electron microscopy mapping of viable and dead spores show a similar amount of intact-looking as well as clearly damaged spores, so this visual information alone is not sufficient to establish firmly the viability of spores.
- Time-resolved luminescence spectroscopy under UV excitation also reveals some differences in the ns-decay components of various emissions from viable and dead spores. Trp-like fluorescence is relatively more intense in viable spores. The decay times for various emissions from dead spores tend to be slightly faster than from their viable counterparts in the amino-acid-related spectral regions, while in the oxidation-product-related region are more similar.

10. SUMMARY IN ESTONIAN

Lokaalne mittekontaktne mikrobioloogilise reostuse tuvastamine fluorestsents-spektroskoopia meetodeil

Käesolevas doktoritöös arendati välja mitmed fotoonikasensorid ning uuriti nendega erinevate bioloogiliste patogeenide optilisi omadusi, kasutades valdavalt fluorestsentsspektroskoopia meetodeid. Esiteks iseloomustati valitud bakterite, viiruste ja pärmide komplekti laser indutseeritud fluorestsentsi ja spektraalse fluorestsents "sõrmejäljega", et teha kindlaks, kas kõiki neid bioloogilisi patogeene saab üksteisest eraldada ainult nendele tüüpiliste fluorestsentsspektrite abil. Teiseks uuritakse kahe spetsiifilise bioloogilise indikaatori käitumist – *Geobacillus stearothermophilus* (GS) ja *Bacillus atrophaeus* (BA) spoore – enne, pärast ja dekontaminatsiooni protsessi ajal aurustatud vesinikperoksiidiga (H_2O_2).

Selle töö peamised tulemused võib kokku võtta järgmiselt:

- Loodud laser-indutseeritud fluorestsentslidari kasutamisel on võimalik biopatogeenide kaugtuvastamine. Bioloogilise saastatuse olemasolu saab sellega tuvastada välihaiglatele tüüpiliste taustmaterjalide peal veamääraga <5%. Loodud spektrofluoromeeter ja fluoromeetrid võimaldavad samuti patogeenide tuvastamist ja eristamist ning ka H_2O_2 gaasi mõju jälgimist.
- Esmaavastusena leiti, et GS ja BA spooridel põhinevad „bioloogilised indikaatorid" näitavad ajalise viiviseta reaktsiooni vesinikperoksiidi aurule nende oma fluorestsentssignaalis. Jälgides seda signaali reaalajas, on võimalik saada viivituseta indikatsioon saastest puhastamise („dekontaminatsiooni") protsessi edukuse kohta. Seda efekti kasutades on võimalik oluliselt vähendada aega, mis kulub saastest puhastamise protseduuri edukuse kontrollimiseks ja dekontamineeritud ruumide avamiseks.
- Veel elujõuliste ja võrdluseks juba surnud GS ja BA bakterispooride spektrid näitavad selgeid erinevusi trüptofaani ja türosiiniga seotud spektripiirkonnas ergastades 280 nm footonitega ja jälgides kiirgust ~330 nm emissioonilainepikkusel. Elujõulistel spooridel on selles spektraalpiirkonnas palju suurem suhteline kiirguse intensiivsus, samas kui pikematel lainepikkustel (oksüdatsiooniproduktid jms) spektripiirkonnad näitavad vastupidist efekti, kus elujõu kaotanud spooride kiirgusribad on seal lainepikkustel intensiivsemad.
- Elujõuliste ja surnud spooride skaneeriva elektronmikroskoobiga läbiviidud analüüs näitab sarnasel hulgal nii terve välimusega ja selgelt kahjustatud ja katkisi spoore, seega ei pruugi sellest teabest üksi piisata bakterispooride elujõulisuse kindlakstegemiseks.
- Sub-nanosekundilise aeglahutusega autofluorestsentsi mõõtmised näitavad ka väikesi erinevusi spooride vahel – elujõuliste spooride kiirgus on veidi pikema elueaga ja suhteline intensiivsus suurem võrreldes H_2O_2 töötluse läbinutega.

11. ACKNOWLEDGEMENTS

I herewith thank my supervisors Prof. Marco Kirm and Dr. Sergey Babichenko for their excellent guidance and support, without which this thesis would not have happened. I would also like to thank Prof. Jean-Luc Gala and his team for the inspiration brought about in the joint EDEN project, which initiated my whole PhD studies and Dr. Larisa Poryvkina for making me rethink my academic goals. Thirdly, I would like to thank Harri Hakkarainen and the Cleamix team (Finland) for the all the help related to hydrogen peroxide experiments, spore sample creation and testing. All my fellow colleagues in LDI Innovation as well as from the laboratory of physics of ionic crystals in Tartu are appreciated for their support. Special thanks go to Leino Vint for all the technical discussions on optomechanical design, Vitali Nagirnyi, Juhan Saaring, Ivo Romet and Sergey Omelkov for their help with synchrotron measurements, time-resolved measurements software and result interpretation. Collaboration with x-ray spectroscopy laboratory for making the SEM measurements happen is also highly appreciated. Last but not least I am grateful to my wife Mariina, my son, my parents, brothers, sister and friends for encouraging me during these years.

This work was supported by smart specialization industrial PhD program from European Regional Development Fund. The work has been supported by ASTRA project PER ASPERA, Graduate School of Functional Materials and Technologies, receiving funding from the European Regional Development Fund under project in University of Tartu, Estonia. I also acknowledge a partial financial support from the Estonian Centre of Excellence TK141 by the EU through the European Regional Development Fund (TK141 “Advanced materials and high-technology devices for sustainable energetics, sensorics and nanoelectronics”, project No. 2014-2020.4.01.15-0011) and TK134 “Emerging orders in quantum and nanomaterials” as well as Estonian Research Council grants PRG-111 and PRG-629. I also acknowledge partial support for using the synchrotron radiation research at Petra III ring, Photon Science DESY (Hamburg, Germany) and at MAX IV Lab (Lund, Sweden), which has been supported by the project CALIPSOplus under the Grant Agreement 730872 from the EU Framework Programme for Research and Innovation HORIZON 2020. The development of electron microscopy at the Institute of Physics is partially supported by the NAMUR+ project (grant no. 2014-2020.4.01.16-0123, University of Tartu), which is also acknowledged The FinEstBeAMS beamline operation costs were partially supported within the MAX-TEENUS project (grant no. 2014-2020.4.01.20-0278) by the ERDF funding in Estonia.

12. REFERENCES

[1] Microbiology by numbers, 2011. Nat Rev Microbiol 9, 628–628. https://doi.org/10.1038/nrmicro2644

[2] Váradi, L., Luo, J.L., Hibbs, D.E., Perry, J.D., Anderson, R.J., Orenga, S., Groundwater, P.W., 2017a. Methods for the detection and identification of pathogenic bacteria: past, present, and future. Chem. Soc. Rev. 46, 4818–4832. https://doi.org/10.1039/C6CS00693K

[3] Pendleton, J.N., Gorman, S.P., Gilmore, B.F., 2013. Clinical relevance of the ESKAPE pathogens. Expert Review of Anti-infective Therapy 11, 297–308. https://doi.org/10.1586/eri.13.12

[4] Otter, J.A., Yezli, S., Barbut, F., Perl, T.M., 2020. An overview of automated room disinfection systems: When to use them and how to choose them, in: Decontamination in Hospitals and Healthcare. Elsevier, pp. 323–369. https://doi.org/10.1016/B978-0-08-102565-9.00015-7

[5] Havill, N.L., Moore, B.A., Boyce, J.M., 2012. Comparison of the Microbiological Efficacy of Hydrogen Peroxide Vapor and Ultraviolet Light Processes for Room Decontamination. Infect. Control Hosp. Epidemiol. 33, 507–512. https://doi.org/10.1086/665326

[6] Arunwuttipong, A., Jangtawee, P., Vchirawongkwin, V., Kangwansupamonkon, W., Asavanant, K., Ekgasit, S., 2021. Public Buses Decontamination by Automated Hydrogen Peroxide Aerosolization System. Open Access Maced J Med Sci 9, 847–856. https://doi.org/10.3889/oamjms.2021.6828

[7] Talmy, D., Beckett, S.J., Zhang, A.B., Taniguchi, D.A.A., Weitz, J.S., Follows, M.J., 2019. Contrasting Controls on Microzooplankton Grazing and Viral Infection of Microbial Prey. Front. Mar. Sci. 6, 182. https://doi.org/10.3389/fmars.2019.00182

[8] Lamei Ramandi, S., Asgharian, R., 2020. Evaluation of swab and rinse sampling procedures and recovery rate determination in cleaning validation considering various surfaces, amount and nature of the residues and contaminants. IJPR 19. https://doi.org/10.22037/ijpr.2020.1101173

[9] Bottiroli, G., Croce, A.C., 2007. Autofluorescence spectroscopy of cells and tissue as a tool for biomedical diagnosis, in: Palumbo, G., Pratesi, R. (Eds.), Comprehensive Series in Photochemical & Photobiological Sciences. Royal Society of Chemistry, Cambridge, pp. 189–210. https://doi.org/10.1039/9781847551207-00189

[10] Leblanc, L., Dufour, E., 2004a. Monitoring bacteria growth using their intrinsic fluorescence. Sci. Aliments 24, 207–220. https://doi.org/10.3166/sda.24.207-220

[11] Nowicki, S., Lapworth, D.J., Ward, J.S.T., Thomson, P., Charles, K., 2019. Tryptophan-like fluorescence as a measure of microbial contamination risk in groundwater. Science of The Total Environment 646, 782–791. https://doi.org/10.1016/j.scitotenv.2018.07.274

[12] Sorensen, J.P.R., Lapworth, D.J., Marchant, B.P., Nkhuwa, D.C.W., Pedley, S., Stuart, M.E., Bell, R.A., Chirwa, M., Kabika, J., Liemisa, M., Chibesa, M., 2015. In-situ tryptophan-like fluorescence: A real-time indicator of faecal contamination in drinking water supplies. Water Research 81, 38–46. https://doi.org/10.1016/j.watres.2015.05.035

[13] Xiong, Y., Shi, C., Li, L., Tang, Y., Zhang, X., Liao, S., Zhang, B., Sun, C., Ren, C., 2021. A review on recent advances in amino acid and peptide-based

fluorescence and its potential applications. New J. Chem. 45, 15180–15194. https://doi.org/10.1039/D1NJ02230J
[14] Glasscock, J.M., Zhu, Y., Chowdhury, P., Tang, J., Gai, F., 2008. Using an Amino Acid Fluorescence Resonance Energy Transfer Pair To Probe Protein Unfolding: Application to the Villin Headpiece Subdomain and the LysM Domain. Biochemistry 47, 11070–11076. https://doi.org/10.1021/bi8012406
[15] Davis, K.B., Zhang, Z., Karpova, E.A., Zhang, J., 2018. Application of tyrosine-tryptophan fluorescence resonance energy transfer in monitoring protein size changes. Analytical Biochemistry 557, 142–150. https://doi.org/10.1016/j.ab.2018.07.022
[16] Lakowicz, J.R. (Ed.), 2006. Protein Fluorescence, in: Principles of Fluorescence Spectroscopy. Springer US, Boston, MA, pp. 529–575. https://doi.org/10.1007/978-0-387-46312-4_16
[17] Vivian, J.T., Callis, P.R., 2001. Mechanisms of Tryptophan Fluorescence Shifts in Proteins. Biophysical Journal 80, 2093–2109. https://doi.org/10.1016/S0006-3495(01)76183-8
[18] Walla, P.J. (Ed.), 2014. Modern Biophysical Chemistry. Wiley-VCH Verlag GmbH & Co. KGaA, Weinheim, Germany, pp. 59. https://doi.org/10.1002/9783527683505
[19] Giana, H.E., Silveira Jr., L., Zângaro, R.A., Pacheco, M.T.T., 2003. Rapid Identification of Bacterial Species by Fluorescence Spectroscopy and Classification Through Principal Components Analysis. Journal of Fluorescence 13, 489–493. https://doi.org/10.1023/B:JOFL.0000008059.74052.3c
[20] Shlosberg, Y., Farber, Y., Hasson, S., Bulatov, V., Schechter, I., 2021. Fast label-free identification of bacteria by synchronous fluorescence of amino acids. Anal Bioanal Chem 413, 6857–6866. https://doi.org/10.1007/s00216-021-03642-8
[21] Yu, Q., Heikal, A.A., 2009. Two-photon autofluorescence dynamics imaging reveals sensitivity of intracellular NADH concentration and conformation to cell physiology at the single-cell level. Journal of Photochemistry and Photobiology B: Biology 95, 46–57. https://doi.org/10.1016/j.jphotobiol.2008.12.010
[22] Blacker, T.S., Mann, Z.F., Gale, J.E., Ziegler, M., Bain, A.J., Szabadkai, G., Duchen, M.R., 2014. Separating NADH and NADPH fluorescence in live cells and tissues using FLIM. Nat Commun 5, 3936. https://doi.org/10.1038/ ncomms4936
[23] Lakowicz, J.R., Szmacinski, H., Nowaczyk, K., Johnson, M.L., 1992. Fluorescence lifetime imaging of free and protein-bound NADH. Proc. Natl. Acad. Sci. U.S.A. 89, 1271–1275. https://doi.org/10.1073/pnas.89.4.1271
[24] Setlow, B., Atluri, S., Kitchel, R., Koziol-Dube, K., Setlow, P., 2006. Role of Dipicolinic Acid in Resistance and Stability of Spores of *Bacillus subtilis* with or without DNA-Protective α/β-Type Small Acid-Soluble Proteins. J Bacteriol 188, 3740–3747. https://doi.org/10.1128/JB.00212-06
[25] Nudelman, R., Feay, N., Hirsch, M., Efrima, S., Bronk, B.V., 1999. Fluorescence of dipicolinic acid as a possible component of the observed UV emission spectra of bacterial spores, in: Leonelli, J., Althouse, M.L. (Eds.), . Presented at the Photonics East (ISAM, VVDC, IEMB), Boston, MA, pp. 190–195. https://doi.org/10.1117/12.336865
[26] Zhang, H., You, C., Ren, J., Xu, D., Han, M., Liao, W., 2014. A Simple One-Step PCR Walking Method and Its Application of Bacterial rRNA for Sequencing Identification. Curr Microbiol 68, 486–494. https://doi.org/10.1007/s00284-013-0488-1

[27] Laflamme, C., 2005. Autofluorescence as a viability marker for detection of bacterial spores. Front Biosci 10, 1647. https://doi.org/10.2741/1648
[28] Zhao, W., Chen, J.J., Foley, S., Wang, Y., Zhao, S., Basinger, J., Zou, W., 2015. Biomarker identification from next-generation sequencing data for pathogen bacteria characterization and surveillance. Biomarkers in Medicine 9, 1253–1264. https://doi.org/10.2217/bmm.15.88
[29] Hayashi Sant'Anna, F., Bach, E., Porto, R.Z., Guella, F., Hayashi Sant'Anna, E., Passaglia, L.M.P., 2019. Genomic metrics made easy: what to do and where to go in the new era of bacterial taxonomy. Critical Reviews in Microbiology 45, 182–200. https://doi.org/10.1080/1040841X.2019.1569587
[30] Tannock, G.W., 1999. Identification of lactobacilli and bifidobacteria. Curr Issues Mol Biol 1, 53–64.
[31] Singhal, N., Maurya, A.K., Virdi, J.S., 2019. Bacterial Whole Cell Protein Profiling: Methodology, Applications and Constraints. CP 16, 102–109. https://doi.org/10.2174/1570164615666180905102253
[32] Lellman, S.E., Cramer, R., 2020. Bacterial identification by lipid profiling using liquid atmospheric pressure matrix-assisted laser desorption/ionization mass spectrometry. Clinical Chemistry and Laboratory Medicine (CCLM) 58, 930–938. https://doi.org/10.1515/cclm-2019-0908
[33] Ratiu, I.-A., Ligor, T., Bocos-Bintintan, V., Buszewski, B., 2017. Mass spectrometric techniques for the analysis of volatile organic compounds emitted from bacteria. Bioanalysis 9, 1069–1092. https://doi.org/10.4155/bio-2017-0051
[34] Forrester, J.B., Valentine, N.B., Su, Y.-F., Johnson, T.J., 2009. Chemometric analysis of multiple species of *Bacillus* bacterial endospores using infrared spectroscopy: Discrimination to the strain level. Analytica Chimica Acta 651, 24–30. https://doi.org/10.1016/j.aca.2009.08.005
[35] Naumann, D., Helm, D., Labischinski, H., 1991. Microbiological characterizations by FT-IR spectroscopy. Nature 351, 81–82. https://doi.org/10.1038/351081a0
[36] Maquelin, K., Choo-Smith, L.-P., van Vreeswijk, T., Endtz, H.Ph., Smith, B., Bennett, R., Bruining, H.A., Puppels, G.J., 2000. Raman Spectroscopic Method for Identification of Clinically Relevant Microorganisms Growing on Solid Culture Medium. Anal. Chem. 72, 12–19. https://doi.org/10.1021/ac991011h
[37] Jarvis, R.M., Brooker, A., Goodacre, R., 2006. Surface-enhanced Raman scattering for the rapid discrimination of bacteria. Faraday Discuss. 132, 281–292. https://doi.org/10.1039/B506413A
[38] Rehse, S.J., 2019. A review of the use of laser-induced breakdown spectroscopy for bacterial classification, quantification, and identification. Spectrochimica Acta Part B: Atomic Spectroscopy 154, 50–69. https://doi.org/10.1016/j.sab.2019.02.005
[39] Karasinski, J., White, L., Zhang, Y., Wang, E., Andreescu, S., Sadik, O.A., Lavine, B.K., Vora, M., 2007. Detection and identification of bacteria using antibiotic susceptibility and a multi-array electrochemical sensor with pattern recognition. Biosensors and Bioelectronics 22, 2643–2649. https://doi.org/10.1016/j.bios.2006.10.037
[40] Yu, L., Hao, L., Meiqiong, T., Jiaoqi, H., Wei, L., Jinying, D., Xueping, C., Weiling, F., Yang, Z., 2019. The medical application of terahertz technology in non-invasive detection of cells and tissues: opportunities and challenges. RSC Adv. 9, 9354–9363. https://doi.org/10.1039/C8RA10605C

[41] Galikowska, E., Kunikowska, D., Tokarska-Pietrzak, E., Dziadziuszko, H., Łoś, J.M., Golec, P., Węgrzyn, G., Łoś, M., 2011. Specific detection of Salmonella enterica and Escherichia coli strains by using ELISA with bacteriophages as recognition agents. Eur J Clin Microbiol Infect Dis 30, 1067–1073. https://doi.org/10.1007/s10096-011-1193-2

[42] Vangindertael, J., Camacho, R., Sempels, W., Mizuno, H., Dedecker, P., Janssen, K.P.F., 2018. An introduction to optical super-resolution microscopy for the adventurous biologist. Methods Appl. Fluoresc. 6, 022003. https://doi.org/10.1088/2050-6120/aaae0c

[43] Sun, Y., Hays, N.M., Periasamy, A., Davidson, M.W., Day, R.N., 2012. Monitoring Protein Interactions in Living Cells with Fluorescence Lifetime Imaging Microscopy, in: Methods in Enzymology. Elsevier, pp. 371–391. https://doi.org/10.1016/B978-0-12-391857-4.00019-7

[44] Schwarz, J.M., Lüpken, R., Seelow, D., Kehr, B., 2021. Novel sequencing technologies and bioinformatic tools for deciphering the non-coding genome. Medizinische Genetik 33, 133–145. https://doi.org/10.1515/medgen-2021-2072

[45] Ammor, M.S., 2007. Recent Advances in the Use of Intrinsic Fluorescence for Bacterial Identification and Characterization. J Fluoresc 17, 455–459. https://doi.org/10.1007/s10895-007-0180-6

[46] Zhao, M., Gao, X., Tao, Z., Wang, X., Lin, X., Wang, S., Liu, Y., 2020. Sugar-metabolism-triggered pathogenic bacteria identification based on pH-sensitive fluorescent carbon dots. Sensors and Actuators B: Chemical 316, 128063. https://doi.org/10.1016/j.snb.2020.128063

[47] Frickmann, H., Zautner, A.E., Moter, A., Kikhney, J., Hagen, R.M., Stender, H., Poppert, S., 2017. Fluorescence *in situ* hybridization (FISH) in the microbiological diagnostic routine laboratory: a review. Critical Reviews in Microbiology 43, 263–293. https://doi.org/10.3109/1040841X.2016.1169990

[48] Ammor, M.S., Delgado, S., Álvarez-Martín, P., Margolles, A., Mayo, B., 2007. Reagentless identification of human bifidobacteria by intrinsic fluorescence. Journal of Microbiological Methods 69, 100–106. https://doi.org/10.1016/j.mimet.2006.12.005

[49] Ammor, S., Yaakoubi, K., Chevallier, I., Dufour, E., 2004. Identification by fluorescence spectroscopy of lactic acid bacteria isolated from a small-scale facility producing traditional dry sausages. Journal of Microbiological Methods 59, 271–281. https://doi.org/10.1016/j.mimet.2004.07.014

[50] Powell, J.L., Bailey, C.L., Coopland, A.T., Otis, C.N., Frank, J.L., Meyer, I., 1994. Nd:YAG laser excision of a giant gingival pyogenic granuloma of pregnancy. Lasers Surg Med 14, 178–183. https://doi.org/10.1002/1096-9101(1994)14:2<178::aid-lsm1900140211>3.0.co;2-w

[51] Alimova, A., Katz, A., Savage, H.E., Shah, M., Minko, G., Will, D.V., Rosen, R.B., McCormick, S.A., Alfano, R.R., 2003. Native fluorescence and excitation spectroscopic changes in *Bacillus subtilis* and *Staphylococcus aureus* bacteria subjected to conditions of starvation. Appl. Opt. 42, 4080. https://doi.org/10.1364/AO.42.004080

[52] Agranovski, V., Ristovski, Z.D., 2005. Real-time monitoring of viable bioaerosols: capability of the UVAPS to predict the amount of individual microorganisms in aerosol particles. Journal of Aerosol Science 36, 665–676. https://doi.org/10.1016/j.jaerosci.2004.12.005

[53] Alimova, A., Katz, A., Siddique, M., Minko, G., Savage, H.E., Shah, M.K., Rosen, R.B., Alfano, R.R., 2005. Native fluorescence changes induced by bactericidal agents. IEEE Sensors J. 5, 704–711. https://doi.org/10.1109/JSEN.2005.845521
[54] Irenge, L.M., Dindart, J.-M., Gala, J.-L., 2017. Biochemical testing in a laboratory tent and semi-intensive care of Ebola patients on-site in a remote part of Guinea: a paradigm shift based on a bleach-sensitive point-of-care device. Clinical Chemistry and Laboratory Medicine (CCLM) 55. https://doi.org/10.1515/cclm-2016-0456
[55] Yoo, J.-H., 2018. Review of Disinfection and Sterilization – Back to the Basics. Infect Chemother 50, 101. https://doi.org/10.3947/ic.2018.50.2.101
[56] MIT EHS, n.d. Decontamination and Disinfection [WWW Document]. Decontamination and Disinfection. URL https://ehs.mit.edu/biological-program/decontamination-and-disinfection (accessed 5.5.22).
[57] Linley, E., Denyer, S.P., McDonnell, G., Simons, C., Maillard, J.-Y., 2012. Use of hydrogen peroxide as a biocide: new consideration of its mechanisms of biocidal action. Journal of Antimicrobial Chemotherapy 67, 1589–1596. https://doi.org/10.1093/jac/dks129
[58] Anthrax in Humans and Animals. 4th edition. Geneva: World Health Organization; 2008. Annex 3, Disinfection, decontamination, fumigation, incineration. Available from: https://www.ncbi.nlm.nih.gov/books/NBK310477/
[59] Ramm, L., Siani, H., Wesgate, R., Maillard, J.-Y., 2015. Pathogen transfer and high variability in pathogen removal by detergent wipes. American Journal of Infection Control 43, 724–728. https://doi.org/10.1016/j.ajic.2015.03.024
[60] Boyce, J.M., Sullivan, L., Booker, A., Baker, J., 2016. Quaternary Ammonium Disinfectant Issues Encountered in an Environmental Services Department. Infect. Control Hosp. Epidemiol. 37, 340–342. https://doi.org/10.1017/ice.2015.299
[61] Boyce, J.M., 2016. Modern technologies for improving cleaning and disinfection of environmental surfaces in hospitals. Antimicrob Resist Infect Control 5, 10. https://doi.org/10.1186/s13756-016-0111-x
[62] Rutala, W.A., Gergen, M.F., Weber, D.J., 2007. Microbiologic evaluation of microfiber mops for surface disinfection. American Journal of Infection Control 35, 569–573. https://doi.org/10.1016/j.ajic.2007.02.009
[63] Boyce, J.M., Havill, N.L., Lipka, A., Havill, H., Rizvani, R., 2010. Variations in Hospital Daily Cleaning Practices. Infect. Control Hosp. Epidemiol. 31, 99–101. https://doi.org/10.1086/649225
[64] Berrington, A.W., Pedler, S.J., 1998. Investigation of gaseous ozone for MRSA decontamination of hospital side-rooms. Journal of Hospital Infection 40, 61–65. https://doi.org/10.1016/S0195-6701(98)90026-3
[65] Unal, N., Yanik, K., Karadag, A., Odabaşı, H., Esen, S., Günaydin, M., 2014. Evaluation of the efficacy of akacid plus® fogging in eradicating causative microorganism in nosocomial infections. Int J Clin Exp Med 7, 5867–5871.
[66] Chen, T.-L., Chen, Y.-H., Zhao, Y.-L., Chiang, P.-C., 2020. Application of Gaseous ClO2 on Disinfection and Air Pollution Control: A Mini Review. Aerosol Air Qual. Res. 20, 2289–2298. https://doi.org/10.4209/aaqr.2020.06.0330
[67] Holmdahl, T., Lanbeck, P., Wullt, M., Walder, M.H., 2011. A Head-to-Head Comparison of Hydrogen Peroxide Vapor and Aerosol Room Decontamination Systems. Infect. Control Hosp. Epidemiol. 32, 831–836. https://doi.org/10.1086/661104

[68] Finnegan, M., Linley, E., Denyer, S.P., McDonnell, G., Simons, C., Maillard, J.-Y., 2010. Mode of action of hydrogen peroxide and other oxidizing agents: differences between liquid and gas forms. Journal of Antimicrobial Chemotherapy 65, 2108–2115. https://doi.org/10.1093/jac/dkq308

[69] Malik, D.J., Shaw, C.M., Rielly, C.D., Shama, G., 2013. The inactivation of *Bacillus subtilis* spores at low concentrations of hydrogen peroxide vapour. Journal of Food Engineering 114, 391–396. https://doi.org/10.1016/j.jfoodeng.2012.08.031

[70] Watson, F., Keevil, C.W., Wilks, S.A., Chewins, J., 2018. Modelling vaporised hydrogen peroxide efficacy against mono-species biofilms. Sci Rep 8, 12257. https://doi.org/10.1038/s41598-018-30706-0

[71] Babichenko, S., Poryvkina, L., Rebane, O., Sobolev, I., 2016. Compact HLIF LiDAR for marine applications. International Journal of Remote Sensing 37, 3924–3937. https://doi.org/10.1080/01431161.2016.1204479

[72] Giamarchi, P., Burel, L., Stephan, L., Lijour, Y., Bihan, A.L., 2002. Laser-induced fluorescence with an OPO system. Part I. Optimisation of the analytical system by use of experimental design methodology. Application to the direct quantification of traces of benzo[a]pyrene. Analytical and Bioanalytical Chemistry 374, 490–497. https://doi.org/10.1007/s00216-002-1472-y

[73] Babichenko, S., Poryvkina, L., Leeben, A., n.d. Spectral fluorescent signatures (SFS) in characterisation of water environment. Presented at the 3rd EARSEL Workshop on Laser Remote Sensing of Land and Sea, Tallinn, pp. 140–144.

[74] Pöhlker, C., Huffman, J.A., Pöschl, U., 2012. Autofluorescence of atmospheric bioaerosols – fluorescent biomolecules and potential interferences. Atmos. Meas. Tech. 5, 37–71. https://doi.org/10.5194/amt-5-37-2012

[75] Khan, A., 2020. The Evolution Of The Deep-UV LED [WWW Document]. The Evolution Of The Deep-UV LED. URL https://compoundsemiconductor.net/article/112266/The_Evolution_Of_The_Deep-UV_LED/feature (accessed 5.5.22).

[76] Recker, M.C., Cazalas, E.J., McClory, J.W., Bevins, J.E., 2019. Comparison of SiPM and PMT Performance Using a Cs_2LiYCl_6: Ce^{3+} (CLYC) Scintillator With Two Optical Windows. IEEE Trans. Nucl. Sci. 66, 1959–1965. https://doi.org/10.1109/TNS.2019.2926246

[77] Turner, W.C., Kausrud, K.L., Beyer, W., Easterday, W.R., Barandongo, Z.R., Blaschke, E., Cloete, C.C., Lazak, J., Van Ert, M.N., Ganz, H.H., Turnbull, P.C.B., Stenseth, N.Chr., Getz, W.M., 2016. Lethal exposure: An integrated approach to pathogen transmission via environmental reservoirs. Sci Rep 6, 27311. https://doi.org/10.1038/srep27311

[78] Robilotti, E., Deresinski, S., Pinsky, B.A., 2015. Norovirus. Clin Microbiol Rev 28, 134–164. https://doi.org/10.1128/CMR.00075-14

[79] Christenson, E.C., Cronk, R., Atkinson, H., Bhatt, A., Berdiel, E., Cawley, M., Cho, G., Coleman, C.K., Harrington, C., Heilferty, K., Fejfar, D., Grant, E.J., Grigg, K., Joshi, T., Mohan, S., Pelak, G., Shu, Y., Bartram, J., 2021. Evidence Map and Systematic Review of Disinfection Efficacy on Environmental Surfaces in Healthcare Facilities. IJERPH 18, 11100. https://doi.org/10.3390/ijerph182111100

[80] Rasko, D.A., Worsham, P.L., Abshire, T.G., Stanley, S.T., Bannan, J.D., Wilson, M.R., Langham, R.J., Decker, R.S., Jiang, L., Read, T.D., Phillippy, A.M., Salzberg, S.L., Pop, M., Van Ert, M.N., Kenefic, L.J., Keim, P.S., Fraser-Liggett, C.M., Ravel, J., 2011. *Bacillus anthracis* comparative genome analysis in support

of the Amerithrax investigation. Proc. Natl. Acad. Sci. U.S.A. 108, 5027–5032. https://doi.org/10.1073/pnas.1016657108
[81] Sweeney, D.A., Hicks, C.W., Cui, X., Li, Y., Eichacker, P.Q., 2011. Anthrax Infection. Am J Respir Crit Care Med 184, 1333–1341. https://doi.org/10.1164/rccm.201102-0209CI
[82] Marquis, R.E., 1998. Bacterial Spores - resistance, dormancy and water status, in: Reid, D.S. (Ed.), The Properties of Water in Foods ISOPOW 6. Springer US, Boston, MA, pp. 486–504. https://doi.org/10.1007/978-1-4613-0311-4_22
[83] Pottage, T., Macken, S., Giri, K., Walker, J.T., Bennett, A.M., 2012. Low-Temperature Decontamination with Hydrogen Peroxide or Chlorine Dioxide for Space Applications. Appl Environ Microbiol 78, 4169–4174. https://doi.org/10.1128/AEM.07948-11
[84] Zhdanova, N.G., Shirshin, E.A., Maksimov, E.G., Panchishin, I.M., Saletsky, A.M., Fadeev, V.V., 2015. Tyrosine fluorescence probing of the surfactant-induced conformational changes of albumin. Photochem. Photobiol. Sci. 14, 897–908. https://doi.org/10.1039/C4PP00432A
[85] Gakamsky, A., Duncan, R.R., Howarth, N.M., Dhillon, B., Buttenschön, K.K., Daly, D.J., Gakamsky, D., 2017. Tryptophan and Non-Tryptophan Fluorescence of the Eye Lens Proteins Provides Diagnostics of Cataract at the Molecular Level. Sci Rep 7, 40375. https://doi.org/10.1038/srep40375
[86] Tikhonova, T.N., Rovnyagina, N.R., Zherebker, A.Y., Sluchanko, N.N., Rubekina, A.A., Orekhov, A.S., Nikolaev, E.N., Fadeev, V.V., Uversky, V.N., Shirshin, E.A., 2018. Dissection of the deep-blue autofluorescence changes accompanying amyloid fibrillation. Archives of Biochemistry and Biophysics 651, 13–20. https://doi.org/10.1016/j.abb.2018.05.019
[87] Semenov, A.N., Yakimov, B.P., Rubekina, A.A., Gorin, D.A., Drachev, V.P., Zarubin, M.P., Velikanov, A.N., Lademann, J., Fadeev, V.V., Priezzhev, A.V., Darvin, M.E., Shirshin, E.A., 2020a. The Oxidation-Induced Autofluorescence Hypothesis: Red Edge Excitation and Implications for Metabolic Imaging. Molecules 25, 1863. https://doi.org/10.3390/molecules25081863
[88] Pärna, R., Sankari, R., Kukk, E., Nõmmiste, E., Valden, M., Lastusaari, M., Kooser, K., Kokko, K., Hirsimäki, M., Urpelainen, S., Turunen, P., Kivimäki, A., Pankratov, V., Reisberg, L., Hennies, F., Tarawneh, H., Nyholm, R., Huttula, M., 2017. FinEstBeaMS – A wide-range Finnish-Estonian Beamline for Materials Science at the 1.5 GeV storage ring at the MAX IV Laboratory. Nuclear Instruments and Methods in Physics Research Section A: Accelerators, Spectrometers, Detectors and Associated Equipment 859, 83–89. https://doi.org/10.1016/j.nima.2017.04.002
[89] Sinha, R.P., Häder, D.-P., 2002. UV-induced DNA damage and repair: a review. Photochem. Photobiol. Sci. 1, 225–236. https://doi.org/10.1039/b201230h
[90] Oberländer, J., Mayer, M., Greeff, A., Keusgen, M., Schöning, M.J., 2018. Spore-based biosensor to monitor the microbicidal efficacy of gaseous hydrogen peroxide sterilization processes. Biosensors and Bioelectronics 104, 87–94. https://doi.org/10.1016/j.bios.2017.12.045
[91] Arreola, J., Keusgen, M., Wagner, T., Schöning, M.J., 2019. Combined calorimetric gas- and spore-based biosensor array for online monitoring and sterility assurance of gaseous hydrogen peroxide in aseptic filling machines. Biosensors and Bioelectronics 143, 111628. https://doi.org/10.1016/j.bios.2019.111628

[92] Melly, E., Cowan, A.E., Setlow, P., 2002. Studies on the mechanism of killing of *Bacillus subtilis* spores by hydrogen peroxide. J Appl Microbiol 93, 316–325. https://doi.org/10.1046/j.1365-2672.2002.01687.x

[93] Hertwig, C., Reineke, K., Rauh, C., Schlüter, O., 2017. Factors involved in *Bacillus* spore's resistance to cold atmospheric pressure plasma. Innovative Food Science & Emerging Technologies 43, 173–181. https://doi.org/10.1016/j.ifset.2017.07.031

[94] Plomp, M., Carroll, A.M., Setlow, P., Malkin, A.J., 2014. Architecture and Assembly of the *Bacillus subtilis* Spore Coat. PLoS ONE 9, e108560. https://doi.org/10.1371/journal.pone.0108560

13. PUBLICATIONS

CURRICULUM VITAE

Name: Ott Rebane
Date of birth: August 3, 1986
Citizenship: Estonian
Address: Institute of Physics, University of Tartu, W. Ostwald Str. 1, 50411, Estonia
E-mail: ott.rebane@ut.ee

Current position: Project Manager, LDI Innovation OÜ
Industry Liaison Officer, Institute of Physics, University of Tartu

Education:

2009–2011	University of Tartu, MSc in Physics, *cum laude*
2005–2009	University of Tartu, BSc in Physics, *cum laude*
2002–2005	Tallinn Secondary Science School, gold medal

Language skills: Estonian (mother tongue), English (very good), Russian (basic), German (basic)

Institution and position held:

2013–	Project Manager, LDI Innovation Ltd
2013–	Industry Liaison Officer, Institute of Physics, University of Tartu

Research interests:
Conceptual and optical design of photonic sensors based mainly on fluorescence.

Publications:

O. Rebane, M. Kirm, L. Poryvkina, H. Hakkarainen, S. Babichenko, Bacterial spore fluorescence dependence on vaporised hydrogen peroxide concentration, *Proceedings of the Estonian Academy of Sciences*, **71** (2021) 117–126. DOI: doi.org/10.3176/proc.2022.2.02

J. Saaring, A. Vanetsev, K. Chernenko, E. Feldbach, I. Kudryavtseva, H. Mändar, S. Pikker, R. Pärna, V. Nagirnyi, S. Omelkov, I. Romet, **O. Rebane**, M. Kirm. Time-resolved luminescence spectroscopy of ultrafast emissions in $BaGeF_6$. *Journal of Luminescence*, 244 (2022) 116729. DOI: 10.1016/j.jlumin.2022.118729.

O. Rebane, H. Hakkarainen, M. Kirm, L. Poryvkina, I. Sobolev, P. Wilska, S. Babichenko, Real-time monitoring of hydrogen peroxide vapour decontamination of bacterial spores by means of UV fluorimetry, *Proceedings of the Estonian Academy of Sciences*, **70** (2021) 51–61.

J. Saaring, A. Vanetsev, K. Chernenko, E. Feldbach, I. Kudryavtseva, H. Mändar, R. Pärna, V. Nagirnyi, S. Omelkov, I. Romet, **O. Rebane**, M. Kirm. Relaxation of electronic excitations in K_2GeF_6 studied by means of time-resolved luminescence spectroscopy under VUV and pulsed electron beam excitation. *Journal of Alloys and Compounds*, 883, 160916 (2021). DOI: 10.1016/j.jallcom.2021.160916.

J.-L. Gala, **O. Rebane**, J. Ambroise, S. Babichenko, Omar Nyabi, Thierry Hance, Acaricidal efficacy of ultraviolet-C irradiation of *Tetranychus urticae* adults and eggs using a pulsed krypton fuoride excimer laser, *Parasites and Vectors*, 14 (2021). DOI: 10.1186/s13071-021-05085-7

P. Saari, **O. Rebane**, I. Besieris, Energy-flow velocities of nondiffracting localized waves, *Physical Review A*, 100 (2019), ARTN 013849. DOI: 10.1103/PhysRevA.100.013849.

M. Bentahir , S. Babichenko, A.S. Piette, L. Poryvkina, **O. Rebane**, B. Smits, I. Sobolev, N. Soboleva, J.L. Gala, Non-contact, real-time laser-induced fluorescence detection and monitoring of microbial contaminants on solid surfaces before, during and after decontamination. *Journal of Biosensors & Bioelectronics*, **9** (2018).

S. Babichenko, L. Poryvkina, I. Sobolev, **O. Rebane**, Compact HLIF LiDAR for marine applications. *International Journal of Remote Sensing*, 37 (2016), 3924−3937. DOI: 10.1080/01431161.2016.1204479.

V. Mitev, S. Babichenko, J. Bennes; R. Borelli, A. Dolfi-Bouteyre, L. Fiorani, L. Hespel, T. Huet, A. Palucci, M. Pistilli, A. Puiu, **O. Rebane**, I. Sobolev, Mid-IR DIAL for high-resolution mapping of explosive precursors. In: U. N. Singh; G. Pappalardo (Ed.). Lidar Technologies, Techniques, and Measurements for Atmospheric Remote Sensing IX (1−13), 2013. SPIE. (*Proceedings of SPIE*; 8894). DOI: 10.1117/12.2028374.

O. Rebane, M. Lõhmus, P. Saari, Image formation of radially and temporally truncated bessel beams. *Lithuanian Journal of Physics*, 50 (2010), 89−94. DOI: 10.3952/lithjphys.50103.

Book chapters:

O. Rebane, S. Babichenko, M. Bentahir, L. Poryvkina, J.-L. Gala. "Non-Contact Real-Time Detection and Monitoring of Microbial Contaminants on Solid Surfaces Using Medium- (BC-Sense) and Short-Distance (H2B-Spectral) Range Sensors". In: Prime Archives in Public Health. Hyderabad, India: Vide Leaf. 2021

Conference presentations:

O. Rebane, "Active Hyperspectral technique for detection of bio and chemical threats in various environments". Oral presentation at the Northern Optics and Photonics international conference, 13.09.2018, Lund, Sweden.

O. Rebane, S. Babichenko, M. Kirm, L. Poryvkina, I. Sobolev, "Autofluorescence detectors development for pathogen decontamination efficiency

quantification on surfaces". Poster presentation at the Functional Materials and Nanotechnologies international conference, 2018, Riga, Latvia.

O. Rebane, S. Babichenko, M. Kirm, L. Poryvkina, I. Sobolev, "Monitoring Pathogen Decontamination Efficiency Using Autofluorescence Spectra". Poster presentation at the annual conference of the Graduate School of Functional Materials and Technologies, 04.-05.02.2019, Tartu, Estonia.

O. Rebane, S. Babichenko, M. Bentahir, A.S. Piette, L. Poryvkina, B. Smits, I. Sobolev, N. Soboleva, J.L. Gala, "Non-Contact Real-Time Detection and Monitoring of Microbial Contaminants on Solid Surfaces". Oral presentation at the Analytix Congress international conference, 13.11.2019, Berlin, Germany.

O. Rebane, M. Kirm, L. Poryvkina, I. Sobolev, S. Babichenko, "Photonic solutions for monitoring of pathogen decontamination efficiency". Oral presentation at the Functional Materials and Nanotechnologies international online conference, 2020, Vilnius, Lithuania.

O. Rebane, M. Kirm, L. Poryvkina, I. Sobolev, S. Babichenko, "Development of photonic sensor for real-time monitoring of H_2O_2 vapor decontamination process using model pathogens". Oral presentation at the annual conference of the Graduate School of Functional Materials and Technologies, 04.02.2020, Tallinn, Estonia.

O. Rebane, M. Kirm, L. Poryvkina, S.Babichenko, "Fluorescence Dependence on Vaporised Hydrogen Peroxide Concentration of Bacterial Spores". Poster presentation at the annual conference of the Graduate School of Functional Materials and Technologies, 14.–15.06.2021, Tartu, Estonia.

O. Rebane, M. Kirm, V. Nagirnyi, I. Romet, "Time-resolved fluorescence study of bacterial spores treated by hydrogen peroxide vapour for monitoring decontamination process". Oral presentation at the LUMDETR international conference, 16.09.2021, Bydgoszcz, Poland.

O. Rebane, M. Kirm, L. Poryvkina, S. Babichenko, "Development of photonic sensor for monitoring of hydrogen peroxide vapour decontamination". Oral presentation at the Baltic Photonics Virtual Vilnius event, 2021, Vilnius, Lithuania.

O. Rebane, M. Kirm, V. Nagirnyi, J. Saaring, "Time-resolved fluorescence of bacterial spores decontaminated by vaporised hydrogen peroxide". Oral presentation at the annual conference of the Graduate School of Functional Materials and Technologies, 17.05.2022, Tallinn, Estonia.

O. Rebane, M. Kirm, V. Nagirnyi, J. Saaring, "Time-resolved fluorescence to determine the viability of bacterial spores". Poster presentation at the joint FMNT and NIBS international conference, 04.07.2022, Riga, Latvia.

Awards and scholarships:

2020 Functional Materials and Technologies Graduate School travel scholarship to attend FinEstBeams beamtime in MAX-IV Lund 24.09–29.09.2020

2020 Functional Materials and Technologies Graduate School travel scholarship to attend FinEstBeams beamtime in MAX-IV Lund 29.01–02.02.2020
2019 Functional Materials and Technologies Graduate School travel scholarship to attend Excimer laser experiments with mites in CTMA, UCL, Brussels, 23.04–26.04.2019.
2009 University of Tartu, Institute of Physics student scholarship

Other activities and membership:

2020, 2021 reviewer of Estonian National Contest for University Students
2021 supervisor of student work practice for Eino Johannes Tiirinen and Rimmo Rõõm
2018 supervisor of student work practice for Hans Daniel Kaimre
2017–... Industry Liaison Officer for F4E/ITER
2013–... Industry Liaison Officer for European Spallation Source
2012–... member of the board of the Baltic Photonics Cluster
2009–2022 assessor of Estonian National Olympiade in Physics

Courses attended:

Training of presentation skills for GSFMT PhD students 2020 March.

ELULOOKIRJELDUS

Nimi: Ott Rebane
Sünniaeg: 3. august 1986
Kodakondsus: Eesti
Aadress: Füüsika Instituut, Tartu Ülikool, W. Ostwaldi tn 1, 50411, Tartu
E-post: ott.rebane@ut.ee

Praegune töökoht: projektijuht, LDI Innovation OÜ
tööstussuhete ekspert, Füüsika Instituut, Tartu Ülikool

Haridus:

2009–2011	Tartu Ülikool, loodusteaduste magister (MSc), füüsika, *cum laude*
2005–2009	Tartu Ülikool, loodusteaduste bakalaureuse kraad (BSc), füüsika, *cum laude*
2002–2005	Tallinna Reaalkool, kuldmedal

Keelteoskus: eesti (emakeel), inglise (väga hea), vene (baasteadmised), saksa (baasteadmised)

Töökogemus:

2013 –	Projektijuht, LDI Innovation OÜ
2013 –	Tööstussuhete ekspert, Füüsika Instituut, Tartu Ülikool

Peamised uurimisvaldkonnad:
Fluorestsentsil põhinevate fotoonikaseadmete kontseptuaalne ja optiline arendus.

DISSERTATIONES PHYSICAE UNIVERSITATIS TARTUENSIS

1. **Andrus Ausmees.** XUV-induced electron emission and electron-phonon interaction in alkali halides. Tartu, 1991.
2. **Heiki Sõnajalg.** Shaping and recalling of light pulses by optical elements based on spectral hole burning. Tartu, 1991.
3. **Sergei Savihhin.** Ultrafast dynamics of F-centers and bound excitons from picosecond spectroscopy data. Tartu, 1991.
4. **Ergo Nõmmiste.** Leelishalogeniidide röntgenelektronemissioon kiiritamisel footonitega energiaga 70–140 eV. Tartu, 1991.
5. **Margus Rätsep.** Spectral gratings and their relaxation in some low-temperature impurity-doped glasses and crystals. Tartu, 1991.
6. **Tõnu Pullerits.** Primary energy transfer in photosynthesis. Model calculations. Tartu, 1991.
7. **Olev Saks.** Attoampri diapasoonis voolude mõõtmise füüsikalised alused. Tartu, 1991.
8. **Andres Virro.** AlGaAsSb/GaSb heterostructure injection lasers. Tartu, 1991.
9. **Hans Korge.** Investigation of negative point discharge in pure nitrogen at atmospheric pressure. Tartu, 1992.
10. **Jüri Maksimov.** Nonlinear generation of laser VUV radiation for high-resolution spectroscopy. Tartu, 1992.
11. **Mark Aizengendler.** Photostimulated transformation of aggregate defects and spectral hole burning in a neutron-irradiated sapphire. Tartu, 1992.
12. **Hele Siimon.** Atomic layer molecular beam epitaxy of A^2B^6 compounds described on the basis of kinetic equations model. Tartu, 1992.
13. **Tõnu Reinot.** The kinetics of polariton luminescence, energy transfer and relaxation in anthracene. Tartu, 1992.
14. **Toomas Rõõm.** Paramagnetic H^{2-} and F^+ centers in CaO crystals: spectra, relaxation and recombination luminescence. Tallinn, 1993.
15. **Erko Jalviste.** Laser spectroscopy of some jet-cooled organic molecules. Tartu, 1993.
16. **Alvo Aabloo.** Studies of crystalline celluloses using potential energy calculations. Tartu, 1994.
17. **Peeter Paris.** Initiation of corona pulses. Tartu, 1994.
18. **Павел Рубин.** Локальные дефектные состояния в CuO_2 плоскостях высокотемпературных сверхпроводников. Тарту, 1994.
19. **Olavi Ollikainen.** Applications of persistent spectral hole burning in ultrafast optical neural networks, time-resolved spectroscopy and holographic interferometry. Tartu, 1996.
20. **Ülo Mets.** Methodological aspects of fluorescence correlation spectroscopy. Tartu, 1996.
21. **Mikhail Danilkin.** Interaction of intrinsic and impurity defects in CaS:Eu luminophors. Tartu, 1997.

22. **Ирина Кудрявцева.** Создание и стабилизация дефектов в кристаллах KBr, KCl, RbCl при облучении ВУФ-радиацией. Тарту, 1997.
23. **Andres Osvet.** Photochromic properties of radiation-induced defects in diamond. Tartu, 1998.
24. **Jüri Örd.** Classical and quantum aspects of geodesic multiplication. Tartu, 1998.
25. **Priit Sarv.** High resolution solid-state NMR studies of zeolites. Tartu, 1998.
26. **Сергей Долгов.** Электронные возбуждения и дефектообразование в некоторых оксидах металлов. Тарту, 1998.
27. **Kaupo Kukli.** Atomic layer deposition of artificially structured dielectric materials. Tartu, 1999.
28. **Ivo Heinmaa.** Nuclear resonance studies of local structure in $RBa_2Cu_3O_{6+x}$ compounds. Tartu, 1999.
29. **Aleksander Shelkan.** Hole states in CuO_2 planes of high temperature superconducting materials. Tartu, 1999.
30. **Dmitri Nevedrov.** Nonlinear effects in quantum lattices. Tartu, 1999.
31. **Rein Ruus.** Collapse of 3d (4f) orbitals in 2p (3d) excited configurations and its effect on the x-ray and electron spectra. Tartu, 1999.
32. **Valter Zazubovich.** Local relaxation in incommensurate and glassy solids studied by Spectral Hole Burning. Tartu, 1999.
33. **Indrek Reimand.** Picosecond dynamics of optical excitations in GaAs and other excitonic systems. Tartu, 2000.
34. **Vladimir Babin.** Spectroscopy of exciton states in some halide macro- and nanocrystals. Tartu, 2001.
35. **Toomas Plank.** Positive corona at combined DC and AC voltage. Tartu, 2001.
36. **Kristjan Leiger.** Pressure-induced effects in inhomogeneous spectra of doped solids. Tartu, 2002.
37. **Helle Kaasik.** Nonperturbative theory of multiphonon vibrational relaxation and nonradiative transitions. Tartu, 2002.
38. **Tõnu Laas.** Propagation of waves in curved spacetimes. Tartu, 2002.
39. **Rünno Lõhmus.** Application of novel hybrid methods in SPM studies of nanostructural materials. Tartu, 2002.
40. **Kaido Reivelt.** Optical implementation of propagation-invariant pulsed free-space wave fields. Tartu, 2003.
41. **Heiki Kasemägi.** The effect of nanoparticle additives on lithium-ion mobility in a polymer electrolyte. Tartu, 2003.
42. **Villu Repän.** Low current mode of negative corona. Tartu, 2004.
43. **Алексей Котлов.** Оксианионные диэлектрические кристаллы: зонная структура и электронные возбуждения. Tartu, 2004.
44. **Jaak Talts.** Continuous non-invasive blood pressure measurement: comparative and methodological studies of the differential servo-oscillometric method. Tartu, 2004.
45. **Margus Saal.** Studies of pre-big bang and braneworld cosmology. Tartu, 2004.

46. **Eduard Gerškevitš.** Dose to bone marrow and leukaemia risk in external beam radiotherapy of prostate cancer. Tartu, 2005.
47. **Sergey Shchemelyov.** Sum-frequency generation and multiphoton ionization in xenon under excitation by conical laser beams. Tartu, 2006.
48. **Valter Kiisk.** Optical investigation of metal-oxide thin films. Tartu, 2006.
49. **Jaan Aarik.** Atomic layer deposition of titanium, zirconium and hafnium dioxides: growth mechanisms and properties of thin films. Tartu, 2007.
50. **Astrid Rekker.** Colored-noise-controlled anomalous transport and phase transitions in complex systems. Tartu, 2007.
51. **Andres Punning.** Electromechanical characterization of ionic polymer-metal composite sensing actuators. Tartu, 2007.
52. **Indrek Jõgi.** Conduction mechanisms in thin atomic layer deposited films containing TiO_2. Tartu, 2007.
53. **Aleksei Krasnikov.** Luminescence and defects creation processes in lead tungstate crystals. Tartu, 2007.
54. **Küllike Rägo.** Superconducting properties of MgB_2 in a scenario with intra- and interband pairing channels. Tartu, 2008.
55. **Els Heinsalu.** Normal and anomalously slow diffusion under external fields. Tartu, 2008.
56. **Kuno Kooser.** Soft x-ray induced radiative and nonradiative core-hole decay processes in thin films and solids. Tartu, 2008.
57. **Vadim Boltrushko.** Theory of vibronic transitions with strong nonlinear vibronic interaction in solids. Tartu, 2008.
58. **Andi Hektor.** Neutrino Physics beyond the Standard Model. Tartu, 2008.
59. **Raavo Josepson.** Photoinduced field-assisted electron emission into gases. Tartu, 2008.
60. **Martti Pärs.** Study of spontaneous and photoinduced processes in molecular solids using high-resolution optical spectroscopy. Tartu, 2008.
61. **Kristjan Kannike.** Implications of neutrino masses. Tartu, 2008.
62. **Vigen Issahhanjan.** Hole and interstitial centres in radiation-resistant MgO single crystals. Tartu, 2008.
63. **Veera Krasnenko.** Computational modeling of fluorescent proteins. Tartu, 2008.
64. **Mait Müntel.** Detection of doubly charged higgs boson in the CMS detector. Tartu, 2008.
65. **Kalle Kepler.** Optimisation of patient doses and image quality in diagnostic radiology. Tartu, 2009.
66. **Jüri Raud.** Study of negative glow and positive column regions of capillary HF discharge. Tartu, 2009.
67. **Sven Lange.** Spectroscopic and phase-stabilisation properties of pure and rare-earth ions activated ZrO_2 and HfO_2. Tartu, 2010.
68. **Aarne Kasikov.** Optical characterization of inhomogeneous thin films. Tartu, 2010.
69. **Heli Valtna-Lukner.** Superluminally propagating localized optical pulses. Tartu, 2010.

70. **Artjom Vargunin.** Stochastic and deterministic features of ordering in the systems with a phase transition. Tartu, 2010.
71. **Hannes Liivat.** Probing new physics in e+e− annihilations into heavy particles via spin orientation effects. Tartu, 2010.
72. **Tanel Mullari.** On the second order relativistic deviation equation and its applications. Tartu, 2010.
73. **Aleksandr Lissovski.** Pulsed high-pressure discharge in argon: spectroscopic diagnostics, modeling and development. Tartu, 2010.
74. **Aile Tamm.** Atomic layer deposition of high-permittivity insulators from cyclopentadienyl-based precursors. Tartu, 2010.
75. **Janek Uin.** Electrical separation for generating standard aerosols in a wide particle size range. Tartu, 2011.
76. **Svetlana Ganina.** Hajusandmetega ülesanded kui üks võimalus füüsikaõppe efektiivsuse tõstmiseks. Tartu, 2011
77. **Joel Kuusk.** Measurement of top-of-canopy spectral reflectance of forests for developing vegetation radiative transfer models. Tartu, 2011.
78. **Raul Rammula**. Atomic layer deposition of HfO_2 – nucleation, growth and structure development of thin films. Tartu, 2011.
79. **Сергей Наконечный.** Исследование электронно-дырочных и интерстициал-вакансионных процессов в монокристаллах MgO и LiF методами термоактивационной спектроскопии. Тарту, 2011.
80. **Niina Voropajeva.** Elementary excitations near the boundary of a strongly correlated crystal. Tartu, 2011.
81. **Martin Timusk.** Development and characterization of hybrid electro-optical materials. Tartu, 2012, 106 p.
82. **Merle Lust.** Assessment of dose components to Estonian population. Tartu, 2012, 84 p.
83. **Karl Kruusamäe.** Deformation-dependent electrode impedance of ionic electromechanically active polymers. Tartu, 2012, 128 p.
84. **Liis Rebane.** Measurement of the $W \to \tau\nu$ cross section and a search for a doubly charged Higgs boson decaying to τ-leptons with the CMS detector. Tartu, 2012, 156 p.
85. **Jevgeni Šablonin.** Processes of structural defect creation in pure and doped MgO and NaCl single crystals under condition of low or super high density of electronic excitations. Tartu, 2013, 145 p.
86. **Riho Vendt**. Combined method for establishment and dissemination of the international temperature scale. Tartu, 2013, 108 p.
87. **Peeter Piksarv.** Spatiotemporal characterization of diffractive and non-diffractive light pulses. Tartu, 2013, 156 p.
88. **Anna Šugai.** Creation of structural defects under superhigh-dense irradiation of wide-gap metal oxides. Tartu, 2013, 108 p.
89. **Ivar Kuusik.** Soft X-ray spectroscopy of insulators. Tartu, 2013, 113 p.
90. **Viktor Vabson**. Measurement uncertainty in Estonian Standard Laboratory for Mass. Tartu, 2013, 134 p.

91. **Kaupo Voormansik.** X-band synthetic aperture radar applications for environmental monitoring. Tartu, 2014, 117 p.
92. **Deivid Pugal.** hp-FEM model of IPMC deformation. Tartu, 2014, 143 p.
93. **Siim Pikker.** Modification in the emission and spectral shape of photostable fluorophores by nanometallic structures. Tartu, 2014, 98 p.
94. **Mihkel Pajusalu**. Localized Photosynthetic Excitons. Tartu, 2014, 183 p.
95. **Taavi Vaikjärv.** Consideration of non-adiabaticity of the Pseudo-Jahn-Teller effect: contribution of phonons. Tartu, 2014, 129 p.
96. **Martin Vilbaste.** Uncertainty sources and analysis methods in realizing SI units of air humidity in Estonia. Tartu, 2014, 111 p.
97. **Mihkel Rähn.** Experimental nanophotonics: single-photon sources- and nanofiber-related studies. Tartu, 2015, 107 p.
98. **Raul Laasner.** Excited state dynamics under high excitation densities in tungstates. Tartu, 2015, 125 p.
99. **Andris Slavinskis.** EST Cube-1 attitude determination. Tartu, 2015, 104 p.
100. **Karlis Zalite**. Radar Remote Sensing for Monitoring Forest Floods and Agricultural Grasslands. Tartu, 2016, 124 p.
101. **Kaarel Piip.** Development of LIBS for *in-situ* study of ITER relevant materials. Tartu, 2016, 93 p.
102. **Kadri Isakar.** ^{210}Pb in Estonian air: long term study of activity concentrations and origin of radioactive lead. Tartu, 2016, 107 p.
103. **Artur Tamm.** High entropy alloys: study of structural properties and irradiation response. Tartu, 2016, 115 p.
104. **Rasmus Talviste.** Atmospheric-pressure He plasma jet: effect of dielectric tube diameter. Tartu, 2016, 107 p.
105. **Andres Tiko.** Measurement of single top quark properties with the CMS detector. Tartu, 2016, 161 p.
106. **Aire Olesk.** Hemiboreal Forest Mapping with Interferometric Synthetic Aperture Radar. Tartu, 2016, 121 p.
107. **Fred Valk.** Nitrogen emission spectrum as a measure of electric field strength in low-temperature gas discharges. Tartu, 2016, 149 p.
108. **Manoop Chenchiliyan.** Nano-structural Constraints for the Picosecond Excitation Energy Migration and Trapping in Photosynthetic Membranes of Bacteria. Tartu, 2016, 115p.
109. **Lauri Kaldamäe.** Fermion mass and spin polarisation effects in top quark pair production and the decay of the higgs boson. Tartu, 2017, 104 p.
110. **Marek Oja.** Investigation of nano-size α- and transition alumina by means of VUV and cathodoluminescence spectroscopy. Tartu, 2017, 89 p.
111. **Viktoriia Levushkina.** Energy transfer processes in the solid solutions of complex oxides. Tartu, 2017, 101 p.
112. **Mikk Antsov.** Tribomechanical properties of individual 1D nanostructures: experimental measurements supported by finite element method simulations. Tartu, 2017, 101 p.

113. **Hardi Veermäe.** Dark matter with long range vector-mediated interactions. Tartu, 2017, 137 p.
114. **Aris Auzans.** Development of computational model for nuclear energy systems analysis: natural resources optimisation and radiological impact minimization. Tartu, 2018, 138 p.
115. **Aleksandr Gurev**. Coherent fluctuating nephelometry application in laboratory practice. Tartu, 2018, 150 p.
116. **Ardi Loot**. Enhanced spontaneous parametric downconversion in plasmonic and dielectric structures. Tartu, 2018, 164 p.
117. **Andreas Valdmann.** Generation and characterization of accelerating light pulses. Tartu, 2019, 85 p.
118. **Mikk Vahtrus.** Structure-dependent mechanical properties of individual one-dimensional metal-oxide nanostructures. Tartu, 2019, 110 p.
119. **Ott Vilson.** Transformation properties and invariants in scalar-tensor theories of gravity. Tartu, 2019, 183 p.
120. **Indrek Sünter.** Design and characterisation of subsystems and software for ESTCube-1 nanosatellite. Tartu, 2019, 195 p.
121. **Marko Eltermann**. Analysis of samarium doped TiO_2 optical and multiresponse oxygen sensing capabilities. Tartu, 2019, 113 p.
122. **Kalev Erme**. The effect of catalysts in plasma oxidation of nitrogen oxides. Tartu, 2019, 114 p.
123. **Sergey Koshkarev.** A phenomenological feasibility study of the possible impact of the intrinsic heavy quark (charm) mechanism on the production of doubly heavy mesons and baryons. Tartu, 2020, 134 p.
124. **Kristi Uudeberg.** Optical Water Type Guided Approach to Estimate Water Quality in Inland and Coastal Waters. Tartu, 2020, 222 p.
125. **Daniel Blixt.** Hamiltonian analysis of covariant teleparallel theories of gravity. Tartu, 2021, 142 p.
126. **Ulbossyn Ualikhanova.** Gravity theories based on torsion: theoretical and observational constraints. Tartu, 2021, 154 p.
127. **Iaroslav Iakubivskyi**. Nanospacecraft for Technology Demonstration and Science Missions. Tartu, 2021, 177 p.
128. **Heido Trofimov.** Polluted clouds at air pollution hot spots help to better understand anthropogenic impacts on Earth's climate. Tartu, 2022, 96 p.